Physical Aging and Hygrothermal Response of Polycarbonate/Acrylonitrile-Butadiene-Styrene Polymer Blend

by

Jacky Tang

A Thesis

presented to the University of Waterloo

in fulfilment of the

thesis requirement for the degree of

Master of Applied Science

in

Mechanical Engineering

Waterloo, Ontario, Canada, 2007

DECLARATION

I hereby declare that I am the sole author of this thesis. This is a true copy of the thesis, including any required final revisions, as accepted by my examiners.

I understand that my thesis may be made electronically available to the public.

ABSTRACT

Polycarbonate (PC) is a glassy engineering thermoplastic that has been used for decades because of its superior mechanical properties such as high toughness and stiffness, and for its general thermal stability. However, the industrial demand for higher performance polymers with faster processing times has caused PC to be gradually replaced by different engineered polymer blends, such as polycarbonate/acyrlonitrile-butadiene-styrene (PC/ABS). Blends combine the advantages of the individual components but because they are a relatively new class of materials, their time-dependent behaviour is less well understood.

The goal of the present work is to characterize two primary time-dependent processes in a commercial 75:25 PC:ABS blend that are known to affect the long-term mechanical properties of the individual components. The first is physical aging which is a result of non-equilibrium fast cooling of glassy or amorphous polymers. Physical aging is associated with structural relaxation due to enthalpic and volumetric recovery. The second process is hygrothermal conditioning which is the combined application of thermal aging and moisture absorption. Three sets of characterization tests were conducted using Differential Scanning Calorimetry (DSC) and Fourier Transform Infrared spectroscopy (FTIR).

The enthalpic relaxation results determined from DSC data for aging at nine different combinations of time and temperature showed that aging experiments are best conducted at temperatures between 80 and 90°C. This range is below the glass temperature of the ABS component. The activation energy for enthalpic relaxation for the unaged blend was found to fall between energies for PC and ABS relaxations, but not according to the rule-of-mixtures.

The present study attempted to adopt the Tool–Narayanaswamy-Moynihan (TNM) phenomenological model to predict relaxation kinetics but was found to be complicated by multiple endothermic peaks. It was then concluded that the TNM model, although

very useful for single polymer systems, is unsuitable for blends. A semi-empirical model was applied instead to fit the experimental data which provided a reasonable estimate of the relaxation behaviour. Aging at 80°C for the period investigated did not reach equilibrium and it is expected that aging times of upwards of 2 years will be necessary to minimize the errors associated with the data fitting to provide a better fit of the model.

The FTIR studies revealed that thermal aging at 80°C in dry atmosphere results in oxidation of the butadiene component. However, the addition of moisture to the aging process appears to prevent, or at least impede, oxidation from occurring. The presence of moisture seems to trigger hydrogen bonding, which saturates regardless of the moisture content after approximately 80 days. The initial rate of moisture diffusion in PC/ABS appeared to depend predominantly on temperature while the ambient moisture concentration tends to only affect the final equilibrium content in the blend.

ACKNOWLEDGEMENTS

I wish to extend my sincere gratitude to Dr. Pearl Sullivan for her insight, patience and guidance throughout this work.

This research was made possible in partnership with Research in Motion Ltd. (RIM) and Materials and Manufacturing Ontario (MMO). The assistance provided by lab chemist, Alexandre Romanov, and lab technician, Deepchand Ramjattan of the Materials Interconnect Research lab at RIM are gratefully appreciated. All materials used in the present study were provided by Materials Research Manager, Dr. Dwayne Wasylyshyn, and Materials Interconnect Research Director, Dr. Bev Christian from RIM.

The assistance of Mr. Ross Bradsen, the MMO liaison manager, in coordinating the project is also gratefully acknowledged.

DEDICATION

May the present work inspire those interested in polymer research to pursue knowledge in this field.

My love and thanks are extended to my parents, Danny and Maria, who have patiently encouraged and supported my efforts along this path of life.

TABLE OF CONTENTS

LIST OF FIGURES

LIST OF TABLES

NOMECLATURE

α	Coefficient of thermal expansion
a	Number of levels of a treatment in an experiment
a	Constant in viscosity expression
A	Constant in VTF expression
A	Absorbance in FTIR
b	Constant in viscosity expression
B	Constant in Adam-Gibbs expression
β	Non-exponential shape parameter of KWW expression
c	Concentration
c_∞	Saturated surface concentration
c_o	Equilibrium solvent concentration
C_p	Heat capacity
C_{pe}	Heat capacity at equilibrium
C_{pg}	Heat capacity of glass
δ	Relative departure of specific volume in KAHR expression
δ_p	Relative departure of property, P, from equilibrium
δ_p^o	Initial departure from equilibrium of property, P
δ_H	Relative departure of enthalpy in KAHR expression
D	Coefficient of diffusion
ε_{ij}	Random error associated with the j^{th} replicate and i^{th} treatment
E'	Storage modulus
E''	Loss modulus

E^*	Complex modulus
ϕ	Stretched exponential response of KWW expression
f	Free volume fraction
f	Kinetic or time-dependent componet of total heat flow in MDSC
$\Delta\alpha$	Change in coefficient of thermal expansion between equilibrium and glass state
ΔC_p	Change in heat capacity between equilibrium and glass state
Δh^*	Apparent activation energy for enthalpy relaxation
ΔH_a	Enthalpy change across glass transition due to aging
η	Coefficient of viscosity
h	Thickness of plate in diffusion
H	Enthalpy
H_0	Null hypothesis in a formal test of significance
I	Intensity in FTIR
I_o	Intensity of background spectrum in FTIR
J	Flux of diffusion
k	Empirical constant in sorption curve expression
μ_i	Mean value of the i^{th} treatment
$M(t)$	Mass of sample at time, t, in sorption curve expression
M_t	Mass of sample at time, t, in sorption curve expression
M_∞	Equilibrium mass of sample in sorption curve expression
n	Number of observations under the i^{th} treatment
n	Empirical constant in sorption curve expression
N	Total number of observations in an experimental study

θ	A form of activation energy used in KAHR expression
$P(t)$	Value of property, P, at time, t
P_∞	Equilibrium value of property, P
q_1	Cooling rate from above the glass transition temperature
q_2	Heating rate to above the glass transition temperature
R	Universal gas constant, 8.3145 J K^{-1} mol^{-1}
S_c	Configurational entropy used in Adam-Gibbs expression
SS_T	Total sums of squares
t	Time
t_a	Aging time
T	Temperature
T	Percent transmittance in FTIR
T_β	Mechanical transition temperature β
T_γ	Mechanical transition temperature γ
T_a	Aging temperature
T'_f	Fictive temperature
T_f	Fictive temperature
T_g	Glass transition temperature
T_k	Kauzmaan temperature
T_o	Arbitrary temperature below T_g in VTF expression
T_p	Endothermic peak temperature
T_r	Reference temperature in KAHR expression
$Tan\ \delta$	Ratio of loss to storage modulus, E'' / E'

τ	Relaxation time constant
τ_o	Characteristic relaxation time constant in TNM expression
τ_r	Reference time constant
v	Volume
v_f	Free volume
v_o	Occupied volume
x	Non-linearity parameter in TNM expression
x	Position coordinate in direction of flow
y_{ij}	Experimental observation of the j^{th} replicate and i^{th} treatment

Chapter 1 INTRODUCTION

Polymeric materials have been gaining the attention of manufacturers requiring high performance, non-metallic materials. However, the properties of polymeric materials are somewhat different from metals because of the inherently different molecular structure.

Polymeric materials are strongly *viscoelastic*, meaning its properties are time and temperature dependent. Their reaction to external loads can be characterized in two ways. Under constant strain, the time-dependent stress response is known as *stress relaxation*, while time-dependent strain response is referred to as *creep*. Metals (and alloys) exhibit creep deformation at high temperatures but the difference in polymers is their ability to partially recover creep strain upon the removal of the load. This behaviour can be illustrated by various responses of material to the applied load, shown in Figure 1.1.

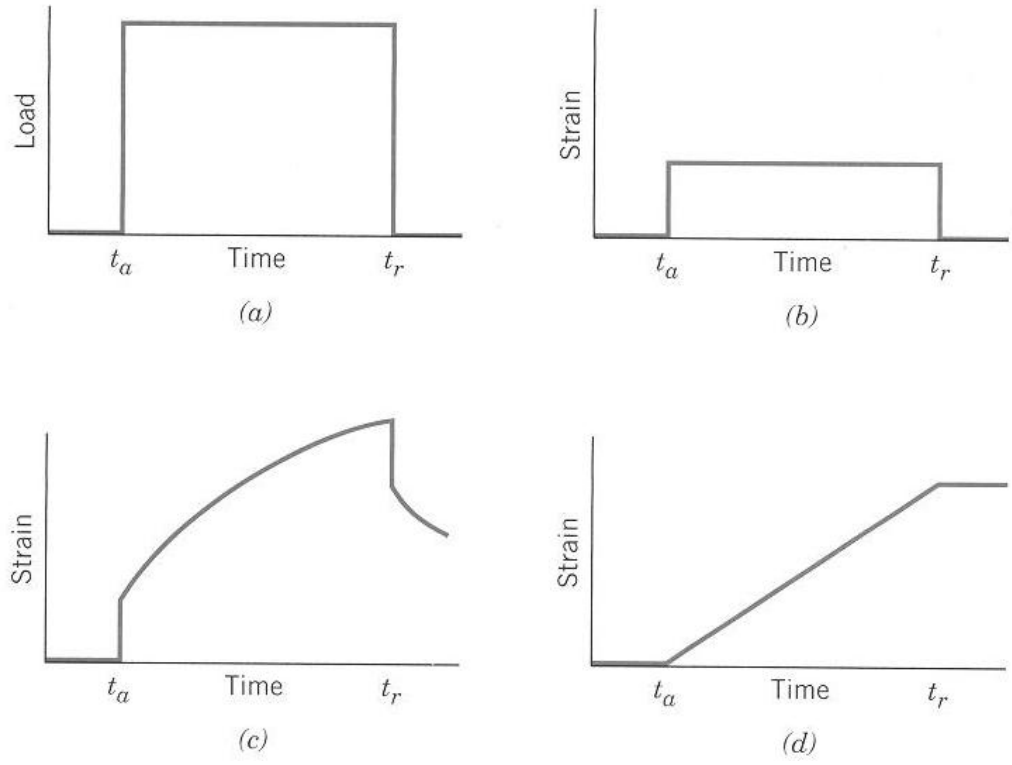

Figure 1.1: (a) Load versus time, where load is applied instantaneously at time t_a and relased at t_r (b) elastic (c) viscoelastic (leathery) (d) viscous behaviour [Callister 1997]

As illustrated, viscoelastic behaviour is a time-dependent phenomenon in which the responses are intermediate of an elastic solid and a viscous liquid. Therefore, the reporting of inherent properties of polymeric materials can be complicated.

Polymer molecules can exist in an orderly *crystalline* state or a random, tangled *amorphous* state. Generally, small molecules (e.g. water) can be entirely crystalline (solid) or entirely amorphous (liquid). The density of a crystalline material will be greater than an amorphous due to the tighter packing. For large molecules, like in polymers, they are often semi-crystalline, having crystalline regions dispersed within amorphous regions or only amorphous [Callister 1997].

The motivation for this work is to study two molecular level processes which are known to affect the viscoelastic (time-temperature dependence) properties of amorphous or glassy polymers. The first is physical aging which is time and temperature-dependent structural relaxation. The second process is hygrothermal structural change due to exposure of moisture and temperature.

Regardless of the glassy polymer systems being studied, it is useful to understand the molecular concepts associated with these processes. The time or rate dependent behaviour of polymers are most readily measured using the glass transition, T_g, which in turn describes the amount of free 'space' or free volume available for molecular movement.

1.1 GLASS TEMPERATURE

An important physical property which is used for engineering design of amorphous polymers is the glass temperature. The glass temperature, T_g, rather than a specific temperature, is a transitional range in which a significant change takes place in some specific physical property (eg. mechanical, electrical, thermal). Above the glass temperature, a material is in an equilibrium state in which the polymer chains can move freely in a liquid state. As the material is cooled below the glass temperature, these motions are limited and the material becomes a glassy solid. It is a very important parameter that can be used to characterize a material, and as expected of viscoelastic materials, this parameter is time or rate-dependent. To add to the complications of time dependence, the use of different thermal analysis techniques (to be discussed later) used to

measure this parameter and different test conditions could result in varying differences in the results. More information on the definition or standards of testing can be found in ASTM E1356-03 and ASTM E1545-00 standards.

The glass temperature for PC is approximately 150°C (143°C - 150°C) depending on technique used to measure [MatWeb–PC]. The glass temperature for ABS is approximately 100°C depending on measurement technique and also the commercial grade [MatWeb–ABS] and consequently, the service temperature range for this material is slightly lower than that of PC.

1.2 FREE VOLUME

Free volume is defined as the space a molecule has for internal movement and it is known to be related to aging [Struik 1978] and penetration by solvents [Vrentas *et al.* 1986]. A simple model describing this is the crankshaft mechanism [McCrum *et al.* 1967]. The crankshaft model treats the molecule as a collection of mobile segments that have some degree of free movement. As the free volume of the chain segment increases, its ability to move in various directions also increases. The increased mobility is the result in greater compliance, and hence a lower modulus. As a material is heated, it passes through a T_γ where bending and stretching such that localized bond movements and side chain movements can occur. Continuing to heat the material, it passes through a T_β which involves the entire side chain and localized groups to have enough space to rotate, hence developing toughness. When T_g is reached, large-scale motions in the chains of the amorphous phase are disentangled.

The concept of free volume is actually an attempt at describing the viscosity, η, of liquids above T_g and has become the basis of different empirical equations developed. The temperature dependence of η was proposed as

$$\ln(\eta) = \frac{A}{T - T_o} \tag{1}$$

by Vogel [1921], Fulcher [1925] and Tammann and Hesse [1926], which is commonly known as the VTF equation. A is a constant and T_o is a temperature below T_g. Also, an alternative equation

that was later proposed by Doolittle [1951] describing the viscosity in terms of the free volume fraction, *f*:

$$\ln(\eta) = a + \frac{b}{f} \tag{2}$$

where a and b are constants, and the free volume fraction is defined as

$$f = \frac{v - v_o}{v} = \frac{v_f}{v} \tag{3}$$

The free volume, v_f, is the difference between the actual volume, v, and the occupied volume, v_o. A physical interpretation of the free volume concept utilizing equation (2) is that the molecular mobility requires a certain critical volume [Cohen and Turnbull 1959; Turnbull and Cohen 1961]. However, an issue that arose with this concept was the poor definition of *occupied volume*. Although this concept is with its own drawbacks, the simplistic nature of it has maintained its popularity amongst researchers.

1.3 PHYSICAL AGING AND STRUCTURAL RECOVERY

The cooling of a material from above the glass temperature to below it, or a temperature jump, will cause excess thermodynamic quantities of enthalpy, volume, etc. This deviation from the equilibrium state is shown in terms of enthalpy in Figure 1.2 (adapted from Moynihan et al. 1976; Richardson and Savill 1975; Moynihan et al. 1996) where point *a* indicates the location of excess enthalpy. A material is first cooled from its liquid state at point *c* to the glass temperature following the unaged line to point *a*. The glass, while in this non-equilibrium state, will spontaneously evolve towards equilibrium. Allowing it to evolve towards equilibrium by storing it at a constant temperature without the application of stress or influence of external conditions is termed *physical aging,* as opposed to chemical or biological aging [Hutchinson 1995]. This term, first introduced by Struik [1978], describes a phenomenon in which changes to a material property are observed as a function of aging time and the monitoring of volume or enthalpy are common parameters to characterize the thermodynamic state of glasses as physical aging is taking place [Liu *et al.* 1992; Cheng *et al.* 1992; Schultheisz and McKenna 1997; Slobodian *et al.* 2003; Hadac *et al.* 2005]. The recovery towards equilibrium state is known as *structural*

relaxation or *recovery*. This process occurs experimentally during isothermal aging at a temperature, T_a. As the aging process progresses, point *b* shifts vertically towards the equilibrium line as the molecules rearrange themselves to an equilibrium state.

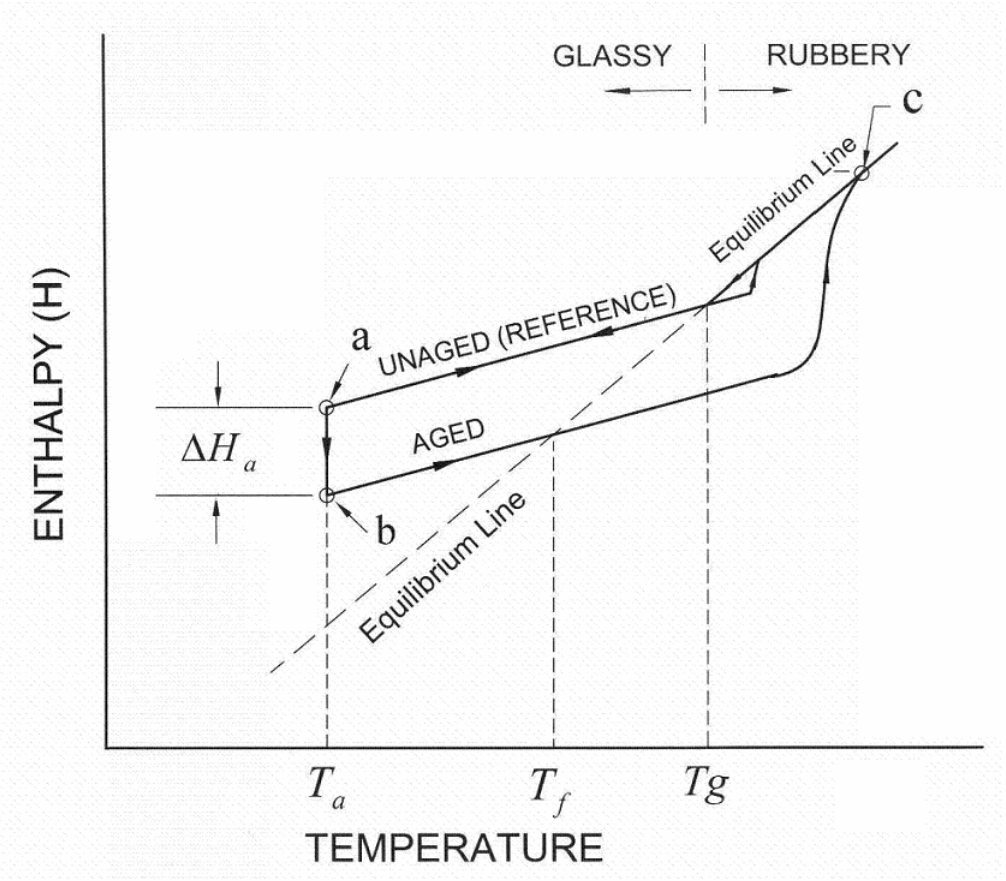

Figure 1.2: Schematic of enthalpy evolution in thermal cycling process

Referring to Figure 1.2, aging at temperature, T_a, causes the monitored parameter, enthalpy, to decrease, or *recover*, from point *a* with an arbitrary enthalpy (h_o) to an equilibrium enthalpy (h_∞). Point *b*, an enthalpy of h_t, is an intermediate point during which equilibrium is approached isothermally after time, *t*. The difference in enthalpy, or the enthalpy recovered as a result of the isothermal aging is denoted as ΔH_a. As time elapses, the structure will recover until equilibrium is reached and the timescale for structural relaxation increases rapidly as T_a is decreased. The rate of structural relaxation can be described by a relaxation time, τ, which is dependent on temperature, *T*, and the fictive temperature, T'_f. This expression is approximated by an Arrhenius expression according to the so-called Tool–Narayanaswamy-Moynihan [Moynihan *et al.* 1976] or TNM equation

$$\tau\left(T,T_f\right)=\tau_o\cdot\exp\left(x\cdot\frac{\Delta h^*}{RT}+\left(1-x\right)\cdot\frac{\Delta h^*}{RT_f}\right) \tag{4}$$

where τ_o is τ at an infinitely high temperature, Δh^* is the apparent activation energy for enthalpy relaxation, R is the ideal gas constant, T_f is the fictive temperature (which will be further discussed), and x ($0 \le x \le 1$) is a non-linearity parameter that describes the relative contributions of temperature and structure to the relaxation time. It can be seen accordingly that τ increases with the decrease of temperature, T.

Another formulation of relaxation, conceptually different from the TNM, but mathematically equivalent was developed by Kovacs, Aklonis, Hutchinson and Ramos, commonly known as KAHR [Kovacs *et al.* 1979].

$$\tau\left(T,T_f\right)=\tau_o\cdot\exp\left(-\theta\left(T-T_r\right)-\left(1-x\right)\cdot\frac{\theta\cdot\delta}{\Delta\alpha}\right) \tag{5}$$

where τ_o is τ in equilibrium at the reference temperature T_r, θ is a form of activation energy in which $\theta\approx\frac{\Delta h^*}{RT_g^2}$, δ is the relative departure of the specific volume from equilibrium, and $\Delta\alpha$ is the difference in the change in the coefficient of thermal expansion between the equilibrium and glass state [Hodge 1994]. The corresponding equation expressed in terms of enthalpy is found by replacing δ with δ_H for the relative departure of enthalpy from equilibrium, and replacing $\Delta\alpha$ with ΔC_p [Hutchinson 1995].

$$\tau\left(T,T_f\right)=\tau_o\cdot\exp\left(-\theta\left(T-T_r\right)-\left(1-x\right)\cdot\frac{\theta\cdot\delta_H}{\Delta C_p}\right) \tag{6}$$

Lastly, another model for structural relaxation is provided by the Adam-Gibbs equation [Hodge 1997, Christiansen and Drozdov 2002]

$$\tau\left(T,T_f\right)=\tau_o\cdot\exp\left(\frac{B}{T\cdot S_c\left(T_f\right)}\right) \tag{7}$$

where B is a constant and $S_c(T_f)$ is the configurational entropy. An advantage of this model is that the entropy can be computed either from calorimetric experiments or from Fourier transform infrared spectroscopy (FTIR). It can be expressed in terms of the fictive temperature as

$$S_c\left(T_f\right) = \Delta C_p \cdot \ln\left(\frac{T_f}{T_k}\right) \tag{8}$$

where ΔC_p is the difference between the liquid and glass heat capacities near T_g, and T_k is the Kauzmaan temperature, the temperature at which the configurational entropy vanishes from equilibrium.

The structural relaxation models introduced have been widely used by researchers; however, they are by no means the only ones available. It should be noted here that the enthalpy and volume relaxes in a similar but non-identical way. In fact, it was noted by Kovacs [1958] and Petrie [1972] that the time required to reach equilibrium is considerably longer in enthalpy relaxation than volume relaxation. The experimentation with polystyrene (PS) by Petrie indicates that enthalpy relaxation requires in excess of 100 hours whereas equilibrium of volume is reached in approximately 10 hours. It is then deduced that there are some molecular motions that contribute to enthalpy relaxation but cause no changes to the volume [Hutchinson 1995].

The formulations shown above only describe one instance of relaxation time with a prescribed set of parameters. A distribution or continuous spectrum can be modeled by the use of a stretched exponential response, the Kohlrausch-Williams-Watts (KWW) function

$$\Phi\left(t\right) = \exp\left[-\left(\frac{t}{\tau}\right)^{\beta}\right] \tag{9}$$

where τ is given by one of the chosen formulations and β ($0 \leq x \leq 1$) is the non-exponentiality parameter inversely proportional to the breadth of the relaxation spectrum. It can also be interpreted as a measure of molecular 'co-operativity'.

1.3.1 Fictive Temperature

Tool [1945; 1946] was the first to develop another important parameter in studying glassy polymers known as the fictive temperature, T'_f, or more commonly written as T_f, used to define the state of the structure of a glass based on its previous thermal history. As such, T_f will vary depending on the rate of cooling, reheating, thermal aging time or temperature or any parameter that affected the previous thermal history of the polymer. Observing Figure 1.2 once again, upon reheating after t_a, the temperature at which the equilibrium line is reached is defined as the fictive temperature, T_f. In the case where there is no recovery or aging process, the temperature measured from the equal area method is comparable to the glass temperature [McKenna and Simon 2002].

Although the fictive temperature is defined, in order to determine the fictive temperature, the heat capacity, C_p, curve must be consulted. The fictive temperature, T_f, can be determined from the equal area method, as described elsewhere [Moynihan *et al.* 1976; Richardson and Savill 1975]. A graphical method of determining T_f was developed by Moynihan as shown in Figure 1.3. By selecting an arbitrary temperature for T_f, balancing area I (the area above the C_p curve between the arbitrarily chosen T_f and the start of the overshoot peak in the liquid state) and area II (the area under the trend line of the glassy C_p curve up to T_f added to the area under the overshoot peak in the liquid state).

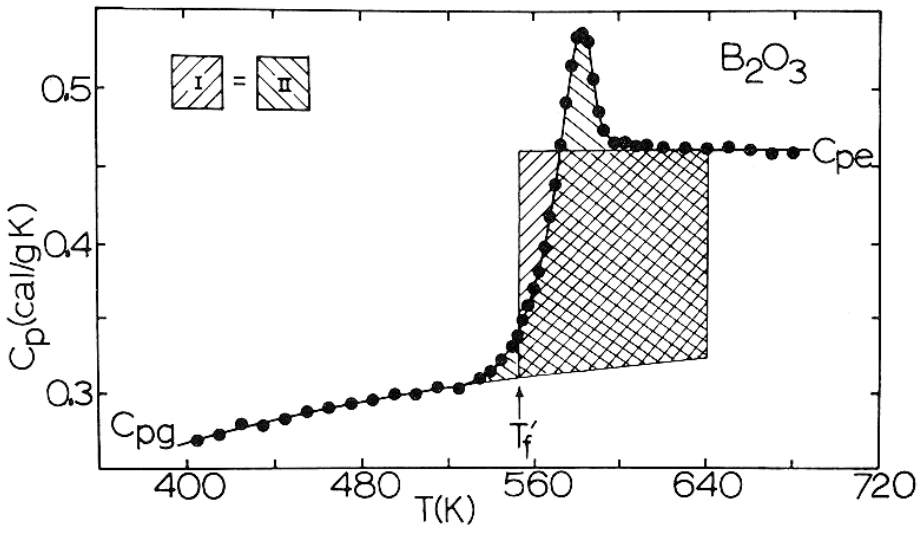

Figure 1.3: Heat capacity versus temperature for B_2O_3 glass during heating at 10 K/min following a rate cool at 10 K/min through the glass transition region [Moynihan *et al.* 1976].

The balancing of the areas can be mathematically represented as

$$\int_{T>>T_g}^{T'_f} \left(C_{pe} - C_{pg}\right) dT = \int_{T>>T_g}^{T<<T_g} \left(C_p - C_{pg}\right) dT \tag{10}$$

where C_{pg} is the glass heat capacity observed below the transition region, and C_{pe} is the equilibrium liquid heat capacity observed above the transition region [Moynihan *et al.* 1976].

1.4 ENTHALPY AND VOLUME RELAXATION

A simple structural recovery experiment involves the monitoring of the change of a property in an isothermal state, following a temperature jump from an equilibrium state (above T_g) to a non-equilibrium state, T_o (below T_g). As mentioned before, this specific property could be that of enthalpy or volume, as these are the most commonly used properties. These changes can be expressed in terms of a departure, δ, for a property, P, from the equilibrium value, P_∞.

$$\delta_p(t) = P(t) - P_\infty \tag{11}$$

The departure of the property is generally shown plotted on a logarithmic time scale as shown in Figure 1.4.

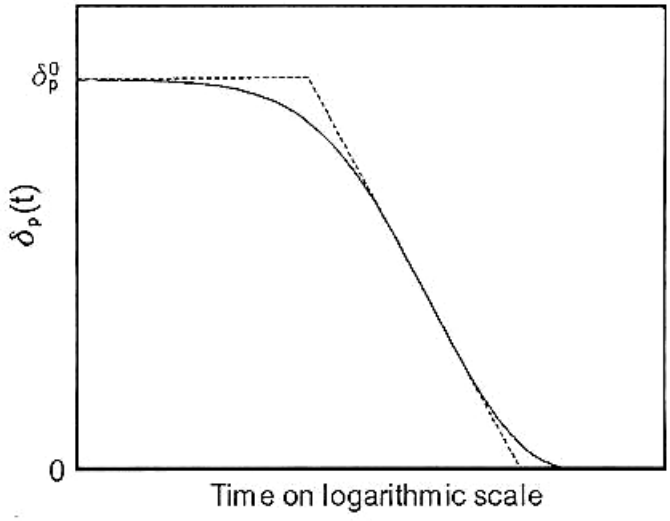

Figure 1.4: Departure of property P from equilibrium versus log(t) [Malek and Mitsuhashi 1999]

The initial departure from equilibrium, denoted by δ_p^o, can be related to the magnitude of the temperature jump, $\Delta T = T_0 - T_\infty$

$$\delta_p^o = \Delta T\left[\left(\frac{dP}{dT}\right)_{liquid} - \left(\frac{dP}{dT}\right)_{solid}\right] \tag{12}$$

In the case of volume relaxation, the term within the bracket is substituted by $V_o\Delta\alpha$, where $\Delta\alpha$ is the change in the coefficient of thermal expansion. Similarly, for enthalpy relaxation, the bracketed term would be replaced by the change in specific heat, ΔC_p. Since these changes are measured across T_g, they are also differences between the parameter in the liquid state and the glassy state.

The slope of the inflectional tangent, $-\left(\frac{d\delta_p(t)}{d\log(t)}\right)$, is referred to as the relaxation rate [Kovacs 1958; Kovacs 1963]. The use of this parameter, introduced by Kovacs, was originally used to measure volume relaxation rate and has since been adopted for enthalpy relaxation as well.

1.5 TIME-DEPENDENT MOISTURE ABSORPTION

The sorption of small molecules – gases, organic solvents or water – by polymers has been of fundamental research interest. When polymers are exposed to liquids, one of the main forms of degradation is swelling during which small molecules diffuse into and are absorbed by the larger polymer molecules. These small molecules fit into and occupy positions amongst the polymer molecules, forcing them apart, causing the expansion or swelling [Callister 1997]. Polymer-water systems studies have been of particular interest. Diffusion is the mechanism by which water molecules are absorbed into polymers through the surface and the most common formulation of the diffusion process is Fick's law [1855].

There are three common modes of transport behaviour, depending on the diffusion and relaxation mechanisms. When diffusion is much slower than relaxation, resembling Fickian diffusion, it is categorized as Case I. If diffusion is rapid compared to relaxation, characterized by a moving

concentration front, it is known as Case II. Lastly, there is an intermediary case when diffusion and relaxation rates are comparable, termed Case III [Barrie 1975].

These different cases can be distinguished by the shapes of their sorption curves and the initial fractional mass uptake during sorption which follows

$$\frac{M_t}{M_\infty} = kt^n \tag{13}$$

where k and n are empirical constants. For a Case I system, n = 0.5 and k is proportional to the diffusion coefficient over the initial half of the sorption experiment. In a Case II system, n= 1.0 and k is directly proportional to the velocity of the moving boundary. For a Case III system, n lies between 0.5 and 1.0 [Lee and Knaebel 1997].

Some common sorption behaviour that do not necessarily fall under the above cases may include, but are not limited to, pseudo-Fickian, sigmoidal, two-stage, overshoot and drastic acceleration. A brief description of some of these is included in the publication by Lee and Knaebel [1997].

The molecular changes caused by the swelling of the free volume due to penetration of water molecules as well as dissociation caused by hygro-degradation are conveniently monitored by FTIR.

1.5.1 Fickian Diffusion

Fick introduced two differential equations that quantified the transport process. His first law, states that the diffusion flux, J, of a component of concentration, c, across a surface of unit area is proportional to the concentration gradient across that plane. D is known as the diffusion coefficient and x is the position co-ordinate in the flow direction. The second law states that the rate of change of concentration in a volume element is proportional to the rate of change of concentration gradient at that point. Fick's two laws are shown in equation (14) and equation (15), respectively.

$$J = -D(c) \cdot \frac{\partial c}{\partial x} \tag{14}$$

$$\frac{\partial c}{\partial t} = \frac{\partial}{\partial x}\left(D(c) \cdot \frac{\partial c}{\partial x} \right) \tag{15}$$

Case I or Fickian diffusion is characterized by increased penetration or weight gain of the polymer system with $t^{1/2}$. Under steady flow conditions, J is constant, and the concentration profile of an initially dry plate of thickness $2h$ which has its surfaces exposed is given by

$$\frac{c(x,t)}{c_o} = 1 - \frac{4}{\pi}\sum_{n=0}^{\infty}\left\{ \frac{(-1)^n}{2n+1} \cdot \exp\left[-D(2n+1)^2 \cdot \frac{\pi^2 \cdot t}{4 \cdot h^2} \right] \cdot \cos\left[\frac{(2n+1) \cdot \pi \cdot x}{2h} \right] \right\} \tag{16}$$

where c_o is the equilibrium solvent concentration. In general, the diffusivity constant is dependent of the concentration and hence equation (15) needs to be solved numerically for most cases.

An analytical solution for the total moisture uptake is given as [Barrie 1975]:

$$\frac{M(t)}{M_\infty} = 1 - \frac{8}{\pi^2}\sum_{n=0}^{\infty}\left\{ \frac{1}{(2n+1)^2} \cdot \exp\left[-D(2n+1)^2 \cdot \frac{\pi^2 \cdot t}{4 \cdot h^2} \right] \right\} \tag{17}$$

where M_∞ is the absorbed moisture at saturation, and the diffusion constant is the initial slope of the moisture absorption curve approximated with about 0.001 per cent error as

$$D = \frac{0.04919}{\left(t / l^2 \right)_{1/2}} \tag{18}$$

1.5.2 Non-Fickian Diffusion

Due to the viscoelastic nature of polymers, polymer-solvent systems often exhibit behaviour different from a simple Fickian diffusion process. One type of non-Fickian behaviour in which the polymer relaxation process is very slow compared to the diffusion process exhibits a sharp concentration front that propagates at constant speed through the polymer. This relaxation controlled transport, known as Case II of diffusion, has been first reported in literature by Alfrey *et al.* [1966].

An example of anomalous absorption behaviour is shown below in Figure 1.5. Two Fickian models of different saturation levels depicted as dashed lines enclose the original two-stage data of the experiment.

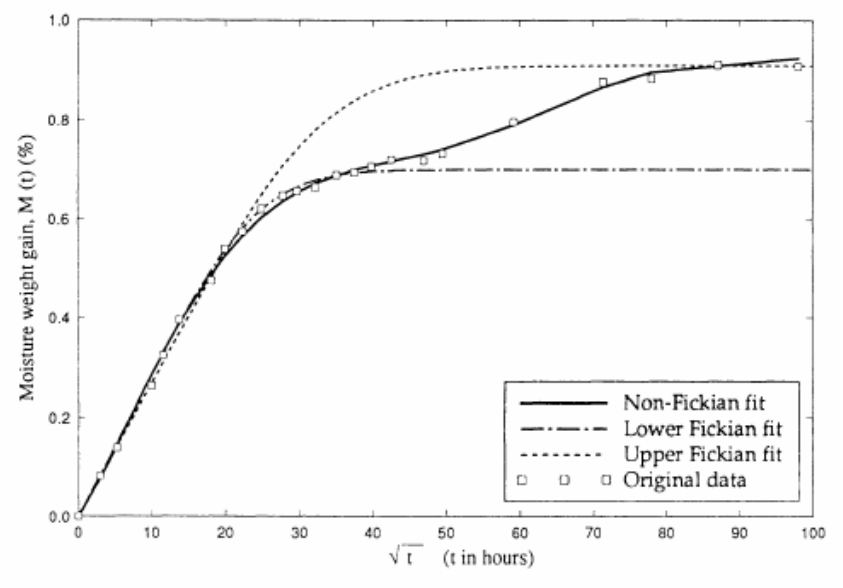

Figure 1.5: 2-step non-Fickian moisture absorption with upper and lower bounds by different concentration in Fickian fitting [Cai and Weitsman 1994]

Departure from idealized diffusion can occur for many different reasons and a study on non-Fickian diffusion by Cai and Weitsman [1994] had been conducted. Even though the ambient conditions remained constant, a time-dependent *boundary condition* was used to reduce the non-Fickian moisture absorption data in order to correlate it with a Fickian model. The boundary condition takes the form of a Prony series:

$$c_o(t) = c_i + \sum_r c_r \left[1 - \exp\left(\frac{-t}{\tau_r} \right) \right] \tag{19}$$

where τ_r is the time constant governing the time-dependence in the surface concentration. In the case where $c_i = 0$, the moisture concentration profile and the moisture uptake is given as [Barrie 1975]

$$\frac{c(x,t)}{c_\infty} = 1 - \exp(-\beta t) \cdot \frac{\cos\left[x\left(\frac{\beta}{D}\right)\right]^{0.5}}{\cos\left[h\left(\frac{\beta}{D}\right)\right]^{0.5}} - \frac{16\beta h^2}{\pi} \times \sum_{n=0}^{\infty}\left\{ \frac{(-1)^n}{2n+1} \cdot \frac{\exp\left[-D(2n+1)^2 \cdot \frac{\pi^2 t}{4h^2}\right]}{4\beta h^2 - D\pi^2 \cdot (2n+1)^2} \cdot \cos\left[\frac{(2n+1)\cdot \pi x}{2h}\right]\right\} \tag{20}$$

$$\frac{M(t)}{M_\infty} = 1 - \exp(-\beta t) \cdot \tan\left(\frac{\beta h^2}{D}\right)^{0.5} - \frac{8}{\pi^2} \cdot \sum_{n=0}^{\infty}\left\{ \frac{1}{(2n+1)^2} \cdot \frac{\exp\left[-D(2n+1)^2 \cdot \frac{\pi^2 t}{4h^2}\right]}{1 - (2n+1)^2 \cdot \left(\frac{D\pi^2}{4\beta h^2}\right)}\right\} \tag{21}$$

where c_∞ is the saturated surface concentration and $\beta = 1 / \tau$.

For a general case, where the surface moisture concentration is given by equation (19), the surface moisture concentration and moisture absorption are given as [Cai and Weitsman 1994]

$$\frac{c(x,t)}{c_\infty} = \frac{c_i}{c_\infty} c_H(x,t) + \sum_{r=1}^{R}\left(\frac{c_r}{c_\infty} \cdot \hat{c}(x,t;\beta_r)\right) \tag{22}$$

$$\frac{M(t)}{M_\infty} = \frac{c_i}{c_\infty} M_H + \sum_{r=1}^{R}\left(\frac{c_r}{c_\infty} \cdot \hat{M}(t;\beta_r)\right) \tag{23}$$

where c_H is Fick's solution, equation (16) and $\hat{c}$ is equation (21). M_H and $\hat{M}$ corresponds to equations (17) and (21), respectively.

In a similar approach attempted by Roy [2000] a time-dependent *diffusion coefficient* in the form of a Prony series was utilized:

$$D(t) = D_i + \sum_r D_r\left[1 - \exp\left(\frac{-t}{\tau_r}\right)\right] \tag{24}$$

where τ_r is the time constant governing the time-dependence in the variation of the diffusion coefficient. The analytical solution for the concentration profile and corresponding moisture uptake curve are given as [Roy 2000]

$$\frac{c(x,t)}{c_o} = 1 - \frac{4}{\pi}\sum_{n=0}^{\infty}\frac{(-1)^n}{2n+1}\cdot\exp\left\{-(2n+1)^2\cdot\frac{\pi^2}{4h^2}\times \left\{D_i t + \sum_{r=1}^{R} D_r\left[t+\tau_r\left(e^{\frac{-t}{\tau_r}}-1\right)\right]\right\}\right\}\cos\left[\frac{(2n+1)\cdot\pi x}{2h}\right] \tag{25}$$

$$\frac{M(t)}{M_o} = 1 - \frac{8}{\pi^2}\sum_{n=0}^{\infty}\frac{1}{(2n+1)^2}\cdot\exp\left\{-[2n+1]^2\cdot\frac{\pi^2}{4h^2}\left[D_i t + \sum_{r=1}^{R} D_r\left[t+\tau_r\left(e^{\frac{-t}{\tau_r}}-1\right)\right]\right]\right\} \tag{26}$$

Subsequently, Roy also attempted to present an approach to model this two-stage behaviour through finite element methods. The results of the approximation clearly indicate that predicted moisture uptake is capable of capturing the two-step behaviour. Although it over-estimates the absorption process, it better models the experimental data than the idealized Fickian prediction as seen in Figure 1.6.

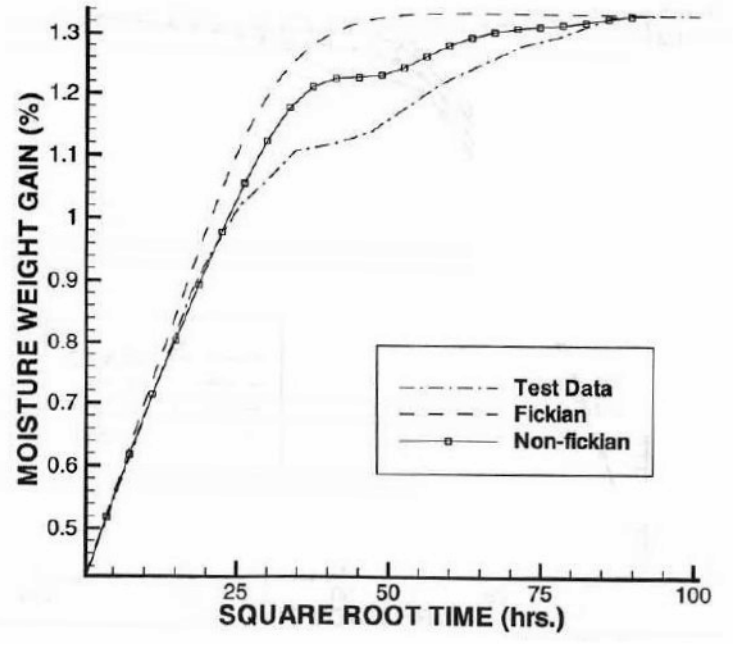

Figure 1.6: Non-Fickian moisture uptake prediction [Roy 2000]

1.6 MOTIVATION FOR RESEARCH WORK

There is significant industrial interest in understanding the time and temperature-dependent behaviour of blends which offer the combination of advantageous properties of individual polymer components. It is not uncommon that a material's properties meet most but not all requirements of a certain design. The lack of a superior material that meets all criteria has led to the need for polymer blends that offer the possibility of combining the properties of available materials to produce unique materials with tailored and enhanced properties. A polymer blend is a mixture of two or more polymers with noticeable differences in chemical composition and/or microstructure. It is also a description of a material rather than of a structure. However, the success of this strategy has been worse than a simple *rule of mixtures* would predict in most cases. The reason for the aforementioned is that most polymers are not *miscibile* in one another. Hence, the typical result of mixing polymers together is a material that consists of two separate phases, and the interface between the phases is often weaker than the polymers themselves.

Careful experiments via multiple techniques are necessary to establish miscibility and in many instances, the conclusions about miscibility drawn from different studies and techniques have been in conflict. Lodge *et al*. describes that this may be due to a well known, but incorrect, rule of thumb: *observing two distinct glass transitions in a binary polymer blend is a signature of immiscibility*. This is a common misconception that Lodge *et al*. [2006] explains

> "much confusion stems from a naive application of a well known but incorrect rule of thumb, namely, that observation of two distinct glass transitions in a binary polymer blend is a signature of immiscibility. The reason for such confusion is that not only do some miscible systems exhibit two transitions, but any one-phase polymer mixture should be expected to exhibit two distinct transitions if the pure component transitions are sufficiently different."

In immiscible polymer blends, their physical properties are poor compared to those of the constituent components because of phase separation due to weak interaction at the boundaries of the components [Sato 2004]. Ionic interactions between components have been used as a method for improving miscibility in polymer-polymer blends [Garton 1992]. These include

intermolecular interactions such as hydrogen bonding and dipole-dipole interactions between component polymers [Sato 2004].

This work has focused on the polycarbonate/acrylonitrile-butadiene-styrene (PC/ABS) blend which has been replacing PC over the past decade due to the advantages it offers over the individual constituents.

1.6.1 Polycarbonate

Polycarbonate (PC) is an amorphous polymer with good mechanical properties. It is a tough, high-impact strength and ductile thermoplastic that can retain mechanical properties over a wide range of service temperatures with good dimensional stability [Callister 1997]. However, its poor chemical resistance make it sensitive to environmental conditioning factors, resulting in brittle failure. Safety equipment is often made from PC or its derivatives. Shown in Figure 1.7 is the molecular structure of PC.

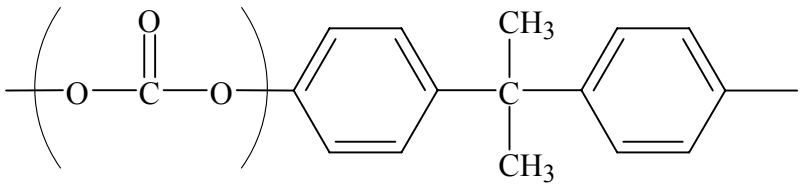

Figure 1.7: Molecular structure of polycarbonate

1.6.2 Acrylonitrile-Butadiene-Styrene

Acrylonitrile-Butadiene-Stryene (ABS) is a common thermoplastic used for its light weight, high impact resistance and dimensional stability. It generally has outstanding strength and toughness, and is resistant to heat distortion [Callister 1997]. However, it has poor weathering resistance and flame resistance, and thus flame retardants are often combined into the ABS production. The actual properties of ABS depend greatly on the blend ratio of the three major components. The acrylonitrile component is responsible for chemical resistance and thermal stability; the butadiene component is the cause of the toughness and impact strength; the styrene gives rigidity and

processability. By altering the composition of the three components, variations of this material may be produced to yield products varying in processability, toughness, and heat resistance. The low water absorption nature of ABS is used in plumbing piping and fittings, refrigerator linings and lawn and garden equipment. Illustrated in Figure 1.8 are the molecular structure of components of ABS.

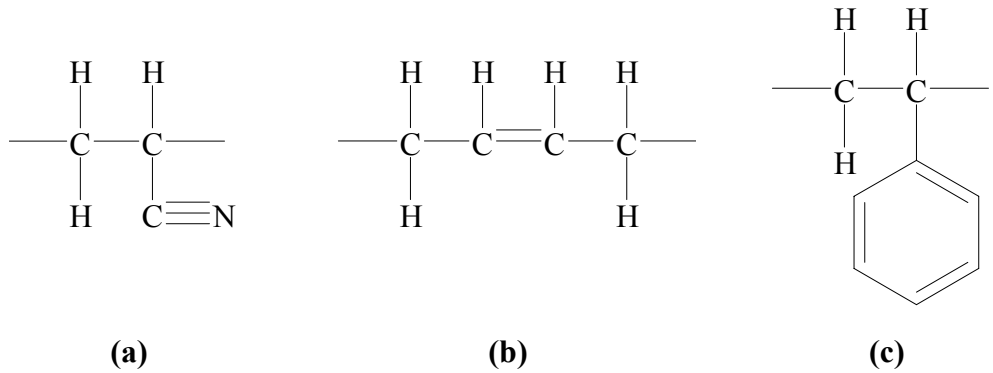

Figure 1.8: Molecular structure of (a) polyacrylonitrile (b) polybutadiene and (c) polystyrene

1.6.3 PC/ABS Blend

PC/ABS is an amorphous resin blend that is widely used for fabricating thin-walled plastic packaging for communication and electronic devices. Blends of PC and ABS can be mixed to improve upon their applications; by combining the exceptional mechanical and thermal properties of PC and the enhanced processability and low-temperature impact strength of ABS, PC/ABS blends result in a useful balance in toughness and stiffness as compared to conventional high impact PC or ABS alone, heat resistance, and better processing capabilities than PC alone – bringing together the advantages of both worlds. This improved processability is a great characteristic that many electronic device manufacturers have taken advantage of and use for the injection moulding of thin-walled casings for products such as desktop and laptop computers, cellular phones, calculators, etc. ABS is a copolymer containing a block polybutadiene to which styrene-acrylonitrile (SAN) random copolymer has been grafted. Thus, in the PC/ABS blend the interface between the two phases consists of PC/SAN [Más *et al.* 2002]. Good chemical resistance and hydrolytic stability under heat and humidity provides increased performance in automotive parts, electronic instruments, computers, telecommunications equipment, toys and especially thin-wall product designs.

1.6.4 Literature on Aging and Hygrothermal Response of PC/ABS to Date

In recent years, the recycling trend has caught onto the reuse, or regrinding, of material into resin for moulding. Many personal computer firms routinely blend virgin material with regrind. This has led to the studies conducted by several researchers [Eguiazabal and Nazabal 1990; Biddle and Christy 1992; Kuczynski *et al.* 1994] with differing results of properties of PC/ABS after numerous regrinding cycles. After six regrinding cycles, Biddle and Christy [1992] found little changes in color and flammability rating, as well as tensile and flexural strength being virtually unaffected. Similarly, Kuczynski *et al.* subsequently performed tests, finding no apparent change in tensile and flexural modulus, yield, ultimate and flexural stresses. These results were obtained from testing on three different commercially available PC/ABS blends after eight regrinding cycles. On the contrary, the study by Eguiazabal and Nazabal reported a substantial decrease in ductility, and tensile and impact strength were also degraded. All this occurred after the third regrinding cycle. Melt flow was also reported to increase, which indicates that there was a molecular weight reduction.

The study conducted by Balart *et al.* on recycled wastes indicates little degradation in PC or ABS was found after its service life as electrical components. This could mean that during the lifetime of the waste material obtained, humidity or thermal condition played a minor role. [Balart *et al.* 2005]

On a similar topic of personal computers, from a study performed by Wang [1995] on PC/ABS blends used for Compaq computers, the effects of humidity and temperature were studied. The impact strength is most affected by different levels of humidity – the higher the humidity the quicker the strength of the blend is reduced and also the higher the temperature at a specific humidity, the more prominent in degradation of strength.

In a thermal aging study [Guest and Van Daele 1995], it was found that PC/ABS blends containing 60% and 75% PC were able to retain high impact performance even after aging at elevated temperatures, as compared to that of just PC. The physical aging process decreases

toughness due to the oxidation of butadiene rubber and also decreases the ductility of blend systems containing ABS.

Generally speaking, residual stresses will form during injection moulding as a result of the temperature gradients that exist during solidification. Normally, the stresses that form in the interior of the moulding are tensile and fairly weak, and those at the surface are compressive and can be quite strong [Li *et al.* 2003]. Hot water conditioning performed by Ram *et al.* [1985] and Qayyum and White [1991] both concluded that the residual stresses in a moulding are reversed, meaning tensile stresses exist on the surface. These tensile stresses on the surface caused flaws to form, which were thought to lead to the decrease in toughness. In a boiling water aging study [Li *et al.* 2003], mechanical properties of PC/ABS were studied, and it was found that it caused a sharp decrease in elongation at break and notched impact strength. It was also found that the T_g of PC in the blend decreased after aging, while the T_g of ABS did not. The clustering of water molecules around impurities also led to microcracks, which were unrecoverable through heat treatment.

It is also observed that with progressive aging and moisture uptake the melt flow rate increases slightly, suggesting shorter polymeric chains, thus making the material less viscous and easier to flow. This implies that the overall molecular weight has decreased. [Patty 2004].

As PC is gradually being replaced by PC/ABS, previous experiments on PC are being slowly adapted to the blend using similar experimental methods. Although there is increasingly more literature on the mechanical properties and morphology of PC/ABS, there have been minimal studies on the hygrothermal aging, enthalpy or volume relaxation of PC/ABS. A rare reporting of PC/ABS relaxation data by Rusch [1968] indicates that the relaxation behaviour is dominated by the continuous phase in the blend with the longest relaxation time.

1.6.5 Objectives of Research Study

The objective of the study is to characterize two time dependent processes in a PC/ABS blend. The first process is physical aging which is related to structural relaxation due to non-equilibrium

cooling of polymers. This investigation will allow understanding of the effects of cooling conditions during moulding of the blend. The second process is the hygrothermal response due to moisture and/or heat conditioning. A key difference between physical aging and hygrothermal moisture absorption is that in physical aging, the main mechanism is volumetric contraction. However, if moisture is diffused through the polymer, the contraction is negated by swelling of the free volume. The competing processes complicate the analysis of hygrothermal conditioning. Although the molecular processes are much more complex, the results of the phenomenological study offer insight into the time-dependent hygrothermal response of the material during service.

1.6.6 Scope of Work

The scope of work consists of two main studies:

(i) Physical aging studies have been conducted to:

(a) evaluate the effects of cooling rate when cooling from above the glass transition in an unaged commercial PC/ABS blend are measured using DSC methods,

(b) compare the effects of cooling rate in short-term aged material under different combinations of time and temperature conditions,

(c) determine the effects of aging time and temperature on enthalpy relaxation,

(d) study the influence of aging on the measured heat enthalpies upon heating through the glass transition, and

(e) analyze the significance of changes in the results with the increase in aging time using statistical methods.

(ii) Hygrothermal conditioning has been performed to:

(a) compare moisture absorption behaviour of the material exposed to environments consisting of different temperature and moisture content.

(b) observe microstructural changes due to physical aging or hygrothermal conditions by infrared spectroscopy.

To achieve the objectives of the research, three sets of experimental studies have been conducted:

(i) cooling rate study

(ii) progressive physical aging study

(iii) hygrothermal study

The requisite data analyses for the final results are presented in a flowchart in Figure 1.9.

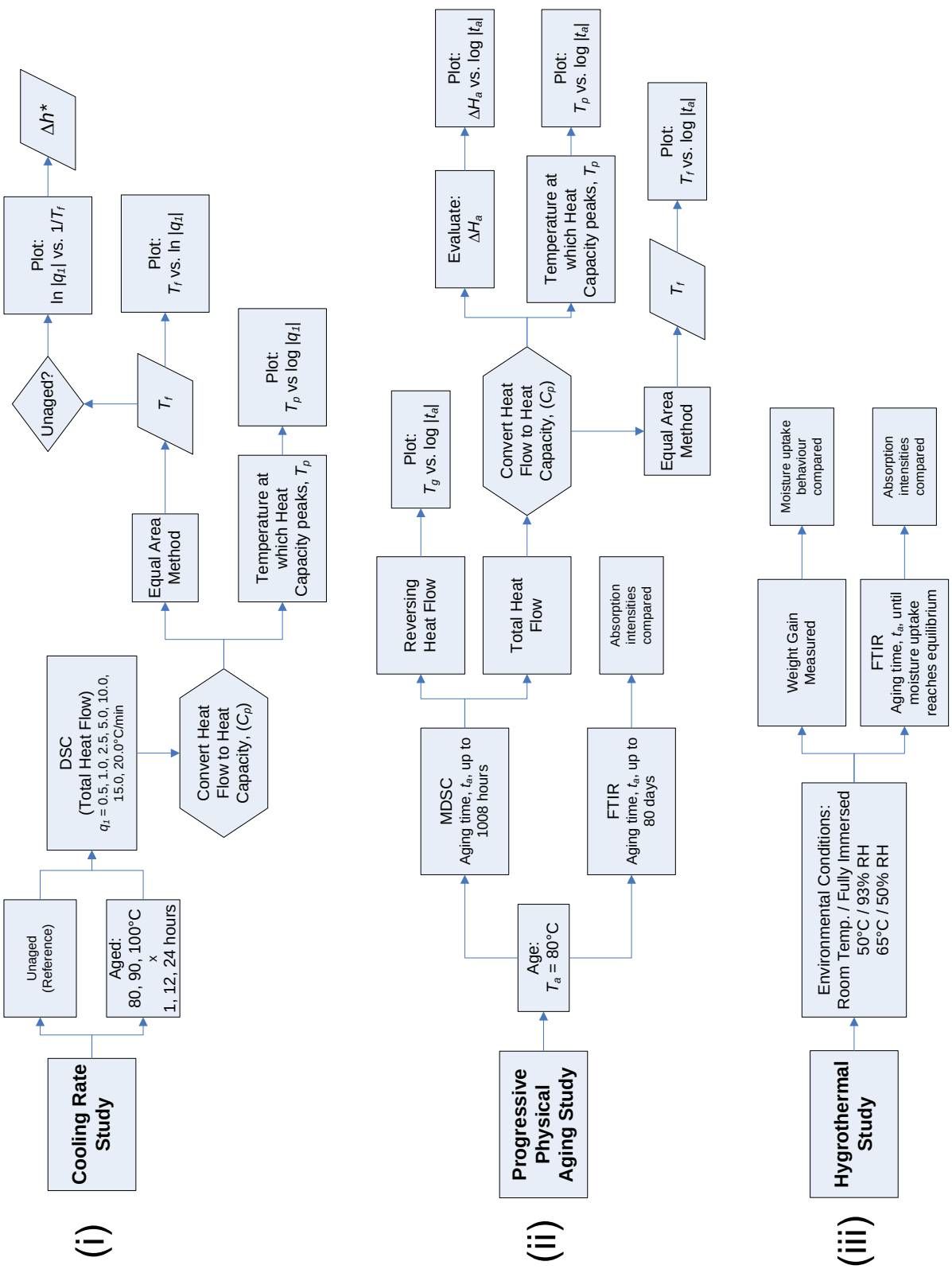

Figure 1.9: Flow chart of experimental work

Chapter 2 POLYMER CHARACTERIZATION TECHNIQUES

As mentioned in Figure 1.1, material properties will vary due to the time or rate-dependent nature of viscoelastic materials. This will lead to complications in the measurement technique and test conditions used. Although there are a variety of thermo-analytical techniques for characterizing polymers, our work has used two common methods that will be discussed. In addition, the Fourier Transform Infrared (FTIR) spectroscopy technique which has been used is discussed in more detail.

2.1 DYNAMIC MECHANICAL ANALYSIS

Dynamic mechanical analysis (DMA) is a technique used to detect major transitions, as well as secondary or tertiary transitions that are not readily identifiable by other techniques. The DMA applies an oscillating force to a sample and analyzes the material's response to that force. Parameters such as the viscosity and stiffness can be measured which corresponds to the ability to dissipate energy as heat (damping) and the ability to recover from deformation (elasticity), respectively. An advantage of DMA is that the stiffness, or modulus, can be obtained during sample oscillation. However, the absolute value of modulus is slightly different than the Young's modulus. The storage modulus (*E'*) and loss modulus (*E"*) are obtained which can be used to calculate the complex modulus, *E**. These moduli allow better characterization of the material and parallel that of real, imaginary and complex numbers. The ratio of *E'/E"* is defined as tan δ or damping [Menard 1999]. Typical dynamic profiles of the *E'* and *E"* variation as a function of temperature are illustrated in Figure 2.1.

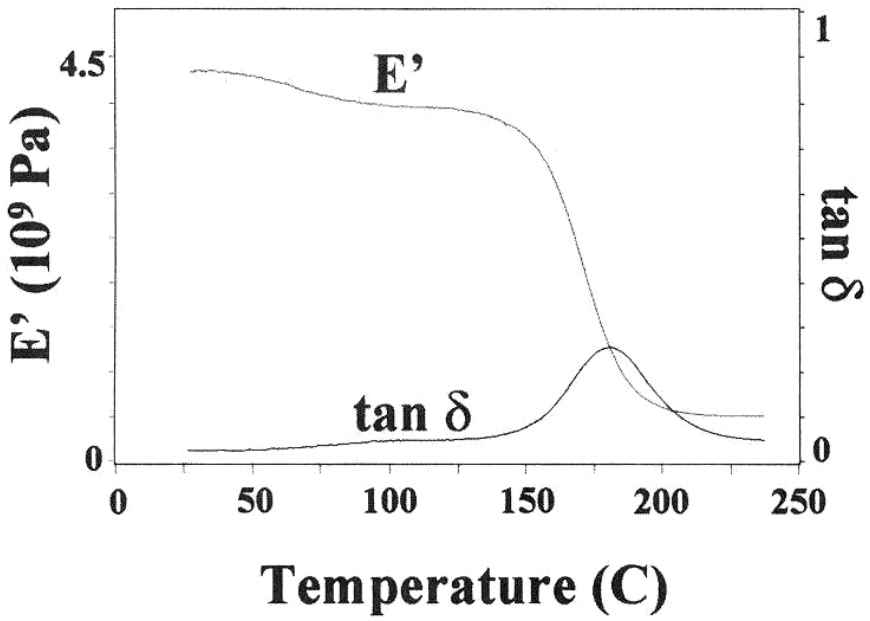

Figure 2.1: Sample DMA temperature scan of E' and tan δ from [Menard 1999]

From the *E'* curve, a transition is observed at approximately 175°C from the change (inflection) in the storage modulus. The peak in the tan δ curve locates where the greatest damping would occur, which is found to be close to the *E'* inflection. Transitions represent points at which the material behaviour has changed dramatically. This first transition, T_α, is known as the glass transition temperature T_g. Counting backwards, the secondary transition is T_β. The beta transition is often associated with side chain movements, related to toughness of a polymer [Menard 1999]. An ideal operating range of a polymer may be between that of the T_g and T_β, where the material possesses the stiffness to resist deformation, yet also maintains the flexibility to not shatter under strain. The use of subsequent methods as described below do not have the same sensitivity as the DMA for detecting secondary transitions such as T_β. Common methods of reporting the glass temperature include the use of *E"* [Seyler 1994] and tan δ peak values, which are comparable to the midpoint technique in a DSC enthalpy graph [Ferrillo and Achorn 1997].

2.2 (MODULATED) DIFFERENTIAL SCANNING CALORIMETRY

Calorimetry, the measurement of heat absorbed or evolved due to chemical reaction or state change, can be used to monitor the heat transfer, or enthalpy change, within a polymer. The glass temperature, T_g, is usually taken as a characteristic point on a plot of a property, such as

enthalpy, H, or of its temperature derivative, such as heat capacity, C_p (= dH/dT). A typical DSC trace in Figure 2.2 illustrates the enthalpy response and its temperature derivative, heat capacity versus temperature.

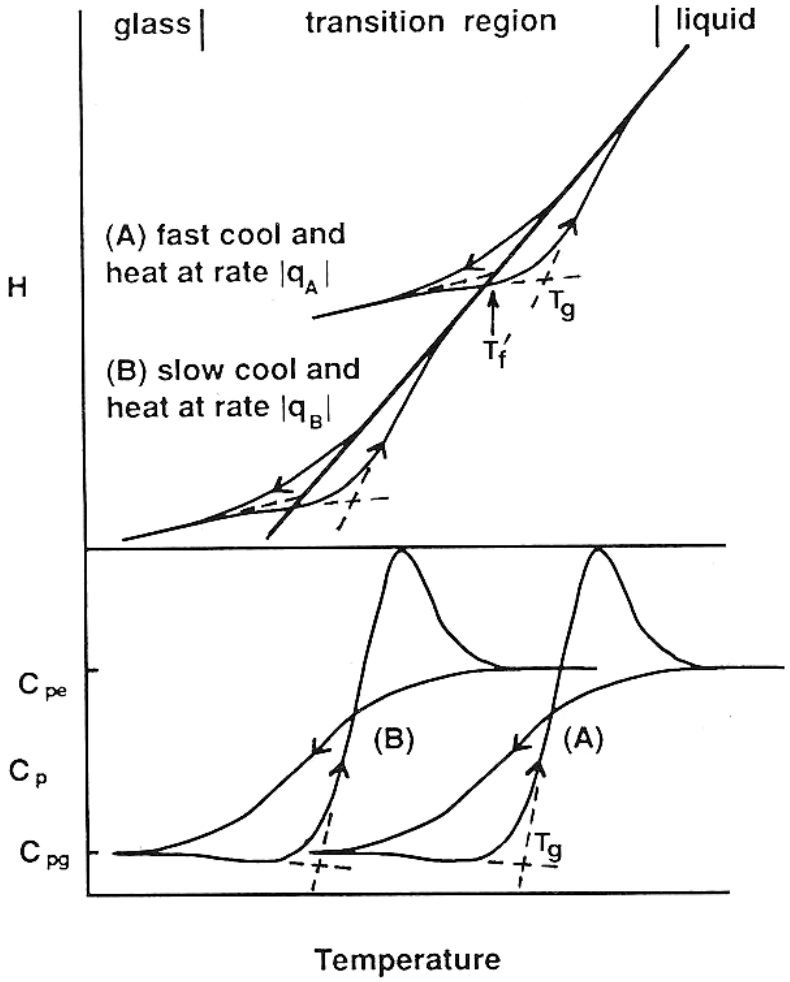

Figure 2.2: Schematic plot of enthalpy, H, and heat capacity, C_p, during cooling and reheating through the glass transition region at two different rates [Moynihan *et al.* 1974]

The enthalpy response to temperature in Figure 2.2 indicates that as the material is cooled from above the glass temperature, the liquid approaches a temperature below the glass temperature and deviates from equilibrium. It is expected that the slower the cooling rate, the better it is able to follow the equilibrium line, and thus at faster cooling rates from above T_g, departure from equilibrium is expected sooner (e.g. at higher temperatures). The fictive temperature for case (A) is comparably close to its T_g, and notably greater than that of case (B), which is also comparably close to its respective T_g.

It can be seen that in the characterization of a material, several parameters are especially important. These parameters occur in three steps of a thermal characterization cycle in which physical aging is part of. The first step of the thermal cycle involves the cooling rate, q_1, used to approach the aging temperature, T_a. Second is the physical aging process that recovers ΔH_a enthalpy, and lastly, the heating rate, q_2, to reach above glass temperature where it is again in equilibrium. This final heating step will produce an observable endothermic peak at the glass transition region. The temperature at which this endothermic peak occurs is dependent on the recovered enthalpy, and thus is affected by the aging temperature, T_a, and time, t_a.

If temperature modulation is applied during differntial scanning calorimetry (MDSC), the heat flow signals can be separated into

$$\frac{dH}{dt} = C_p \frac{dT}{dt} + f(T,t) \qquad \textbf{(27)}$$

where $\frac{dH}{dt}$ is the total heat flow rate due to the underlying linear heating rate, and is equivalent to the standard DSC heat flow obtained at the same overall heating rate. This total heat flow can be separated into a heat capacity and melting component, $C_p \frac{dT}{dt}$, and a kinetic or time-dependent component, $f(T,t)$. The heat capacity component, found as the response to the modulated heating rate, is known as the reversing heat flow signal, and the kinetic component is taken as the difference from the total heat flow and heat capacity component, and is termed the non-reversing heat flow signal. These mathematical expressions for the MDSC technique have been published elsewhere [Thomas TP006]. It was thought that the benefit of this technique is that since enthalpic recovery is a kinetic process, it occurs entirely in the non-reversing heat flow signal. Therefore, it is convenient to isolate and integrate the peak in this signal to measure differences in energy content due to aging. This advantage of using the MDSC technique allows one to associate the enthalpy relaxation of a sample simply by determining the area under the non-reversing heat flow curve, but discussions elsewhere [Hutchinson *et al.* 1999; Simon and McKenna 2000; Simon 2001; Simon and McKenna 2002] have indicated this to be an unreliable method of obtaining the enthalpy relaxation. Due to this, the conventional method of evaluating the difference in areas of the total heat capacity of aged and unaged samples are still used for this

evaluation. The heat capacity is used for quantitative analysis of enthalpy and endothermic peak temperatures, while the reversing heat flow component is employed for qualitative comparisons.

2.3 FOURIER TRANSFORM INFRARED SPECTROSCOPY

Infrared spectroscopy is an analytical technique measuring electromagnetic radiation intensity. It is often used for analysis or identification of substances (organic or inorganic) and to quantify components of an unknown mixture. Infrared spectroscopy is widely used in many different applications because any sample of matter, regardless of solid, liquid or gaseous state, can be measured by infrared spectroscopy. Furthermore, the required amount of a sample to be analyzed is small.

The electromagnetic spectrum covers a large range of wavelengths, from gamma rays to radio waves. The infrared range occupies a small portion of this spectrum and can be classified as *near*, *mid* or *far* infrared, named for their relation to the visible spectrum. Below is an approximation of the ranges of the infrared classification [Alpert *et al.* 1970]:

Infrared	Wavenumber (cm^{-1})	Wavelength (μm)
Near	~ 10,000 to 5,000	~ 1 to 2
Mid	~ 5,000 to 200	~ 2 to 50
Far	~ 200 to 10	~ 50 to 1000

Table 2.1: Infrared rays range

When a sample of matter is exposed to radiation, certain frequencies are absorbed by the material leading to molecular vibrations. Infrared spectroscopy works because it detects the vibration from the matter as the chemical bonds stretch, contract and/or bend. Shown below in Figure 2.3 are common molecular vibration modes induced by infrared radiation [Coleman 1993]:

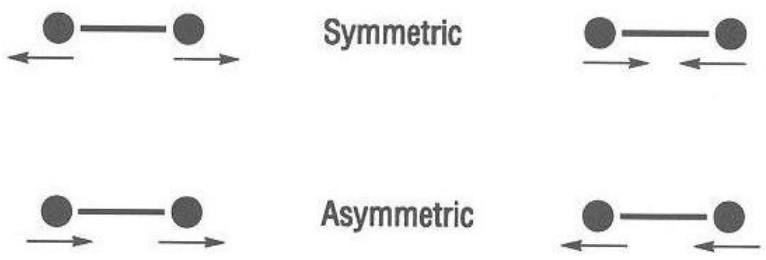

(a) Stretching

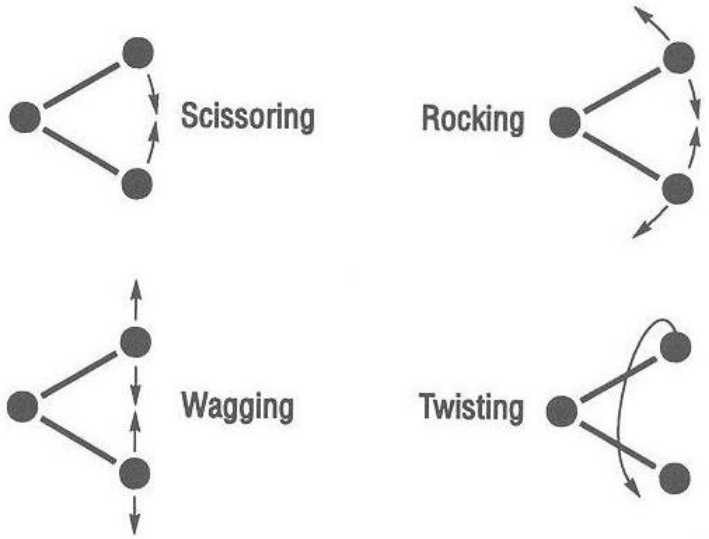

(b) bending

Figure 2.3: Infrared Activated Molecular Vibrational Modes

These chemical bonds have specific frequencies at which they vibrate, corresponding to energy levels. Another reason for the popularity of this technique is due to the fact that the frequencies at which radiation is absorbed are unique and characteristic for different molecules and chemical functional groups, and as a result, infrared radiation is absorbed in a specific wavelength range, which is like the *fingerprint* of the compound.

2.3.1 Apparatus and Theory

A typical infrared spectroscopy apparatus consists of a beam of infrared light produced at a source and then split into two separate beams by a beam splitter, or *interferometer*. One beam is aimed towards a stationary mirror, *F*, and the other to a moving mirror, *M*, as depicted in the

commonly used Michelson interferometer in Figure 2.4. The moving mirror travels uniformly from a starting position to a terminal position, and then returns back to the starting position again to complete a scan [Ning 2002]. As the two beams are then reflected back and recombined at the beam splitter, a portion of the light is passed toward the sample and the remaining towards the radiation source, which in turn reflects the rays back towards the beam splitter [Stuart 2004].

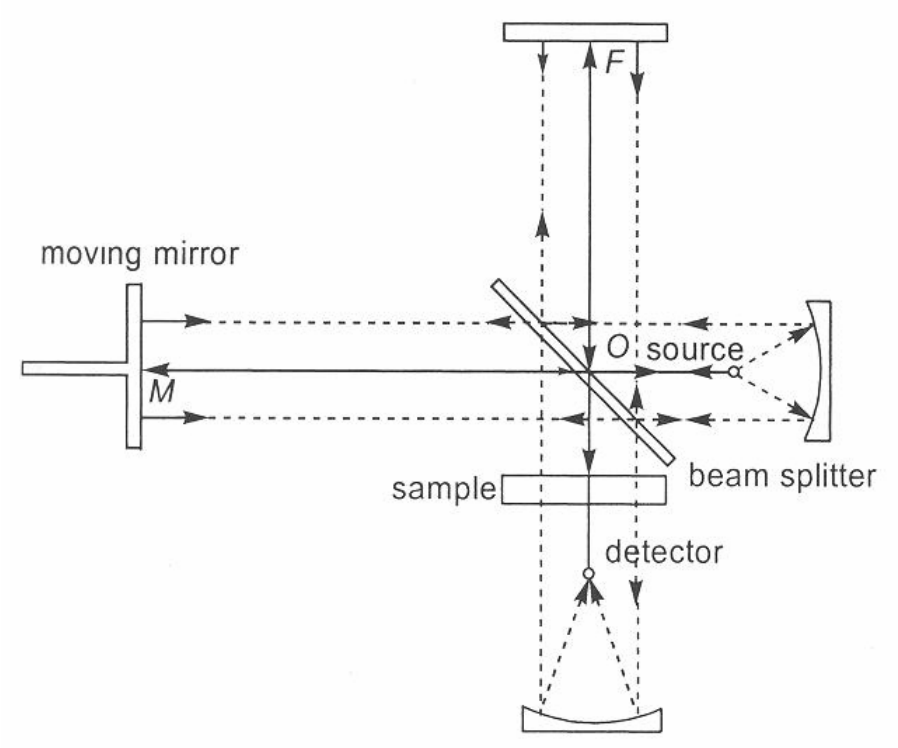

Figure 2.4: Schematic diagram of Michelson interferometer [Ning 2002]

Since the two rays travel different distances, their recombined signal is a result of the "interfering" with each other, thus, resulting in an encoded signal. The two rays have regular variable optical path differences, or optical retardation, when recombined. In one extreme case, the two rays are in-phase (zero optical retardation) which leads to constructive interference. At the other extreme when the two rays are out-of-phase, this leads to destructive interference. Figure 2.5 below shows three discrete frequencies (dashed curves) that combine to produce the solid curve.

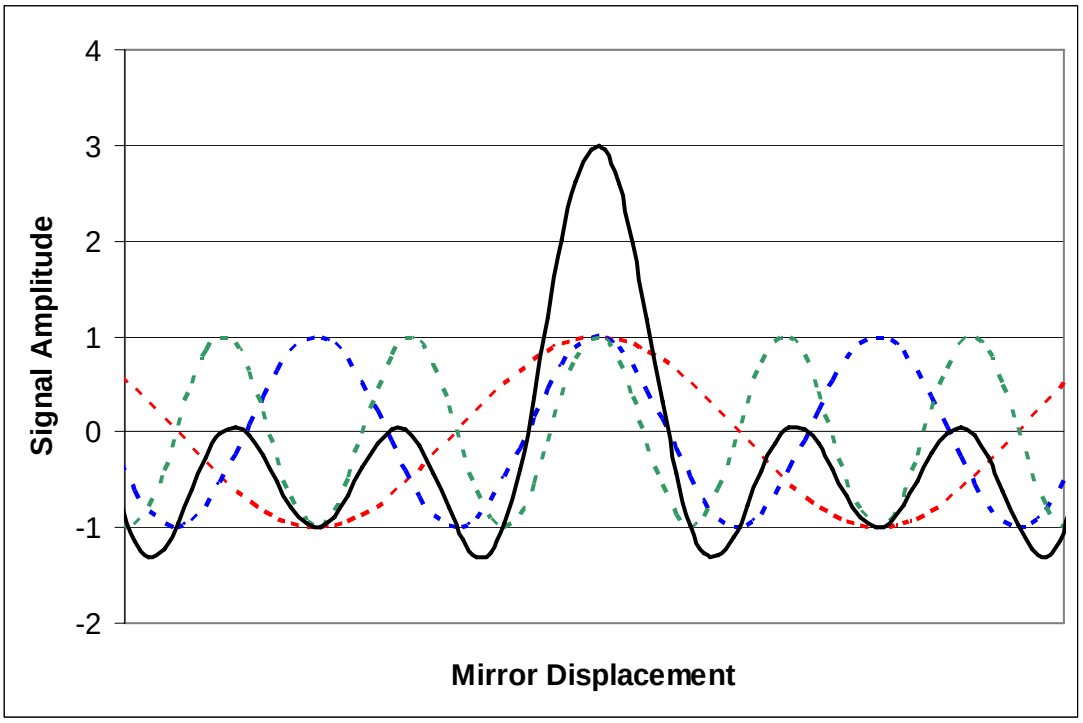

Figure 2.5: Interference due to optical retardation

When the signal is transmitted through (or reflected off of) the sample surface (as will be further discussed), specific frequencies of energy are absorbed, causing the vibration of functional groups. The infrared signal after the interaction with the sample is unique to the material and is then measured by the detector as a function of mirror position to obtain the *interferogram*. By utilizing the Fourier transform theorem, any mathematical function can be expressed as a sum of sinusoidal waves.

The detected signal can then be decoded by performing the Fourier transform to present an infrared spectrum, which plots transmittance (or absorbance) versus wavelength (or wavenumber).

2.3.2 Measuring and Analysis

Calibration is necessary to ensure that the bands are observed at their proper frequencies or wavelengths [Silverstein *et al.* 1991]. This requires a standard material with band features that do not change appreciably as a function of resolution. Calibrations can be performed on polystyrene film as it possesses reasonably sharp bands and are very reproducible from different sources

[Choquette *et al.* 2002]. The characteristic wavelength band observed for this calibration occurs at 1601 cm^{-1}.

In an absorption spectrum, the intensity of the transmitted (or reflected) light through the sample and anything that the infrared beam passes through is what is ultimately measured. The effect of the atmosphere on the resulting data is important since carbon dioxide and water vapour absorbs infrared radiation [Alpert *et al.* 1970]. To eliminate the characteristic absorption bands of anything unrelated to the actual sample, a background scan is completed and subtracted (or normalized) from the sample's spectrum. The difference in the spectrum of the reference background to the actual sample will only be characteristic of the sample. This removes any atmospheric absorption bands within the cell's environment from the raw spectrum data. Consequently, a transmittance spectrum is obtained as

$$T = I / I_o \tag{28}$$

where T is the percent transmittance and I is the intensity measured with a sample in the beam, and I_o is the intensity measured from the background spectrum [Alpert *et al.* 1970]. The absorbance spectrum, A, is related to the transmittance spectrum by

$$A = -log_{10} T \tag{29}$$

For a reference background, a clean crystal window or an open beam air background may be typically used.

2.3.3 Modes of Measurement

The classical method of infrared detection is the transmission of radiation *through* the specimen [Garton 1992], as was depicted in Figure 2.4. Films are commonly used for this technique since the infrared beam can easily pass through the sample. However, if specimens are thick, opaque, or highly reflective, reflection spectroscopy would be more suitable [Garton 1992]. Reflective techniques include, but are not limited to, specular reflectance, attenuated total reflectance (or also known as internal reflectance) and diffuse reflectance.

Attenuated total reflectance (ATR) is a technique used for analyzing the surfaces of materials. This method works well for samples that are too thick or opaque for transmission or reflective spectroscopy, respectively. The sample in this technique is placed in contact with a crystal of high refractive index, commonly ZnSe or Ge [Stuart 2004]. The infared radiation enters the crystal from one end such that reflections occur internally within the crystal, while the number of reflections will depend on the crystal length and thickness and the interface angle, and exits from the other as it is directed back into the normal beam path of the spectrometer. A schematic is illustrated below in Figure 2.6.

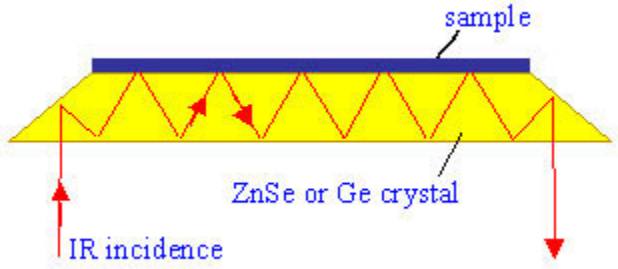

Figure 2.6: Schematic diagram of an ATR setup [Nuance 2006]

With each reflection, the light beam penetrates the sample to a depth of a few microns and is absorbed at the characteristic absorption bands. The intensity also decreases exponentially with reflections. It should be noted that to obtain internal reflectance, the angle of incidence must exceed the critical angle of the crystal. Liquids, and pliable solids, such as rubbers or plastics, are suitable for use with ATR spectroscopy, and the methodology for sample preparation has been discussed above.

2.3.4 Applications and Limitations

The widespread use of infrared spectroscopy has found its way into the analysis and characterization of polymers, amongst many other fields. Infrared spectra of polymers give insight at the molecular level in regards to the orientation of polymer chains. Polymer materials are often moulded and as such are often glossy and smooth. ATR is a method suitable for use with opaque smooth samples of polymer.

Infrared spectroscopy can be used as a tool to characterize miscibility, the premise being that miscibility with a second polymer will perturb the local environment and cause changes and/or shifts in intensity of the absorption bands [Garton 1992]. The way in which the infrared spectrum is disturbed may be informative of the molecular environment, and in particular, the presence of specific interactions, such as the forming or breaking of bond groups (hydroxyl, carbonyl, hydrogen bonding etc.). However, it is important to note that only qualitative conclusions can be drawn from these infrared spectra, since the perturbation of the infrared spectrum is a qualitative criterion of miscibility and a description of the general nature of the interactions between blend components.

Similarly, moisture absorption or hygrothermal conditioning can cause significant changes in spectra. It is customary to compare the difference between the spectrum of a blend (or a blend subjected to certain conditioning) and the weight sum of the spectra of the pure polymers. These changes in the spectrum can easily be made clear by spectral subtraction (or normalization). [Garton 1992]

Despite the many uses and advances in FTIR and infrared spectroscopy in general, there are limitations for each. A general limitation of infrared spectroscopy is that it cannot measure the exact amount of an element in a substance. Also, it is unable to detect single atoms (such as noble gases) and monoatomic ions since they do not produce vibrational motion as they are single entities that contain no chemical bonds and therefore do not possess the vibrational motion needed to absorb infrared radiation. Lastly, noble gases such as helium and argon, and diatomic molecules such as N_2 and O_2 are undetectable. [Alpert *et al.* 1970]

Also, this technique imposes limitations when applied to transient experimental systems. The reason for this is inherent to the method of acquiring the interferogram. As the moving mirror is translating, the interferogram signal is being collected and the continuous optical retardation produces the detected signal modulation. As such, the frequency is then a function of mirror velocity and wavelength of the IR beam. This requires the use of a static sample, which contradicts the initial purpose of the experiment being transient.

Chapter 3 EXPERIMENTAL DETAILS

3.1 MATERIAL AND SPECIMENS

The resin used for this study is a 75:25 PC/ABS blend commercially known as Cycoloy C6600 produced by GE Plastics. The glass transition temperature of the blend was first measured using dynamic mechanical analysis (DMA). The DMA sample consists of a rectangular bar having dimensions 27.0 mm x 12.3 mm x 1.52 mm cut from a flat surface on electronic device housings as-moulded from the provided resin. The extrusion barrel is set to 260°C while the mould temperature is maintained at 80°C, during which the material is injection moulded with a packing pressure of 1160 kg/cm^2. A piece of resin between 10 – 12 mg is encapsulated within aluminum hermatic pans for (M)DSC experiments. All aging was performed in a VWR Signature 1430M vacuum oven. Sheets of the same material were also moulded with conditions similar to the above, and test samples cut in the form of a bar with nominal dimensions of 76.2 mm (3 in.) by 25.4 mm (1 in.) by the thickness of the sheet, 2.84 mm (0.11 in.). These samples were used according to ASTM standard [D570] for experimentation purposes.

3.2 APPARATUS

3.2.1 DMA and Test Parameters

Dynamic mechanical analysis (DMA) was performed on a TA Instruments DMA Model 2980. The sample bar was mounted onto a single cantilever mode clamp and oscillated at 1 Hz frequency and at a heating rate of 1°C/min.

3.2.2 (M)DSC and Test Parameters

All (M)DSC tests were performed on a TA Instruments DSC Model 2920. The Refrigeration Cooling System attached to the DSC provided adequate cooling for the cooling rate studies performed. Baseline calibrations were also performed daily. Indium is used to perform the temperature and heat flow rate calibration, while sapphire is used for the heat capacity calibration. The indium calibration is performed to ensure a proper melting point value of 156.6°C [ASTM

E967-83; ASTM E968-83] and the standard heat of fusion of 28.7 J/g [ASTM E968-83] is used to obtain the cell constant. The results of the heat capacity calibration are compared to the reported sapphire specific heat capacity [ASTM E1269-01] for the temperature range of interest for this study. Modulation parameters for MDSC were selected based on recommendations from TA Instruments technical reports [Thomas TP008; Thomas TP010] and further refined. All MDSC experiments were conducted with an oscillation amplitude of 1°C, period of 70 seconds and an underlying heating rate of 1°C/min.

3.2.3 FTIR and Test Parameters

A Bruker Optics Tensor27 FTIR attached to a Hyperion microscope with an ATR-II 20X objective was used to obtain infrared spectrum. The objective consisted of a germanium tip, approximately 100 μm in diameter. FTIR data were averaged over 100 scans, obtained at a resolution of 4 cm^{-1}.

3.2.4 Other Equipment

An analytical balance capable of reading 0.0001 g is used to record the mass of prepared specimens. A VWR Signature 1430M vacuum oven is used to maintain uniform temperatures for specimens conditioned at 8 hours of aging or more.

3.3 DATA ANALYSIS OF AGING AND MOISTURE ABSORPTION

3.3.1 Determination of Enthalpy Loss

The term physical aging is known as the process by which a material is allowed to evolve toward equilibrium isothermally without the influence of external conditions [Hutchinson 1995]. Excess enthalpy due to non-equilibrium cooling, is lost during aging, in which the material is relaxing or recovering towards equilibrium. It is common for aging effects to be investigated approximately 20°C below T_g, as the aging rate is generally most prominent in this region [Hodge 1987; Hutchinson *et al.* 1999; Guest and Van Daele 1995].

Since structural recover is completely reversible, all experimental characterization of physical aging must begin by the erasing of the sample thermal history. This is done by heating up the sample and isothermally holding at 130°C for 5 minutes. After erasing the thermal history, it is then cooled to the aging temperature, T_a. The enthalpy loss on aging, ΔH_a, is found simply from the difference in the area under the heat flow signals of a DSC scan, and in the case of MDSC, the non-reversing heat flow signal, for the aged and reference scan, where the reference will herein for the rest of the paper refer to the scan of the thermally erased sample. The integral is to be performed between the aging temperature, T_a, and a temperature, T_c, above the glass temperature at which both attain equilibrium.

$$\Delta H_a = \int_{T_a}^{T_c} \left(C_p\right)_{aged} dT - \int_{T_a}^{T_c} \left(C_p\right)_{ref} dT \tag{30}$$

3.3.2 Determination of Fictive Temperature

The fictive temperature, T_f, can be determined from the equal area method, as mentioned above. Since T_f will vary depending on the rate of cooling, reheating, thermal aging time or temperature or any parameter that affects the previous thermal history of the polymer, this parameter is used to describe a structural state. As such, T_f is an appropriate temperature at which to evaluate ΔC_p. In this work, the fictive temperature will be used to compare the material's structural state and wherever necessary, the glass transition temperature will be analyzed for completeness.

The equal area technique in determining the fictive temperature was implemented through a MatLAB program written to consistently determine the fictive temperature, and an example of it is illustrated in Figure 3.1.

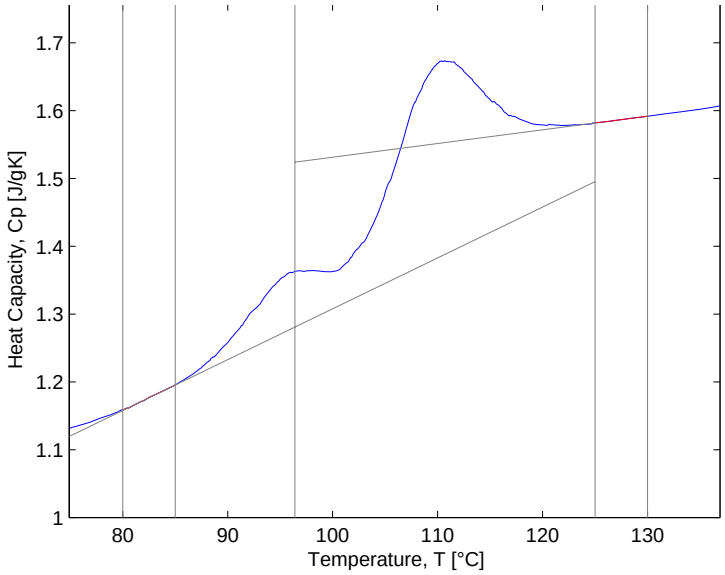

Figure 3.1: Equal area method by MatLAB used to determine T_f

By determining the fictive temperature, it is also possible to evaluate the apparent activation energy for enthalpy relaxation, Δh^*. From the relation in equation (31), it can be seen that Δh^* can be found from the slope of a plot of ln $|q_1|$ against $\frac{1}{T_f}$ which requires a varying range of cooling rates.

$$\frac{d\left(\ln\left|q_1\right|\right)}{d\left(\frac{1}{T_f}\right)} = -\frac{\Delta h^*}{R} \tag{31}$$

Although the analysis presented thus far has been entirely given in the perspective of enthalpy or calorimetric studies, a correlation between volume or dilatometric work is always appropriate. As previously mentioned, enthalpy and volume relaxation are similar, but of different time scale. Thus, a comparison of enthalpy and volume relaxation is not possible as there is no direct correlation between the two [Hutchinson 1995]. The main problem of such a comparison is that $\Delta\alpha$, for volume relaxation, and ΔC_p, for enthalpy relaxation, are not fully comparable quantities. It has been proposed [Málek J and Shanelova 2000; Málek 1998; Málek and Montserrat 1998] that the fictive relaxation rate, R_f, can be a useful comparison of the relaxation rate as measured by either volume or enthalpy. Such a rate is defined as a function of the fictive temperature, which can be determined in either an enthalpic or volumetric study, and is shown below

$$R_f = -\frac{d\Delta T_f}{d\log t} \tag{32}$$

3.3.3 Investigation of Infrared Spectrum

The molecular structure of the mer groups of the constituent materials were illustrated in Figure 1.7 and Figure 1.8. Characteristic of PC is the carbonate linkage (or the carbonyl functional group, C=O). The infrared absorption band for the carbonyl group occurs near 1770 cm^{-1}, but with contributions from *trans-trans* (*t-t*) conformers at 1767 cm^{-1} and *trans-cis* (*t-c*) at 1785 cm^{-1} [Heymans 1997]. The terms *trans-trans* and *trans-cis* refer to the conformation of the carbonate linkage. The stretching of the C–O bond occurs around 1150 to 1250 cm^{-1}. The stretching of the C–C bond in the phenyl group (benzene ring) is found at approximately 1600 cm^{-1} with contributions of *t-t* and *t-c* conformers at 1594 and 1604 cm^{-1}, respectively [Heymans 1997]. Characteristic of polyacrylonitrile is the C≡N bond which is seen approximately at 2250 cm^{-1} and for polybutadiene, the C=C bond occurs at 960 cm^{-1}. The presence of polystyrene is noted by the phenyl group, which exists also in PC. These noted wave numbers characteristic of the components of the polymer blend are investigated in this study.

3.4 EXPERIMENTAL PROCEDURE

3.4.1 Controlled Cooling Rate Study

Cooling rate studies were performed to determine the apparent activation energy, Δh^*, in equation (31). The study was performed in standard DSC mode using a single specimen to minimize the effects of variability in the sample. For this study, nominal cooling rates of q_1 = 0.5, 1.0, 2.5, 5.0, 10.0, 15.0 and 20°C/min were used to cool from above the glass transition temperature to the aging temperature, T_a. In total, ten conditions were studied: no aging as a reference and aging at T_a = 80, 90 and 100°C for three aging times, t_a = 1, 12 and 24 hour(s). After each aging condition, the sample is further cooled to room temperature, before subsequently reheated at a rate of q_2 = 10°C/min to above the glass transition temperature. Data was collected from both the equilibrium cooling (q_1) and re-heating scans (q_2), used for the fictive temperatures to obtain Δh^*.

3.4.2 Enthalpic Relaxation Study

The endothermic overshoot seen in DSC heat-up scans is not only dependent on the prior cooling and heating history, but also heavily dependent on the physical aging treatment. The location as well as the size of the endothermic peak is analyzed and discussed quantitatively as well as qualitatively through the heat flow graphs obtained from MDSC mode. The temperature at which the peak of the endotherm occurs, T_p, is a function of three experimental parameters, q_1, ΔH_a and q_2. A similar procedure as outlined in the *Cooling Rate Study* is used: controlled cooling (q_1) from above the glass transition to the aging temperature, aging for a specified time, controlled cooling at q_1 to room temperature, and finally, reheating (q_2) to above the glass transition temperature. Since the objective of this study is to characterize aging affects by studying the peak endotherm, the cooling (and heating rate) were held constant and identical, $q_1 = q_2 =$ 10°C/min. Generally, enthalpy recovery is dictated by the aging temperature, T_a, and aging time, t_a . In this work, all samples were aged in an oven at only one aging temperature, $T_a = 80$°C , which is the practical service temperature limit for the material. For each aging time, $t_a = 0.5$, 2, 8, 96, 336 and 1008 hours, there were 4 replicates, and for each replicate the aged and the reference (unaged) scan with thermal history erased were recorded. For samples that are aged for longer than 8 hours, aging was performed in an oven and then transferred to the DSC in a metal cylindrical container maintained at the same aging temperature.

The bar samples that were cut to ASTM standard for moisture studies were also used for the investigation of the relaxation process by FTIR. These specimens were conditioned prior to moisture absorption and physical aging, respectively, in order for all testing to start at the same reference point. First, moisture was eliminated from the specimens and kept dry by storing in a desiccator for 48 hours. They were then placed into an oven at 135°C for 10 minutes which maintained a dry atmosphere while erasing any previous thermal history. They were then stood on end in grooves machined into an aluminum block such that both surfaces of the sample were equally exposed to the environment. FTIR spectra were obtained on these samples immediately after the thermal history was erased, after 1, 3, 7 and 10 days, and then once every week thereafter for a total of approximately 80 days. The results were replicated twice, and these samples that are removed from the oven for FTIR were not reused. Hence, there were twice as many samples placed into the oven as there were scheduled days.

3.4.3 Hygrothermal Study

Moisture absorption samples were conditioned prior to hygrothermal studies as they were prepared above for FTIR. The specimens were then stored under 3 different hygrothermal conditions: (i) at room temperature fully immersed in distilled water (ii) in an environmental chamber at 50°C and 93% relative humidity (RH), and lastly (iii) an environmental chamber at 65°C and 50% RH. 50°C and 93% RH is a standard condition used for testing purposes by the industrial partner in this research, while that of 65°C and 50% RH was an arbitrary condition selected with parameters between that of 50°C and 93% RH and thermal aging at 80°C. All samples in the environmental chambers stood on end in grooves machined into an aluminum block such that both surfaces of the sample were equally exposed to their conditioning environment. Samples fully immersed rested on end within a glass container.

ASTM standard [D570-98] is used as a guideline and adapted for the moisture uptake weighing frequency. Samples are initially weighed prior to conditioning, after 1, 3, 7 and 10 days, and then once every week thereafter until the increase in weight indicated by three consecutive readings average less than 1% of the total increase in weight or 5 mg, whichever greater. Each condition was replicated with 3 samples for moisture uptake monitoring. Each time the 3 samples are removed for weighing, two other specimens are also removed from the conditioning environment and an infrared spectrum is obtained of the sample, and then immediately placed back into their respective conditioning environment. Samples removed for the FTIR scan are not reused; hence, there were as many samples used as there were scheduled data collection times, and often extra samples left over.

3.5 STATISTICAL ANALYSIS

Although there is a large volume of published data on DSC analysis of polymers which consist of studies involving replications, there has been very little analysis on the repeatability of the data [Dykeman and Lee-Sullivan 2003]. The replicated data collected from the peak shift study was analyzed using Analysis of Variance (ANOVA) to ascertain the repeatability of the results. Experiments were planned so that sufficient data can be collected and analyzed by statistical

methods. The peak shift study is one with a single factor: aging time, t_a, with six levels of the factor. The analysis of a single-factor with a levels of the factor (or treatments) is suitably analyzed by ANOVA, which is a useful tool for comparing the observed response of the a treatments. This is also known as a one-way ANOVA experiment. It is useful to describe these observations from an experiment with the *means model:*

$$y_{ij} = \mu_i + \varepsilon_{ij} \begin{cases} i = 1, 2, ..., a \\ j = 1, 2, ..., n \end{cases} \tag{33}$$

where y_{ij} is the j^{th} observation (or j^{th} replicate) taken under factor level or treatment i. There will be in general n observations under the i^{th} treatment. μ_i is the mean of the i^{th} treatment and ε_{ij} is the random error that encompasses all sources of error in the experiment. The experiment would then consist of $a \cdot n = N$ total observations [Montgomery 2001].

The term analysis of variance (ANOVA) originates from the partitioning of the total variability into components. The sum of squares, denoted as *SS,* is used as a measure of overall variability in the data. The total sum of squares, SS_T, then is representative of the variability in the entire experimental study:

$$SS_T = \sum_{i=1}^{a} \sum_{j=1}^{n} \left(y_{ij} - y_{..} \right)^2 \tag{34}$$

Dividing by the degrees of freedom, $a \cdot n - 1 = N - 1$, the sample variance of the observations can be obtained [Montgomery 2001]. A more common term, the square root of the sample variance, is the standard deviation, σ.

Since ANOVA is used for a comparison of the observations from an experiment, it is necessary for a formal test investigating the hypothesis of no difference in treatment means, the null hypothesis:

$$H_0 : \mu_1 = \mu_2 = ... = \mu_a \tag{35}$$

If the above null hypothesis is false, then the alternative must be valid, that *any* one pair of the above comparisons are not true. This is often misunderstood as *all* comparisons must be unequal, which does not necessarily have to be the case. However, all comparisons being unequal is *one* of the combinations that would result in the rejection of the null hypothesis. Standard statistical practice tests the null hypothesis at a confidence level of 95%, or statistical significance of less

than 5% (P-value ≤ 0.05), which concludes significant statistical differences. A word of caution for researchers is to recognize the difference between practical and statistical significance. Because two different experimental treatments produce statistically different results does not necessarily mean that they are of practical value or interest [Montgomery 2001]. ANOVA is but a tool for analysis and in the end it is the researcher who must make practical judgements of analyzed data results, and not the statistician.

For more detailed analysis, other statistical techniques can be used in conjunction with ANOVA. While ANOVA can reveal statistically significant experimental data, it is not apparent *which* comparison in the null hypothesis has caused the significance (if there is more than one pair of comparisons). Of further interest may be which specific pair(s) of combinations cause(s) significance. This can be analyzed by a multiple comparisons test that shows the comparison of each possible combination of treatments and reports the P-value for each. Another point of interest may be any trends that occur due to the aging process. It can be determined whether results follow an n^{th} order fit by using a technique called *polynomial contrasts*. More detailed information on polynomial contrasts can be found in reference [Montgomery 2001].

The use of ANOVA implies specific assumptions about the data, and it is important that these assumptions must hold true for the analyzed data in order for the conclusions to be valid. After ANOVA has been performed on the data, the results of the model can be used to verify the assumptions which are (i) independence of observations (ii) normality of observations and (iii) not severely leveraged by outlying observations. All data obtained must be independent of each other, and this can be checked by plotting the residuals of the ANOVA model against the predicted values. There should not be *fanning out* or *fanning in*, but an even spread in the residuals. Figure 3.2(a) below illustrates an example of unacceptable variance, showing residuals fanning out. This point about constant variance is crucial for the application of ANOVA. A desirable normal probability plot is shown in Figure 3.2(b) with data following the diagonal, while, deviations at the ends are tolerable. Lastly, Cook's distance is used to check for outlying points causing misleading conclusions. Points on a Cook's distance plot should lie close in relation to the next highest point on the plot. Outlying points *could* cause severe leveraging of analysis results. Outlying points may or may not cause a change in the overall conclusion

(significance), when comparing the ANOVA results before and after of the removal of the observation. In general, these graphical techniques are for determining whether sample data conform to a hypothesized distribution based on a subjective visual examination [Montgomery 2001].

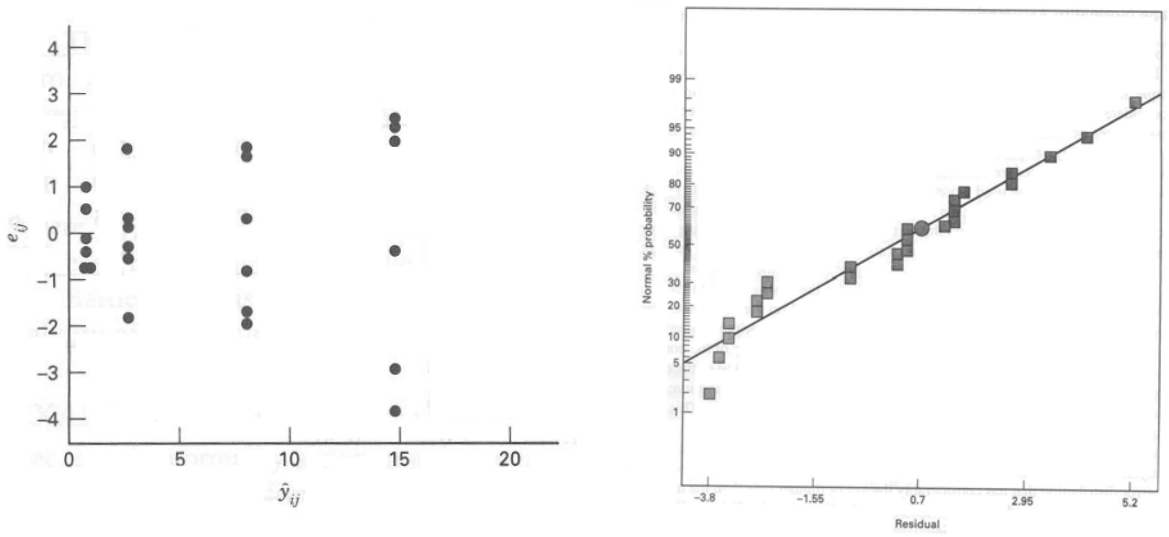

(a) Uneven spread of residuals (fanning out) **(b) Normal probability plot**

Figure 3.2: Example visual examinations of ANOVA assumptions [Montgomery 2001]

If the above techniques yielded unacceptable results in the verification process, then ANOVA is not suitable for use. It is then advisable to either resort to a different analysis technique, or apply a variance-stabilizing transformation to correct the violations of assumptions. The transformation is applied to the observed data and the analysis is performed again on the transformed data [Montgomery 2001]. The transformed data is then verified to meet the above assumptions and thus the analysis of variance applies to the transformed populations.

Chapter 4 RESULTS AND DISCUSSION

4.1 IDENTIFIED GLASS TRANSITIONS

4.1.1 DMA Results

The DMA glass transition temperature can be identified using either the loss modulus, *E*" [Seyler 1994] or the tan δ [Ferrillo and Achorn 1997] peak values. The former has been used in this study on a heat-up scan. According to the DMA profiles shown in Figure 4.1(a), the glass transition peak is apparent at approximately 112°C from the *E*" curve but is accompanied by a small shoulder. Using mathematical software, the peak was mathematically deconvoluted which revealed a second peak occurring near 100°C, Figure 4.1(b). The preliminary results were used in order to determine a range of temperatures for subsequent (M)DSC experiments. The temperature region of interest occurs between 80 to 120°C.

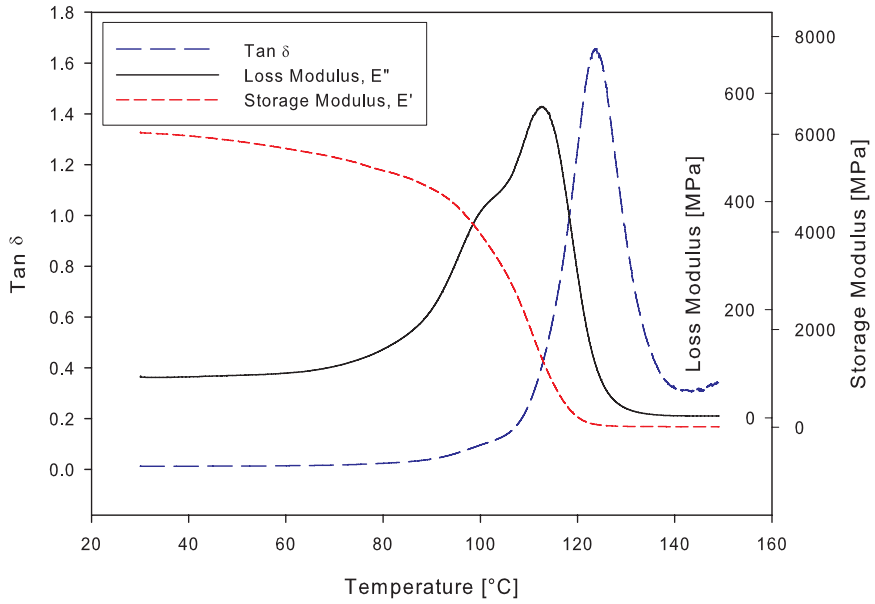

(a) Tan δ, loss and storage modulus obtained by DMA

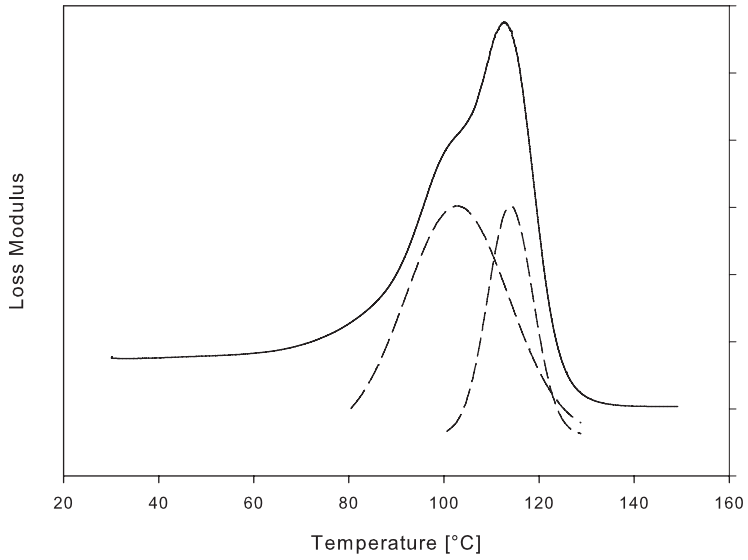

(b) Deconvolution of loss modulus

Figure 4.1: DMA Response of PC/ABS as-received material in single cantilever mode

4.1.2 DSC Results

The heat flow diagram obtained from a DSC heat-up scan of the sample from room temperature to just below 200°C shown in Figure 4.2 indicates the onset of melting to occur around 180°C. The result is reasonably consistent with the temperature region of interest of 80 to 120°C where the step changes are encompassed.

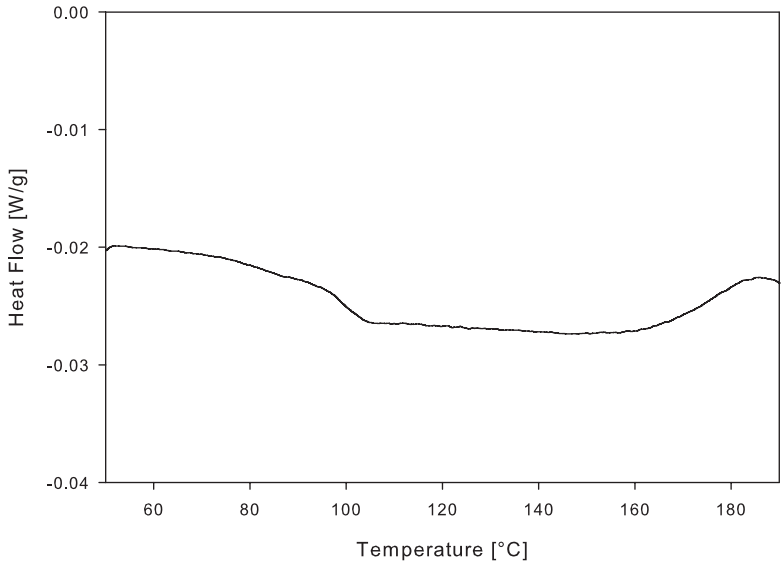

Figure 4.2: DSC Scan of PC/ABS material from room temperature to 200°C

4.2 REPEATABILITY OF DSC TESTS

To ensure that isothermal holding for 5 minutes above the glass transition is sufficient time for equilibrium to be reached and that all thermal history to be removed, samples were held isothermally for 5, 30, and 60 minutes and the heat flows were compared. Figure 4.3 illustrates that the three isothermal hold times produced identical results, thereby validating our technique.

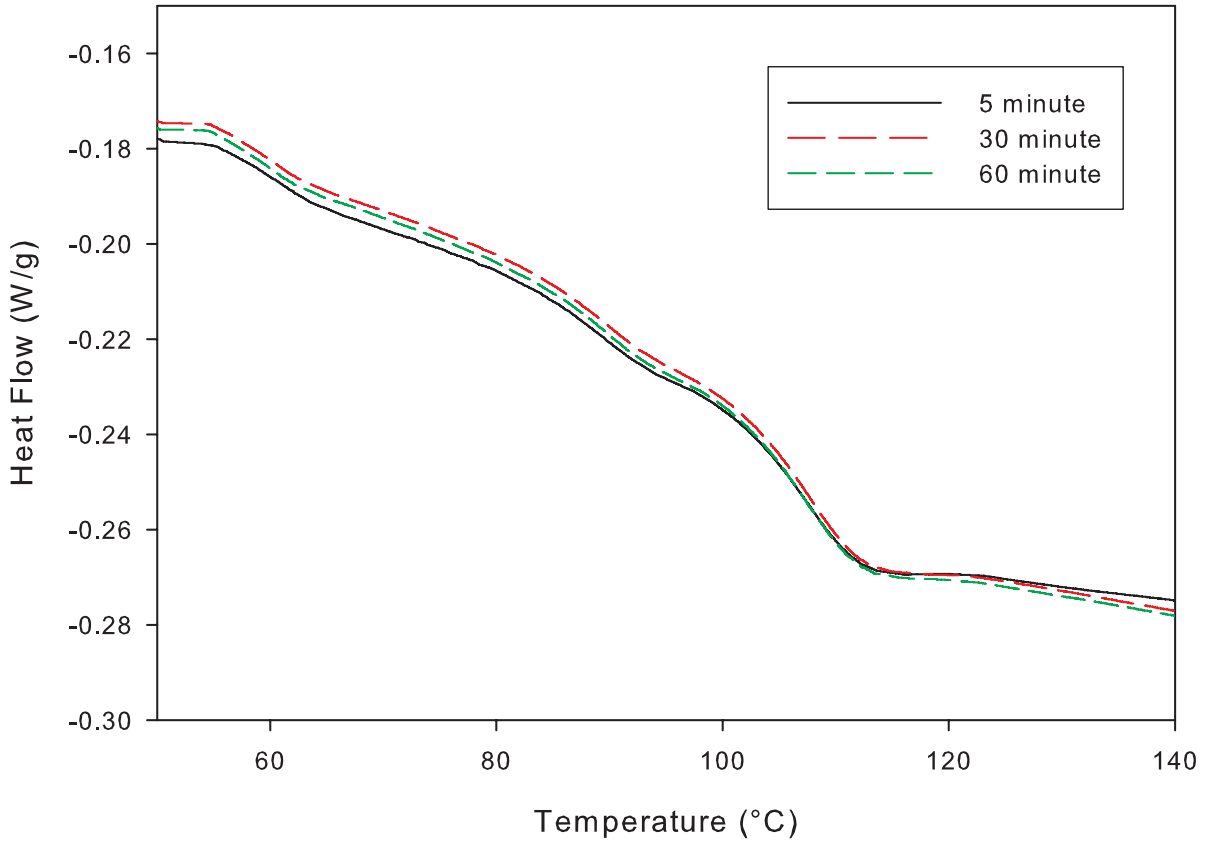

Figure 4.3: Dependence of isothermal hold times above T_g on thermal history removal

4.3 CONTROLLED COOLING RATE ANALYSIS

4.3.1 Reference Sample

The objective of the cooling rate study is to investigate the effects of different cooling rates on the heat flow (or heat capacity) response of the unaged blend. In this first set of samples, the material is not subjected to any physical aging. All heat-up scans after cooling were performed in normal DSC mode for this unaged condition. The results in Figure 4.4 show the effect of

different cooling rates, q_2, on the heat capacities of an *unaged* reference sample, following the same trend as reported in literature [Hutchinson *et al.* 1999; Hutchinson and Kumar 2002] with the size of the endothermic peak inversely proportional to the magnitude of cooling.

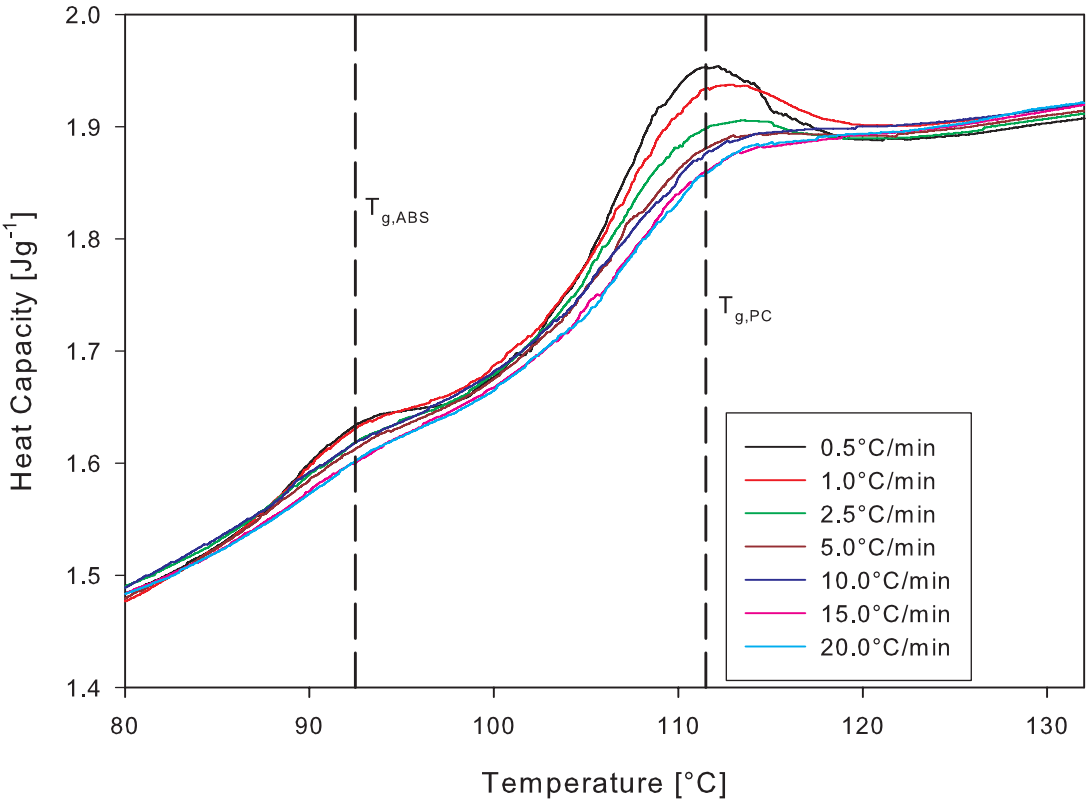

Figure 4.4: Heat capacity at different cooling rates for reference material

The scans reveal two enthalpic peaks – a main one at ~112°C, which is believed to correspond to PC ($T_{g,PC}$), and a much weaker one at ~92°C, which is believed to correspond to ABS ($T_{g,ABS}$). It is noted that the large peak corresponds with the T_g found by DMA (~112°C), but, the shoulder found in the DMA scan is at a higher temperature than the smaller enthalpic peak in the DSC scan. From the work by Ferrillo and Achorn [1997] which compared the glass temperature assignment for DSC and DMA techniques, the values generally agreed to within ± 4°C. In contrast, McKenna and Simon [2002] indicates they could differ by up to 10–15°C. Since the blend is composed of a smaller percentage of the ABS component, the relatively smaller enthalpic peak is reasonable.

From Figure 4.4, ΔC_p for the blend was found by evaluating $C_{pl} - C_{pg}$ at T_f. ΔC_p was determined to be 0.21 ± 0.02 J/gK, which is comparable to values of 0.258 and 0.234 J/gK for polycarbonate [Hutchinson *et al.* 1999; Bauwens-Crowet and Bauwens 1986].

The peak temperature for the reference sample has been plotted as a function of cooling rate in Figure 4.5. In comparing this reference curve (●) for the blend with PC results provided in [Hutchinson *et al.* 1999], the shape of the curve appears to be similar to PC although the initial decrease of the PC curve is steeper than the PC/ABS blend. It is interesting that in both studies, the cooling rate of 2.5°C/min (i.e. log $|q_1|$ = 0.4) is a critical rate at which the trends reverse. Intuitively, slower cooling rates should produce more stable (closer to equilibrium) structures with the peak temperatures remaining fairly constant. The reference curve is plotted along with the aged states at T_a = 80, 90 and 100°C in Figure 4.5 (a), (b) and (c), respectively. It can be seen that in Figure 4.5(c), the shape of the curves have reversed completely to concave-down. From these figures, it is seen that the peak temperature is sensitive to cooling rates even at cooling rates slower than 2.5°C/min except for the poorly aged state, i.e. 80°C at 1 hr. At present, it is not clear what the significance of the blend behaviour changes at 2.5°C/min are.

The fictive temperature determined by the method of equal areas is shown in Figure 4.6. The reference curve is indicated by (●) and it can be seen from the results that the slower the cooling rate, the lower the fictive temperature, which is expected since faster cooling rates will cause an earlier deviation from equilibrium. An earlier deviation while being cooled from above the glass transition will mean the departure occurred at a higher temperature, hence the higher fictive temperature. This is consistent with the concepts proposed by Moynihan *et al.* [1976]. The change in this curve was evaluated to be 1.5°C with the natural logarithm of cooling rate.

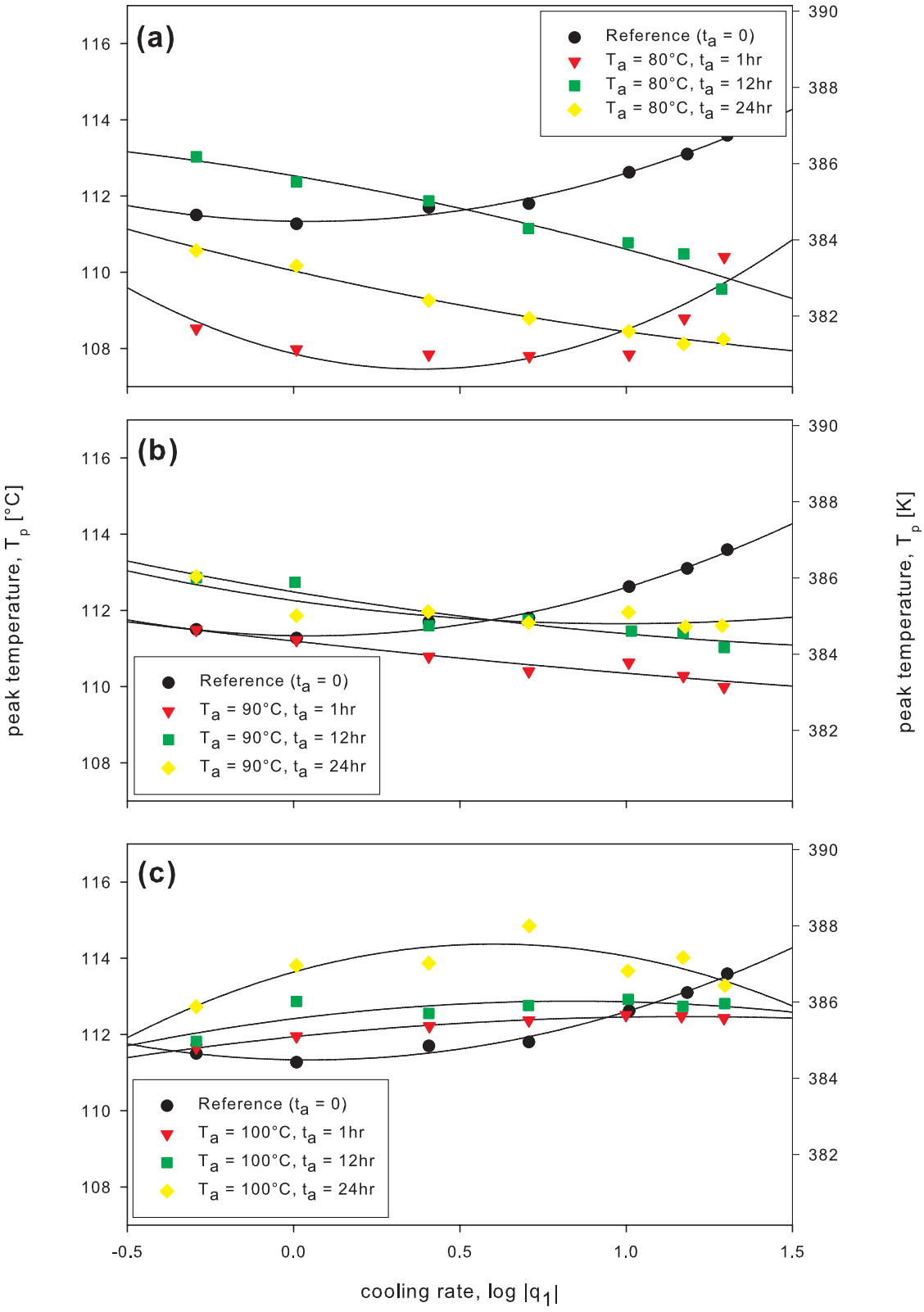

Figure 4.5: Dependence of enthalpic peak temperature on cooling rate for various aged states (a) 80°C, (b) 90°C and (c) 100°C

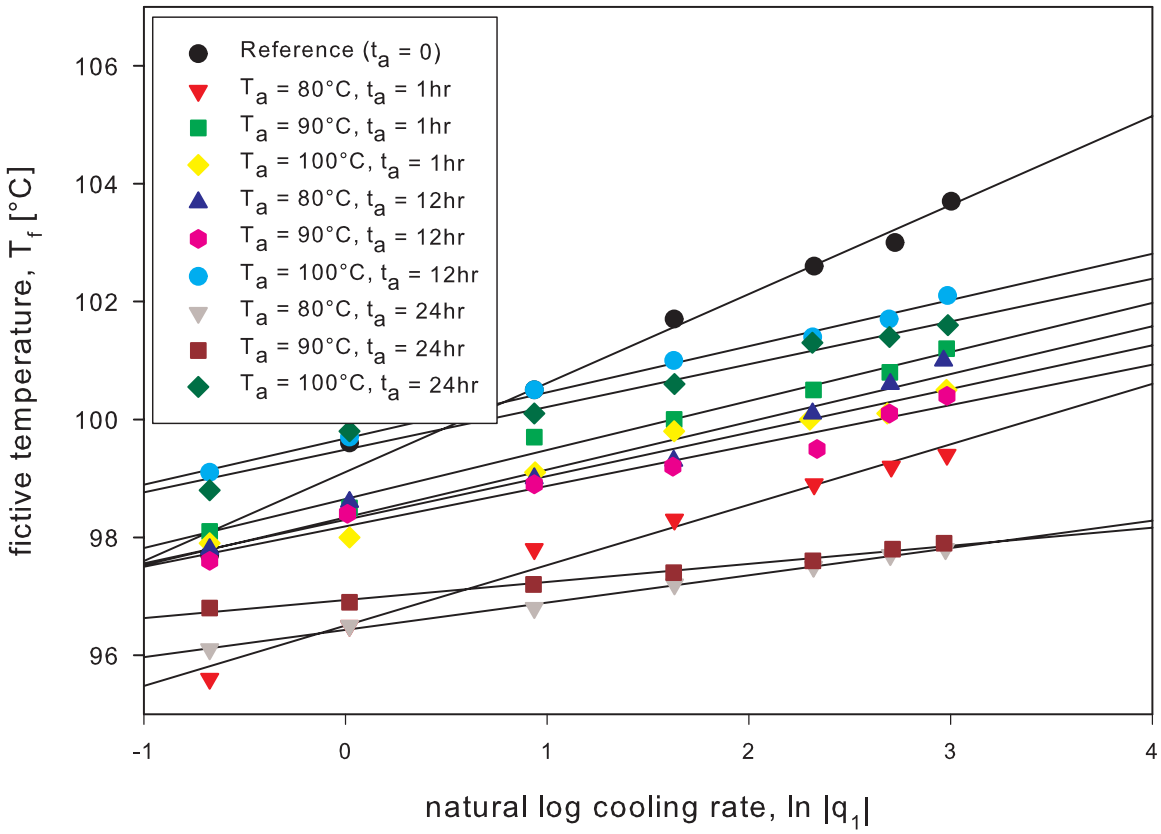

Figure 4.6: Dependence of fictive temperature on cooling rate at various aged states

The apparent activation energy for enthalpy relaxation was also evaluated using the fictive temperature of the unaged sample and plotted in Figure 4.7. Using equation (31), it was found to be $\Delta h^* = 757$ kJ/mol ($\Delta h^*/R = 91$ kK) for this specific blend of PC/ABS material. In comparison, typical values for unaged PC reported in the literature include 1160 kJ/mol [Hutchinson *et al.* 1999], 1130 and 1310 kJ/mol for different molecular mass polycarbonates [Lee-Sullivan and Bettle 2005]. For polystyrene (majority of ABS), the typical value found in literature was in the 500 kJ/mol range [Hutchinson and Ruddy 1988; Avramov 2000; Hodge 1987]. It appears that the PC/ABS activation energy determined here does indeed lie between that of its component materials, but does not necessarily follow a simple *rule-of-mixtures*.

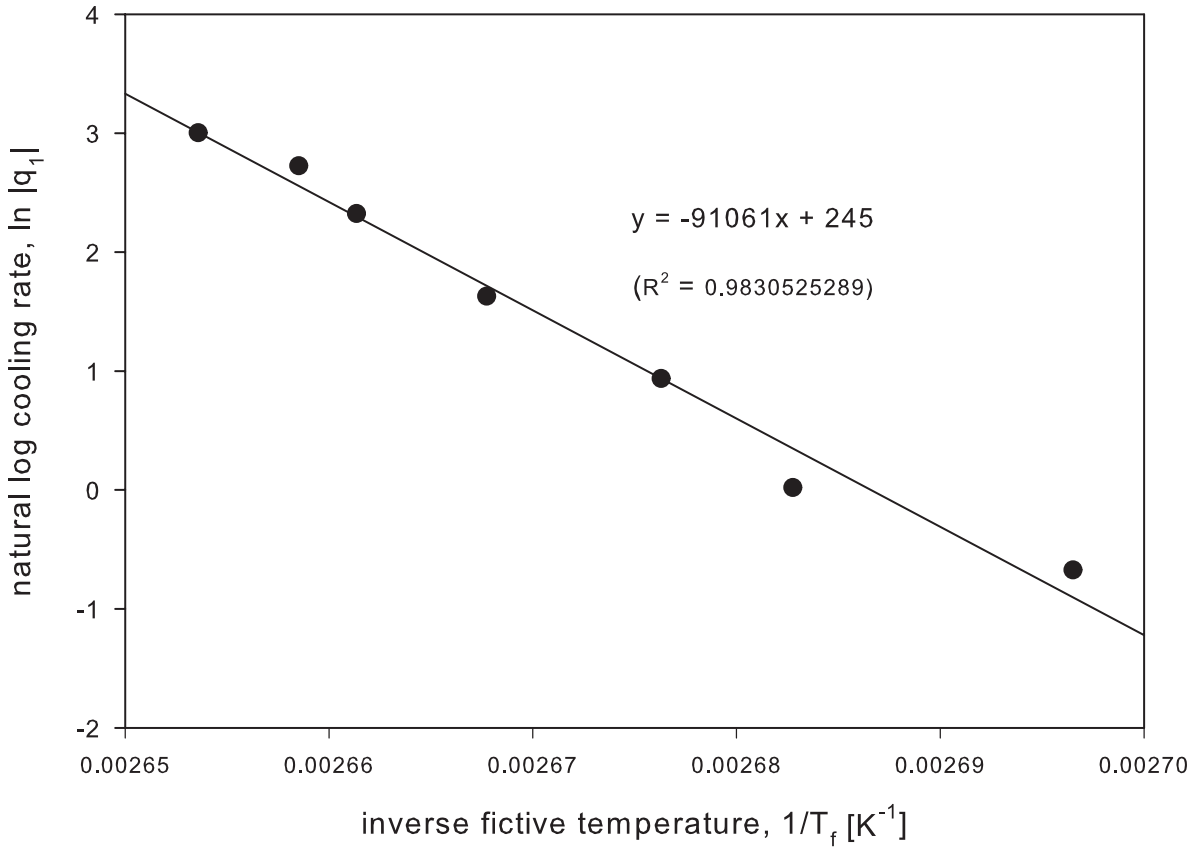

Figure 4.7: Apparent activation energy determined from equation (31)

4.3.2 Aged Samples

As stated earlier, the cooling rate study has been used to determine the effects of different cooling rates on the heat flow response. A similar technique is used to study the effects of cooling rate on *aged* material, however, the intention here is to determine the dependence of the fictive temperature change on cooling rate among the various aged states. A total of nine different conditions were investigated to capture behaviour after aging at temperatures near $T_{g,ABS}$ and $T_{g,PC}$. Again, the standard DSC mode is adequate. Using the same analyses for the reference sample, the results for the endothermic peak temperature and fictive temperature at various aged conditions have also been overlaid in Figure 4.5 and Figure 4.6.

When the peak temperatures of the aged samples are plotted together with the unaged reference in Figure 4.5, it is seen that only the poorly aged sample at 80°C for 1 hour behaves similarly;

both curves concave upward. However, the magnitudes of the peak temperature for the poorly aged state are considerably lower than the other aged states. There are two important observations in Figure 4.5: (i) the curves evolve in shape with increased aging and (ii) the shape of the curves at highest aging temperature at 100°C is completely reversed from the unaged state (eg. concave-down as opposed to concave-up).

It is useful to note here that relaxation inherently occurs, although minimally, when far below the glass temperature. While aging at 80°C, it is reasonable that both components undergo molecular relaxation, although the degree of relaxation are likely different. However, 80°C is just above the optimal aging temperature for ABS component but much farther below that for PC component, it is reasonable to expect that the structural relaxations are mostly associated with the weaker $T_{g,ABS}$ relaxation peak than the $T_{g,PC}$ peak.

The effects of different aging conditions on fictive temperature with increasing cooling rates are shown in Figure 4.6. Generally, fictive temperature increases with cooling rate as previously mentioned. To compare the effects of the different aging conditions, the values of the slopes for these curves are summarized in Table 4.1 and plotted in Figure 4.8.

Aging Temp., T_a	**Aging Time, t_a**		
	1 hr	**12 hr**	**24 hr**
80°C	1.03	0.81	0.46
90°C	0.83	0.69	0.31
100°C	0.74	0.75	0.73

Table 4.1: Summary of the rate of change in fictive temperature with the natural logarithm of cooling rate evaluated from slopes of Figure 6 (units of slopes evaluated in °C)

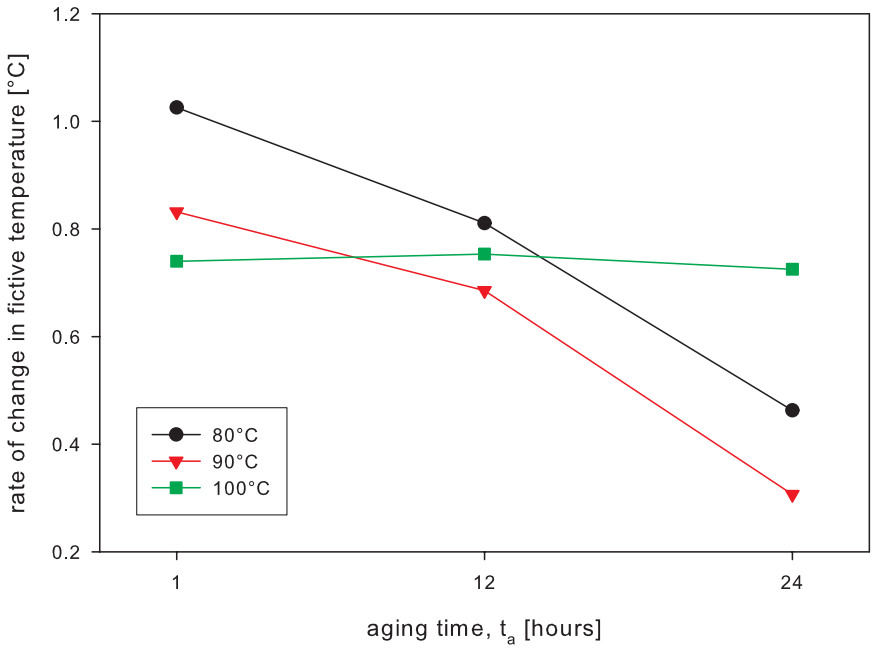

Figure 4.8: Rate of change of fictive temperature as a function of cooling rate with different aging conditions

Figure 4.8 compares the rate of change in fictive temperature (as a function of cooling rate) for the nine different combinations of aging time and temperature. Although the combination data set is limited, there is strong indication that the highest rate is associated with the poorly aged condition of 1 hour aging at 80°C. With longer times, up to 24 hours, the rate decreases. Aging at 90°C results in the same behaviour but the lowest rate is found when aging for 24 hours. Both aging temperatures appear to exhibit self-retardation behaviour, already seen in single polymeric systems. Surprisingly, however, the fictive temperature change is almost independent of aging time when aging at 100°C. As can be seen in Figure 4.4, this temperature lies between the T_g of the two components, PC and ABS, which leads to a significantly different relaxation mechanism. Although the rate change is constant, it is not the lowest among the conditions studied, which suggests that the structural state has not yet reached equilibrium and self-retardation is not evident when aging at temperatures above $T_{g,ABS}$.

4.4 Effects of Aging on Enthalpy Relaxation

The heat capacity of the sample, as a function of temperature, is found by dividing the total heat flow by the heating rate of 1°C/min. Figure 4.9 shows a typical overlay of the total heat capacity

curves obtained from heat flow scans during heat-up which were used to study the peak temperature and enthalpic change after aging at 80°C. At first glance that the endothermic ABS and PC peaks appear to increase in magnitude with increasing aging times. Less obvious, however, is that the endothermic peak temperature for PC actually decreases first before increasing dramatically with the aging time. This initial drop has also been noted elsewhere, for example with PVAc [Hutchinson and Kumar 2002]. Table 1 summarizes the endothermic peak temperatures of the replicated data (along with the mean, standard deviation, and the percent relative standard deviation). The tabulated values confirm the initial decrease and subsequent increase in endothermic PC peak. These values also indicate a very low variance. These peak endothermic temperatures are graphically illustrated (T_p vs log $|t_a|$) in Figure 4.10.

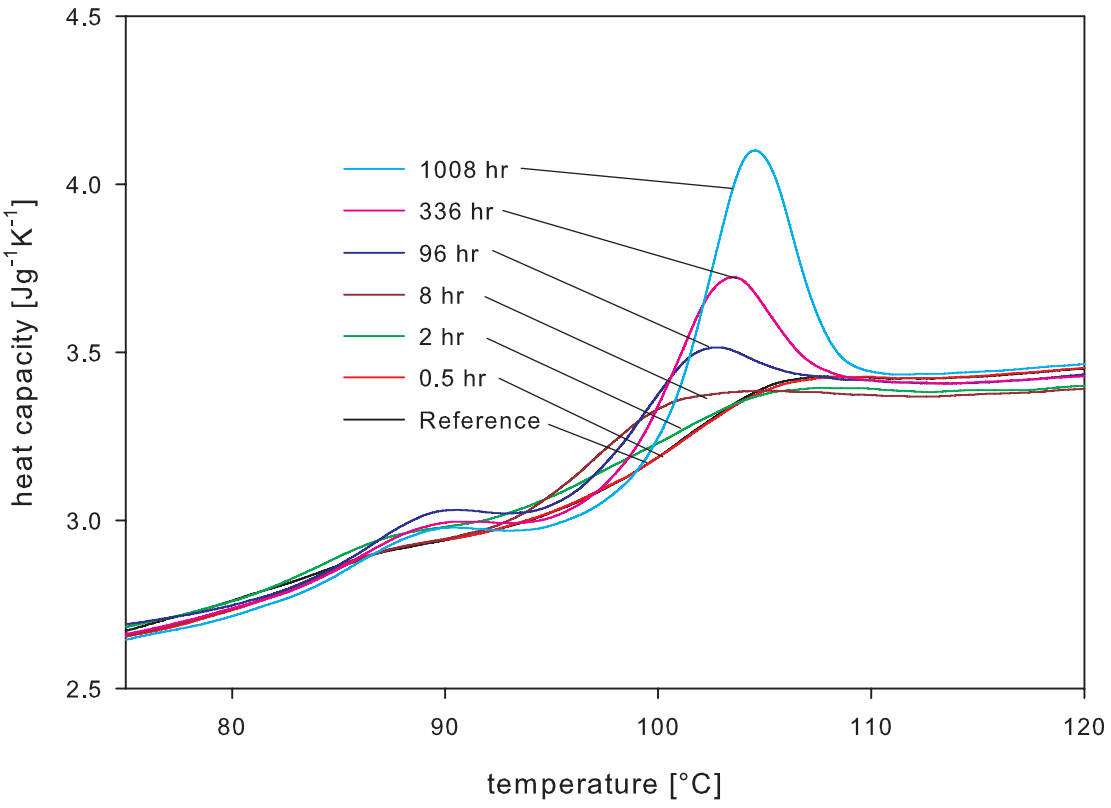

Figure 4.9: Heat-up scans of heat capacity overlay aged at 80°C for various aging times

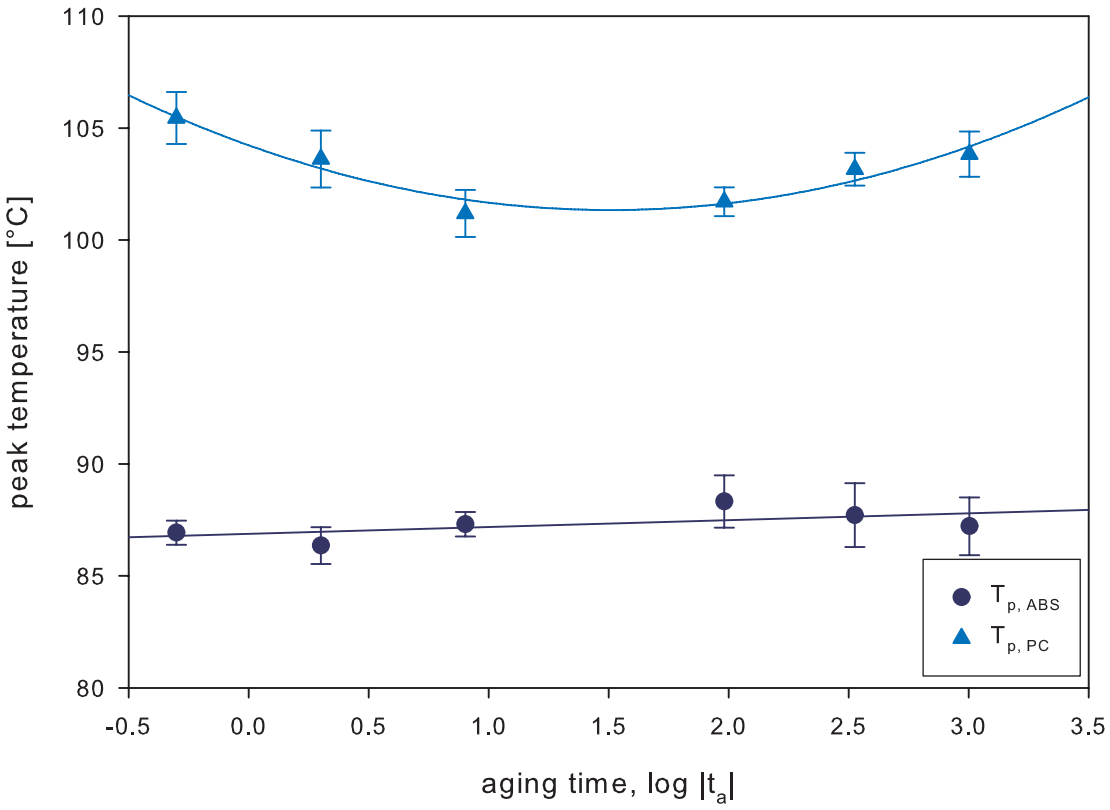

Figure 4.10: Dependence of peak endothermic temperature on aging time from heat capacity

To analyze enthalpic recovery due to physical aging, ΔH_a is evaluated from the difference in the area under the aged and reference heat capacity curve and are tabulated in Table 4.2. This data is graphically illustrated in a ΔH_a vs log $|t_a|$ plot, shown in Figure 4.11, which shows a linear dependence with an increasing rate of change of $\left(\frac{\partial \Delta H_a}{\partial log|t_a|}\right)_{q_1,T_a,q_2}$ = 0.62 J/g per decade. As expected, the enthalpy recovered, ΔH_a, increases as the aging time increases, as indicated by a more prominent enthalpic peak. It is interesting that the rate of enthalpy relaxation in this study is identical to that tabulated in other reported literature for PC [Lee-Sullivan and Bettle 2005; Hutchinson 1995].

Aging Time, t_a (hrs)	Area Under Curve		Enthalpy Recovered (J/g)	Ave. (J/g)	Std. Dev. (J/g)	RSD (%)
	Aged (J/g)	Reference (J/g)				
0.5	1.85	1.61	0.24	0.24	0.012	5.05
	1.93	1.70	0.23			
	1.87	1.62	0.25			
	1.92	1.69	0.22			
2	1.98	1.55	0.43	0.44	0.032	7.26
	2.12	1.65	0.47			
	2.13	1.73	0.40			
	2.20	1.74	0.46			
8	2.21	1.46	0.75	0.72	0.070	9.62
	2.34	1.71	0.63			
	2.31	1.58	0.73			
	2.22	1.43	0.79			
96	2.92	1.60	1.32	1.44	0.086	5.97
	2.98	1.52	1.46			
	2.94	1.41	1.53			
	2.86	1.43	1.43			
336	3.70	1.71	1.99	1.83	0.16	8.53
	3.44	1.68	1.76			
	3.41	1.50	1.91			
	3.08	1.44	1.64			
1008	4.40	1.69	2.71	2.27	0.33	14.50
	3.72	1.73	1.99			
	3.42	1.36	2.06			
	4.15	1.84	2.31			

Table 4.2: Summary of enthalpy recovery, aged at 80°C for various times, t_a

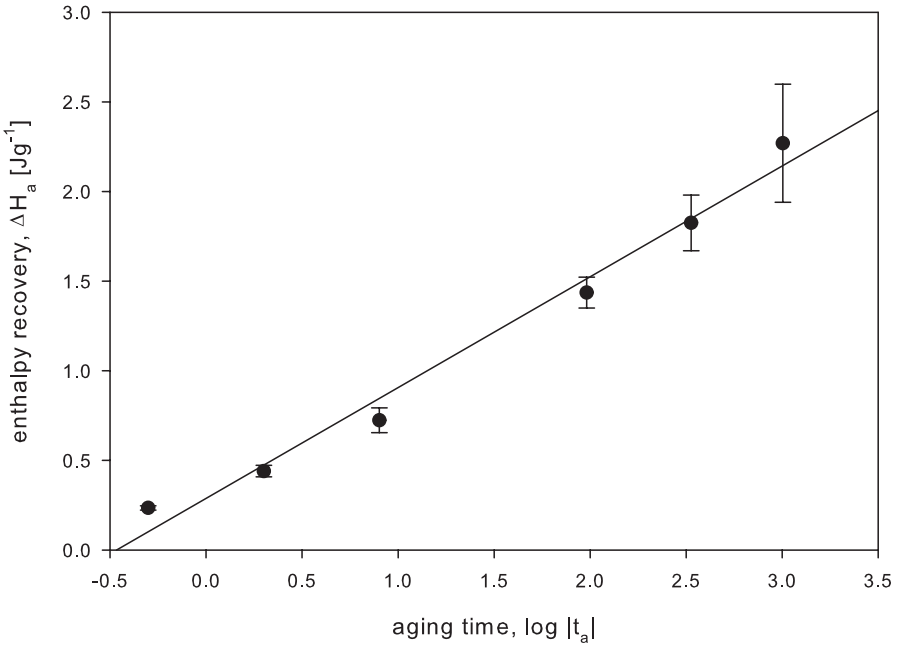

Figure 4.11: Dependence of enthalpy recovery on aging time (hours)

When plotting the endothermic peak temperature as a function of aging time, as shown in Figure 4.10, it can be seen that aging has a negligible effect on the ABS component's peak. In contrast, the endothermic peak associated with PC aging is non-linear. Seen recently elsewhere [Su and Shih 2006], physical aging *could* cause the miscibility of a material to change, as observed by the convergence of two glass temperatures into one. Therefore, it is not surprising that with an increase in aging time, the individual endotherms of PC and ABS could also behave in the same way. This suggests that aging may have influenced the miscibility of the blend.

The heat flow data deconvoluted into the reversing and non-reversing signals, as described in equation (27), is further investigated. As described elsewhere [Thomas TP006], the MDSC reversing signal permits a convenient qualitative analysis of the polymer's glass temperature. When the reversing heat flow for all the aging times are overlaid in Figure 4.12(a), the PC transition inflection temperature appears to decrease with aging time. This is more clearly shown when the derivatives of the curves are plotted in Figure 4.12(b), while Figure 4.13 illustrates the changes of the glass temperature of the two components in the blend.

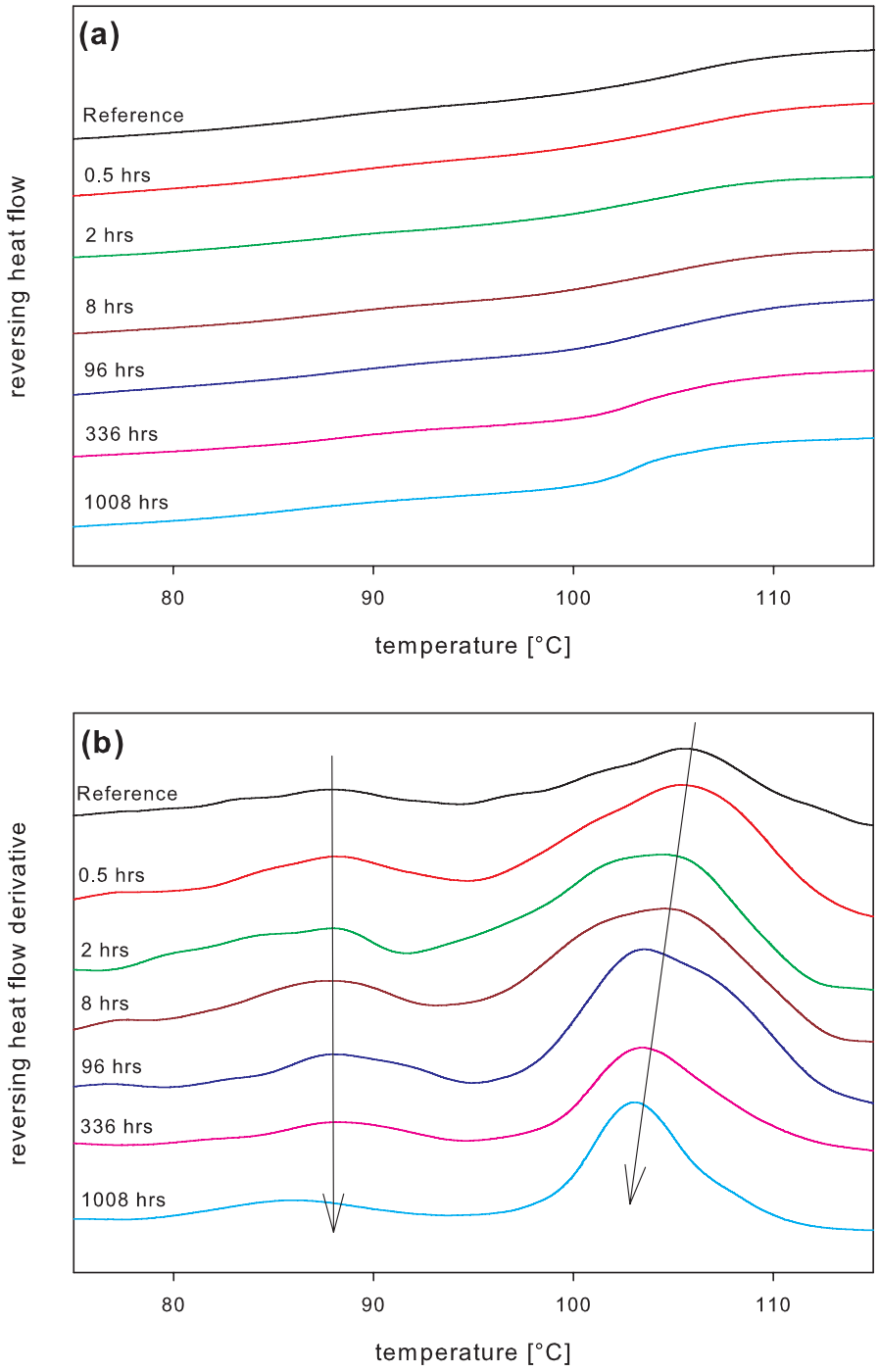

Figure 4.12: Aging at 80°C for different aging times and corresponding derivatives (a) Heat-up scans of reversing heat flow of peak shift study and (b) Derivative of corresponding heat-up reversing heat flow

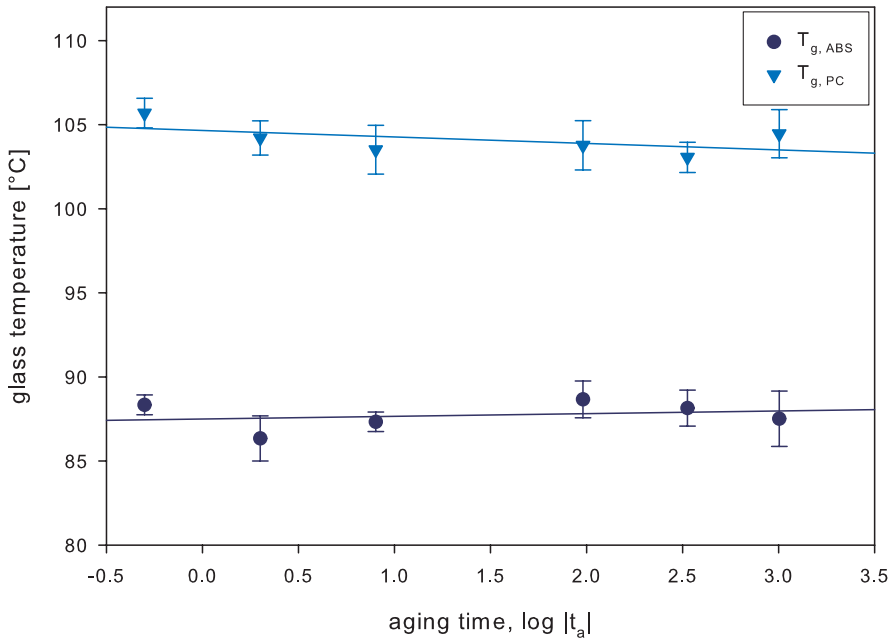

Figure 4.13: Dependence of glass temperature on aging time (hours)

Not only are the PC transitions shown more clearly, it reveals the ABS transition that was otherwise unnoticeable in Figure 4.12(a). These figures clearly indicate that the ABS transition shows little to no change for the duration of the aging study. These results are consistent with the boiling water aging experiments by Li *et al*. [2003] in which the results indicated little to no change in the ABS transition temperature in the PC/ABS blend, whereas the PC transition temperature decreased with aging. They, as other researchers [Balart *et al.* 2005; Nigam *et al.* 2005; Keitz *et al.* 1984; Santana *et al.* 1998], have indicated partial miscibility in studies of PC/ABS systems, while others [Guest and Van Daele 1995; Más *et al.* 2002] have indicated immiscibility. Although two peaks are clearly visible, it was pointed out earlier by Lodge *et al*. [2006] that this *may* not necessarily indicate immisciblity. With the noticeable shift in the inflection of the reversing heat flow, one might be quick to jump to the conclusion that the present PC/ABS blend is partially miscible. However, this is far from certain as a blend's miscibility requires extensive studies by a variety of techniques.

Lastly, since the fictive temperature, T_f, is a more accurate representation of aged state than the glass transition, T_g, the effects of aging on T_f can be observed in Figure 4.14. It has been commonly reported that T_f decreases with aging, and specifically with PC as well [Lee-Sullivan

and Bettle 2005; Ho and Vu-Khanh 2004]. If we employ the concept of fictive relaxation rate as a cursory comparison, the T_f decreases at R_f = 1.64°C per decade of aging time when aging PC/ABS at 80°C in this study, in contrast to R_f = 1.9 for PC evaluated at approximately 10°C below T_g [Málek and Shanelova 2000]. However, this may not be a valid comparison because the aging temperature in this blend study is 10°C below $T_{g,ABS}$ and not $T_{g,PC}$.

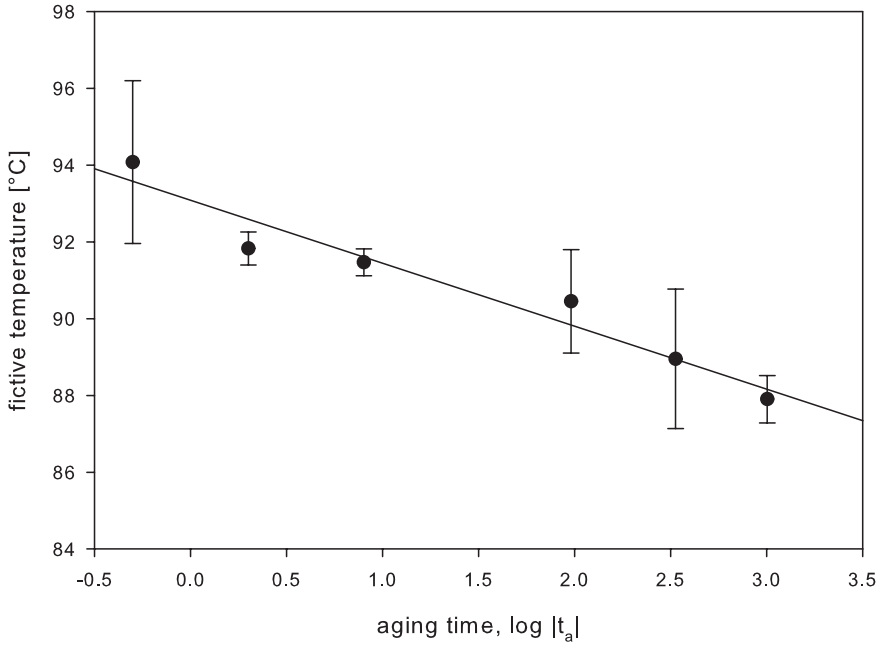

Figure 4.14: Dependence of fictive temperature on aging time (hours)

4.4.1 ATR-FTIR Measurements

In accordance to the flowchart shown in Figure 1.9, it is appropriate to discuss the FTIR results from thermal aging of the blend. The results shown in Figure 4.15(a) of the reference PC/ABS material (eg. not subjected to any conditioning, only thermal history erased) appear similar to that of the PC component as studied elsewhere [Balart *et al.* 2005], as is expected since the majority of the blend consists of PC. This spectra is also visually very similar to that reported by Kuczynski *et al.* [1994] of their PC/ABS blend. The spectra of the aged samples in the study are overlaid in Figure 4.15(b).

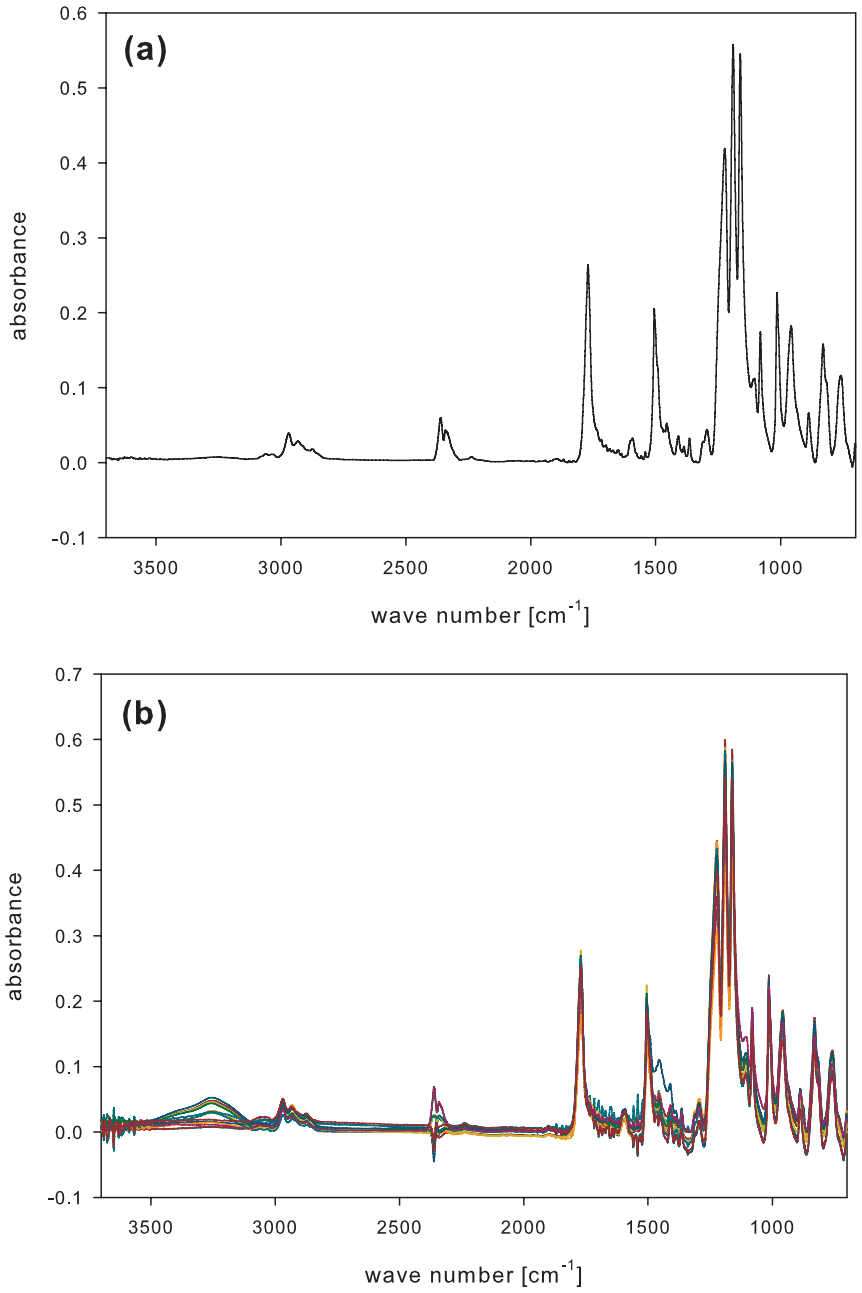

Figure 4.15: ATR-FTIR spectra of (a) reference (b) aged PC/ABS

In a thermal degradation study of ABS by Motyakin and Schlick [2002], the degradation of ABS was found not only to decrease in the absorption intensity in the butadiene region (960 cm^{-1}), but also indicated that degradation products were formed that lead to an increase in the absorption intensity in the carbonyl region. The oxidation process of butadiene lead to the formation of carbonyl (around 1770 cm^{-1}) and hydroxyl groups (between 3000-3500 cm^{-1}).

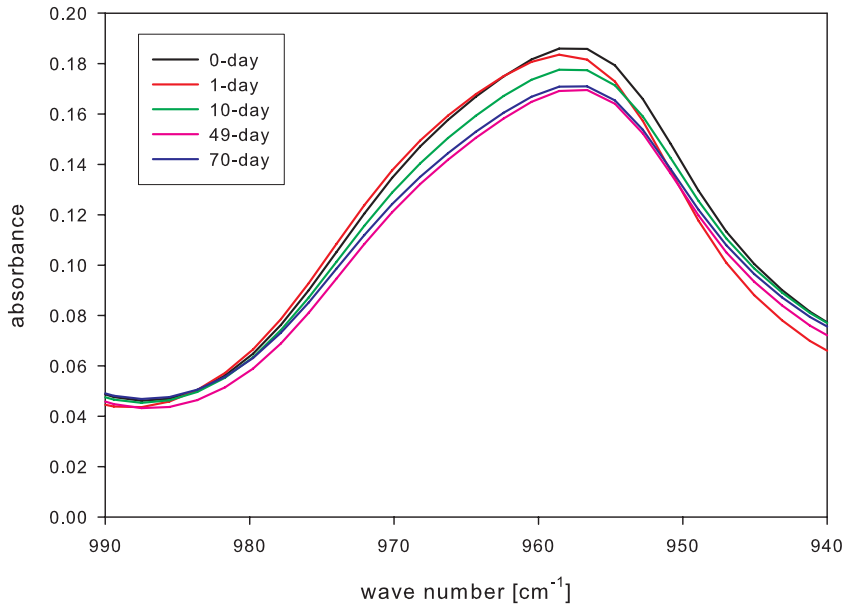

Figure 4.16: Absorbance intensity of polybutadiene region (960 cm^{-1})

A decrease in the absorption intensity of the butadiene region is also seen during the aging process in this study, as shown in Figure 4.16. It is widely known that during oxidation, carbonyl and hydroxyl degradation products are formed and have been monitored in literature, for example by Motyakin and Schlick [2002], Rjeb *et al.* [2000], and Gugumus [1998]. ABS is an easily oxidized material, and it is evident in Figure 4.15(b) that oxidation has occurred. The reference (unaged) sample shown in Figure 4.15(a) showed no traces of hydroxyl groups present. However, the spectrum obtained after subsequent aging showed notable increases in the hydroxyl degradation products after 10 days of aging.

Upon magnification of the carbonyl (C=O) region (1770 cm^{-1}), it can be seen in Figure 4.17 that there is indeed an increase in the absorbance intensities over time which supports the oxidation notion. Although both products of oxidation are formed, the carbonyl region is also the characteristic group in the carbonate linkage. The C=O bond in the carbonate linkage has a very high dissociation energy as indicated by Li and Huang [1999] which makes it suitable for monitoring changes in the spectrum during aging studies.

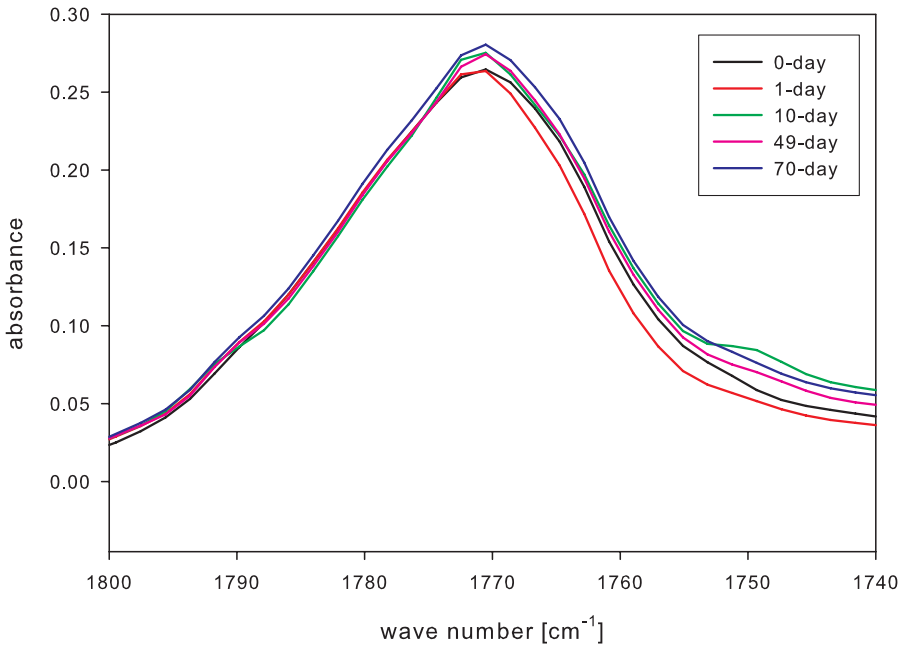

Figure 4.17: Absorbance of C=O carbonate stretching (1770 cm^{-1})

The peaks of all aged samples at various times are normalized to the height of the reference, unaged, spectrum. The normalized peak heights are plotted in Figure 4.18. The results indicate an overall increase of 8% in the intensity of the carbonyl region over the duration of the study, while the butadiene absorbance decreased by approximately 8%. The increase in the absorbance intensities of C=O can possibly be associated with the degradation of butadiene or with the aging of the PC system as found by Heymans [1997]. Observing Figure 4.18 shows gradual increase in the carbonyl absorbance at approximately 10 days, while butadiene shows a decrease beginning at about the same time. It is also noted that the hydroxyl degradation products began to form after 10 days of aging. It is reasonable to assume that the oxidation process of butadiene occurs at this time to produce the hydroxyl and carbonyl degradation products. However, it should also be noted that after the initial drop in the absorption intensity of the butadiene region, the values remained relatively stable after approximately 25 days. The fact that the absorption intensity reaches a steady value quickly could possibly tie into the cause of $T_{g,ABS}$ not shifting. Interestingly, for the duration of the aging study, the enthalpy recovery had yet to achieve equilibrium (Figure 4.11), and similarly the absorbance intensities for the carbonyl region has yet to reach a steady state. It could be reasoned that after the butadiene stabilized, the increase in the carbonyl region could be attributed to the aging process of polycarbonate.

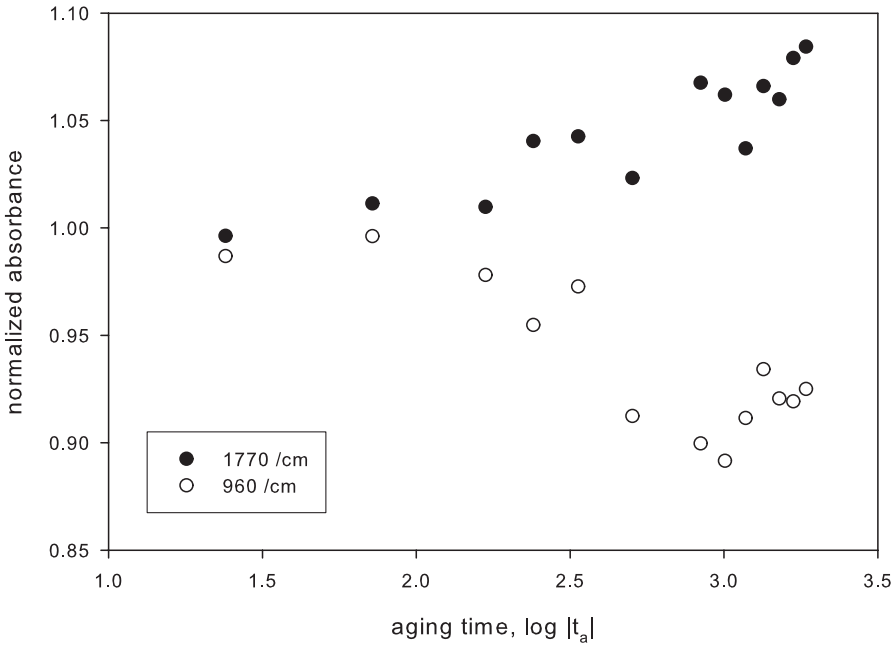

Figure 4.18: Normalized absorbance intensities of carbonyl (1770 cm^{-1}) and butadiene (960 cm^{-1}) region

Not only did Heymans show that the absorbance intensities for the carbonyl group increase with aging in PC, but the aging process was seen to have caused conformational changes from a high energy *trans-cis* arrangement to a lower energy, *trans-trans* arrangement [Lu *et al.* 2000; Heymans 1997] which indicates a shift from 1785 towards 1767 cm^{-1}. It is evident in Figure 4.17 that the carbonyl peak in the reference state occurs at approximately 1770 cm^{-1}, which is already very close to the lower energy *t-t* conformation. Moreover, no noticeable shifts were observed during the subsequent aging process. This can be attributed to the addition of the ABS which may be restricting further conformational rearrangements, or more likely, that the PC region already exists in a lower energy state (1770 cm^{-1}).

The ring stretching vibration bands of the phenyl groups (benzene ring) which exist in both the PC and ABS (as part of the styrene component) occurs around 1600 cm^{-1}. Heymans [1997] had first reported conformational changes in PC by the investigation of the C=O stretching in the carbonate linkage, but had since moved on to investigate the potentially cleaner band, 1600 cm^{-1}, free of Fermi resonance that could obscure changes expected to be seen in physical aging [Heymans and Van Rossum 2002]. However, that study was not successful in observing any conformational changes. The contributions from the *t-t* and *t-c* conformers can be clearly seen in

our study in Figure 4.19 without deconvolution. The 2-peak region of the absorption intensities appear to maintain a reasonably steady absorbance for the duration of the aging study, but also shows no shifting towards either *t-t* or *t-c* contributions.

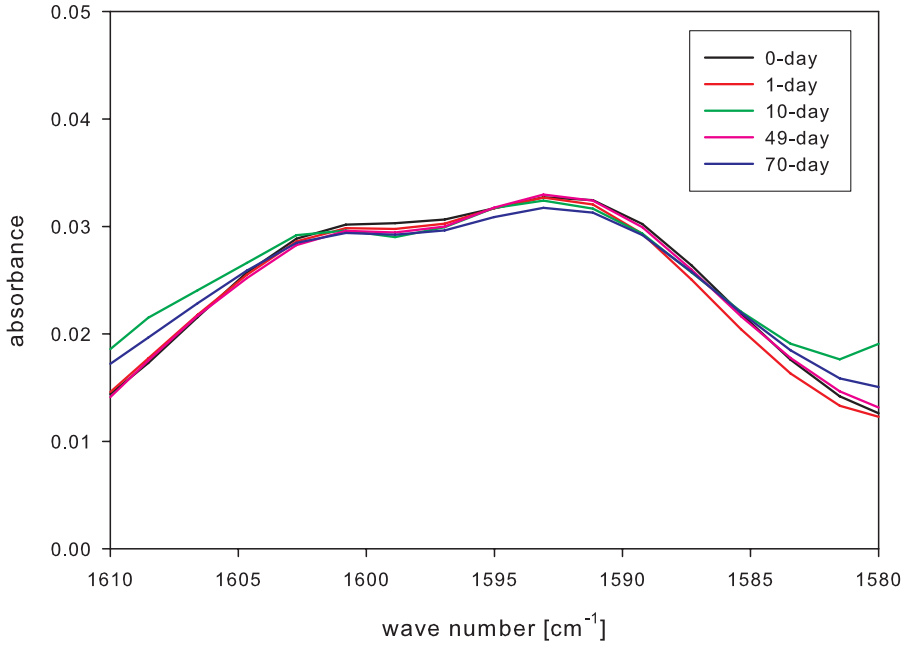

Figure 4.19: Absorbance of phenyl group stretching (around 1600 cm^{-1})

With this in mind, this peak is chosen for a more common method for comparisons of absorbance intensities involving an *internal standard*. Absorbencies at wave numbers of interest are compared to a peak insensitive to change with the treatment, the aging process in this case, in the study. For continuity reasons, the ratios for aged states are then normalized to the ratio for the unaged sample to produce comparable results to Figure 4.18. The absorbance intensity of the larger peak at approximately 1593 cm^{-1} is chosen as the internal standard and the results of the trends are shown in Figure 4.20. It is observed that this method yields a similar result as compared to Figure 4.18, but with slightly more scatter. The internal standard chosen, 1593 cm^{-1}, although appears to be insensitive to the aging process, still is subjected to very minor fluctuations attributed to experimental scatter, thus the original normalized data yield more conclusive observations.

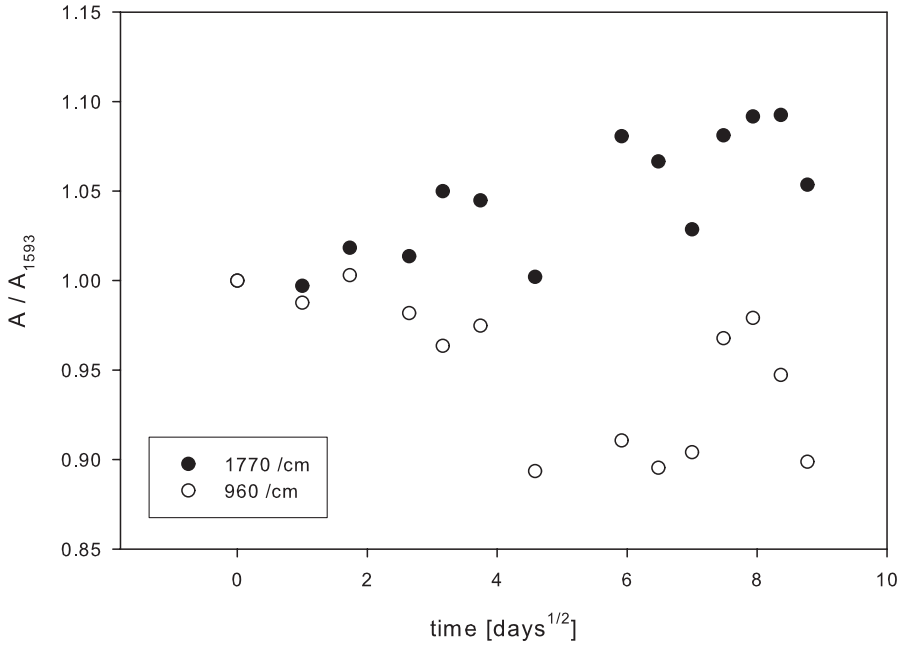

Figure 4.20: Normalized absorbance intensities of carbonyl (1770 cm^{-1}) and butadiene (960 cm^{-1}) region using 1593 cm^{-1} as an internal standard

Also of interest to note is that the characteristic C≡N absorption band for the acrylonitrile component near 2250 cm^{-1} is almost non-existent in the blend. Only a very tiny peak is seen that does not change with aging time. This is evident in the full spectrum seen in Figure 10 of our results, as well as in the work of Kuczynski *et al.* [1994].

4.4.2 Statistical Data Analysis

ANOVA was utilized on the data obtained in the above aging study to determine whether changes in the DSC data with increasing aging time, t_a, are indeed significant. This is to verify observations made earlier. Changes include shifts of the glass temperature, T_g, and enthalpic peak temperature, T_p, for each component in the blend, the overall enthalpy loss, Δh^*, and the structural state of the material described by the fictive temperature, T_f.

Experimental data have been validated before performing ANOVA analysis, and in our validation analysis, it was found that variance, normality and Cook's distance for all independent variables were acceptable, except for the enthalpy recovery data. Enthalpy recovery observations were found to show variance that was fanning out, shown in Figure 4.21(a). As seen from Figure 4.11,

the error bars are gradually increasing, which means non-constant variance. By performing variance-stabilizing (logarithmic) transformations on the enthalpy recovery data, the violation of the assumptions was corrected and the residuals are shown once again in Figure 4.21(b). A desirable normal probability plot is shown in Figure 4.21(c) with data following the diagonal, while deviations at the ends are tolerable. The outlying point on a plot of Cook's distances, shown in Figure 4.21(d) was also corrected by the data transformation, producing an acceptable Cook's distance plot after the data transformation. It is now possible to continue with the ANOVA interpretation.

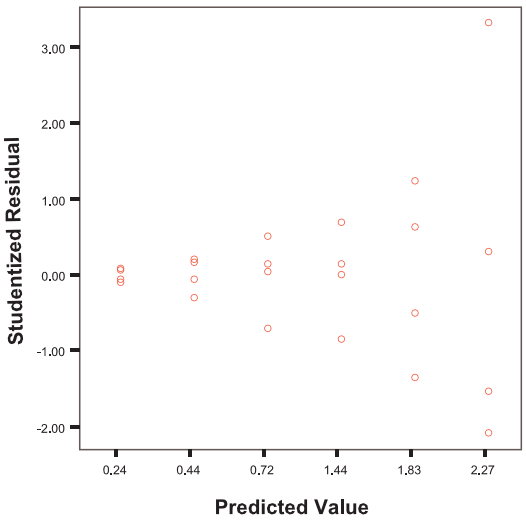

(a) Fanning out of residuals in enthalpy data

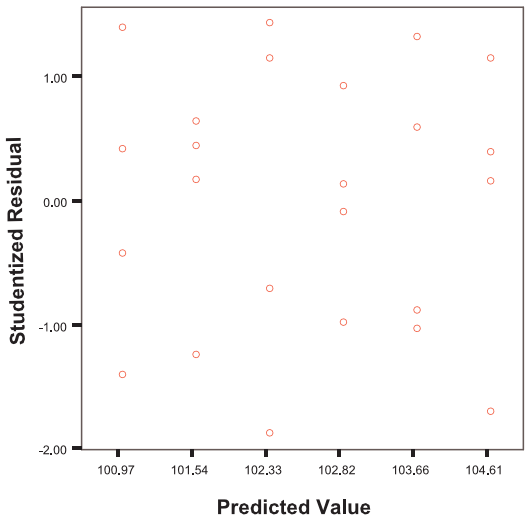

(b) Even spread of residuals for transformed data

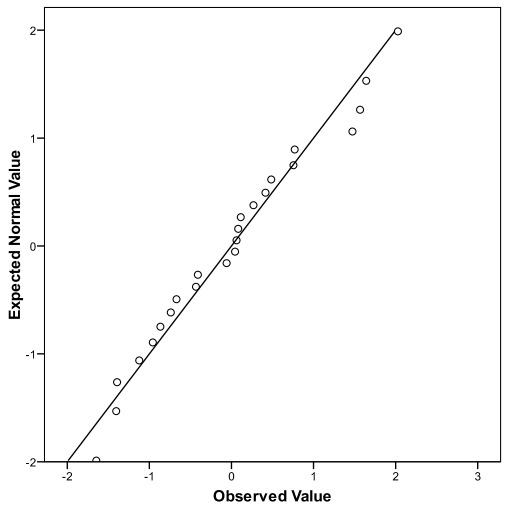

(c) Normal probability plot

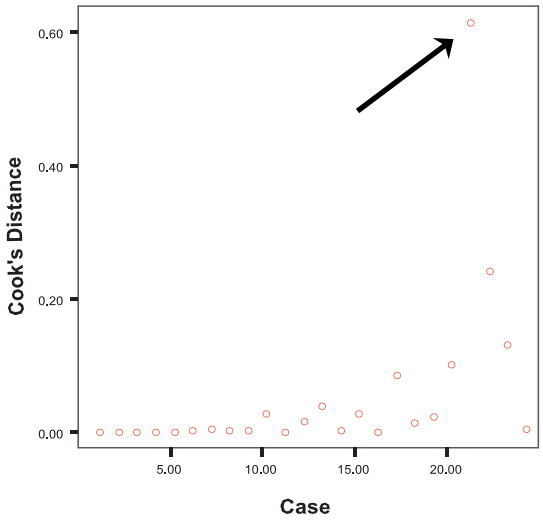

(d) Outlying point in Cook's distance plot

Figure 4.21: Visual examination of ANOVA assumptions

Source	Variable	Sums of Squares	Degrees of Freedom	Mean Square	*P*-value
t_a	$T_{p,ABS}$	7.61	5	1.52	.265
	$T_{p,PC}$	36.22	5	7.24	.001
	$T_{g,ABS}$	14.19	5	2.84	.092
	$T_{g,PC}$	18.31	5	3.66	.025
	Δh^*	2.95	5	0.59	.000
	T_f	96.737	5	19.35	.000
Error	$T_{p,ABS}$	19.31	18	1.07	
	$T_{p,PC}$	19.30	18	1.07	
	$T_{g,ABS}$	22.60	18	1.26	
	$T_{g,PC}$	19.54	18	1.09	
	Δh^*	0.03	18	0.02	
	T_f	30.72	18	1.71	
Total	$T_{p,ABS}$	26.92	23		
	$T_{p,PC}$	55.52	23		
	$T_{g,ABS}$	36.79	23		
	$T_{g,PC}$	37.84	23		
	Δh^*	2.98	23		
	T_f	127.46	23		

Table 4.3: Summary of ANOVA for peak shift experimental study

The ANOVA table is shown in Table 4.3, and recalling that the sums of squares is a measure of variability, it can be seen that the treatment, t_a, as compared to the error, accounts for a large amount of the total variability for $T_{p,PC}$, which is favourable. This means that the differences in the observations are accounted for by the applied treatment, as opposed to random errors, ε. The same can be said of the observations for the fictive temperature, but not for $T_{p,ABS}$ in which there is greater uncertainty and hence a much weaker significance ($P = 0.265$) as compared to $T_{p,PC}$, ($P = 0.001$). Differences found in $T_{p,ABS}$ may not be a direct result of the aging time, but partly affected by the variability encompassed in the random error. The statistically insignificant differences between the peak endothermic temperatures for ABS are consistent with Figure 4.10. On the other hand, the strong significance of $T_{p,PC}$ concludes that its null hypothesis can be rejected. Although it is understood that there are notable differences amongst the different treatments (different aging times) for $T_{p,PC}$, it is unclear which pair of comparisons has caused the significant statistical differences. From the statistical method Tukey's Multiple Comparisons

shown in Table 4.4 for $T_{p,PC}$, each level of the treatment is compared directly to all other levels of the treatment. Those that yield significant statistical differences ($P \leq 0.05$) are marked with an asterisk.

t_a (i)	t_a (j)	*P*-value
0.5	2.0	0.057
	8.0	0.001*
	96.0	0.006*
	336.0	0.192
	1008.0	0.783
2.0	0.5	0.057
	8.0	0.455
	96.0	0.883
	336.0	0.984
	1008.0	0.480
8.0	0.5	0.001*
	2.0	0.455
	96.0	0.967
	336.0	0.168
	1008.0	0.018*
96.0	0.5	0.006*
	2.0	0.883
	8.0	0.967
	336.0	0.522
	1008.0	0.086
336.0	0.5	0.192
	2.0	0.984
	8.0	0.168
	96.0	0.522
	1008.0	0.854
1008.0	0.5	0.783
	2.0	0.480
	8.0	0.018*
	96.0	0.086
	336.0	0.854

Table 4.4: Tukey's multiple comparisons for endothermic peak temperature of PC component

The multiple comparisons from Table 4.4 indicates that the short and long-term aging treatments for $T_{p,PC}$ are not much different, but the differences are significant as compared to the intermediate length aging times. This suggests a parabolic shape which the polynomial contrasts confirm. The polynomial contrasts in Table 4.5 indicate that $T_{p,PC}$ results are significant to a 2nd-order least-squares ($P = 0.00$) fit and not at other (higher) orders, whereas it has been found in literature that the peak endothermic temperature for PC increases linearly (1st order) with aging time [Hutchinson *et al.* 1999]. $T_{p,ABS}$ was found to be significant at a 3rd-order polynomial fit. However, with small data set (6 treatments), it is not possible to confidently assume that higher orders (3rd-order) would apply.

Polynomial Contrast	***P*-value**
Linear	0.539
Quadratic	0.000
Cubic	0.150
Order 4	0.441
Order 5	0.779

Table 4.5: Polynomial contrasts for peak endothermic temperature of PC component

Also, from the ANOVA in Table 4.3, it can be said that the glass temperatures of the ABS component yields near significant results ($P = 0.09$), as the *P*-value is much closer to the 5% significance level as compared to $T_{p,ABS}$, although it is still statistically insignificant. Because of this, it becomes a judgemental decision on the part of the researcher whether this is of practical value and this uncertainty, as depicted by the relatively flat linear fit in the figure, is also reflected in the *P*-value from ANOVA which indicates near significance. Prior to the statistical analysis, it was observed in Figure 13 that there was a subtle decrease in the PC component glass temperature, as was found in literature as well [Su and Shih 2006]. The observed decrease is confirmed with $P = 0.025$ for $T_{g,PC}$ indicating statistical significance in the observed data.

Following a similar approach, enthalpy recovery was also analyzed for the transformed data, it is noted that the ANOVA table indicates a strong significance ($P = 0.00$) for the aging treatment on Δh^*, which prompts further detailed investigation. While observing Figure 12, it is quite apparent that there are prominent differences with increasing aging. In fact, through a test of multiple comparisons, every combination was indicated to be significant, meaning all treatments

of aging times produced samples with significant statistical differences from one another. The polynomial contrasts also confirm the linear increase that is fitted in the aforementioned figure.

Lastly, the ANOVA for fictive temperature had already indicated that the aging conditions rather than errors accounted for a large amount of the variability, and thus leads to the conclusion that the effect of aging is highly significant (P = 0.00). The polynomial contrast confirmed that it follows a strong linear dependence with aging time.

4.5 FURTHER INVESTIGATION BY DSC ANALYSIS

A widely known phenomenological model known as the TNM model, has been applied to single polymer systems by determining the model parameters through experimental studies. The activation energy for enthalpy relaxation for the unaged material has even been adopted in this work for the PC/ABS blend using the same methods, as described in section 4.3.1. Furthermore, this method has also been applied for various aged states. The attempted application of similar experimental methods for application of the TNM model, along with the complications encountered are outlined below. Lastly, an alternative, empirical data fitting model applied to provide similar relaxation spectrum is discussed and illustrated.

4.5.1 Determination of TNM Parameters

It has been proposed by Hutchinson's work in the literature that parameters in the TNM expression can be determined from a series of DSC studies. Although there has been skepticism in these methods, its validity remains to be confirmed, and it is presently used as exploratory insight in determining β and x.

The non-exponentiality parameter, β, can be determined through a set of varying cooling rate experiments. For each cooling rate, the heating scan produces an upper peak in the heat capacity. According to [Hutchinson and Ruddy 1988], the magnitude of this upper peak, $C_{p,u}$, is dependent on the ratio of the cooling to heating rate, the parameter β and to a lesser extent, x. First, plot the

dependence of the normalized upper peak, defined in equation (36), against the ratio of cooling to heating rate.

$$C_{p,u}^{N} = \frac{C_{p,u}}{\Delta C_p} \qquad \textbf{(36)}$$

After x is determined (further below), β can be estimated by using different values of β and x values to bound the experimental curve and obtain a range for β. The normalized upper peak height, $C_{p,u}^{N}$ shown in Figure 4.22, was determined for each condition studied in the cooling rate experiments; 1 unaged reference material, and 9 various aged conditions.

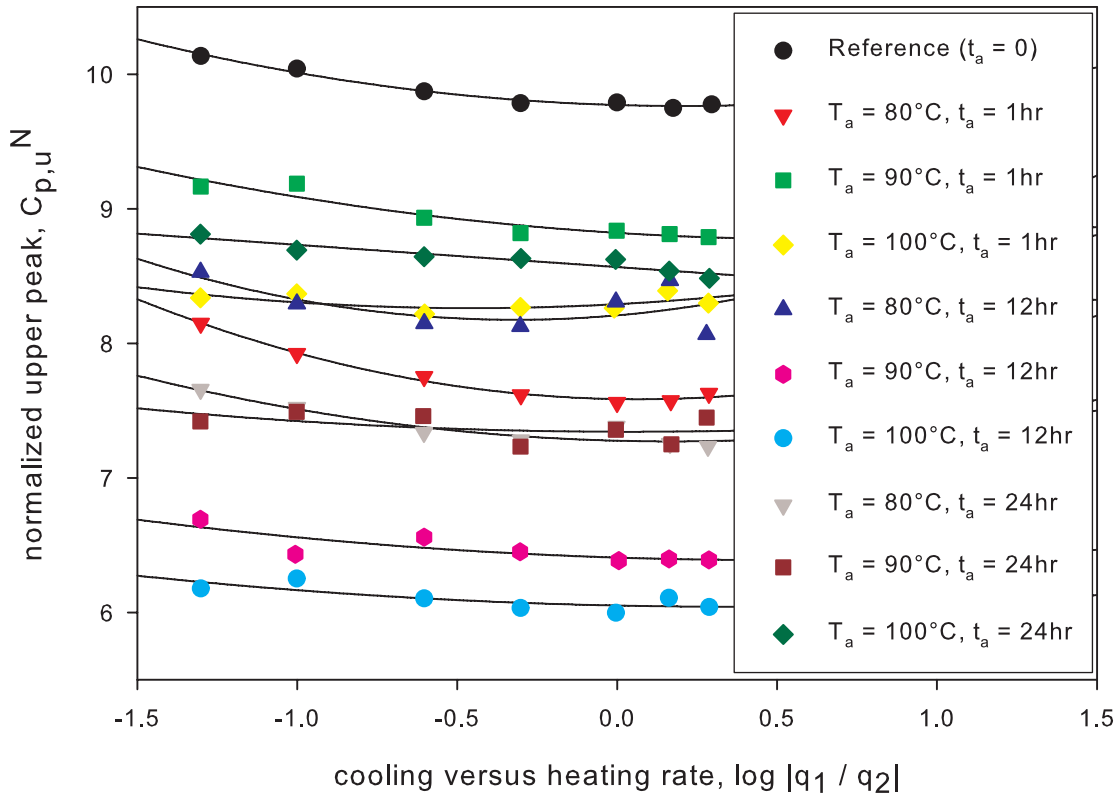

Figure 4.22: Dependence of normalized upper peak heat capacity on ratio of cooling to heating rate

The observed non-linear form in the normalized upper peak for the reference curve corresponds well to previous work [Hutchinson *et al.* 1999]. All $C_{p,u}^{N}$ for the various aged conditions show very similar behaviour, while the magnitudes of the values do not seem to follow any time or temperature dependence. It is noted that the plotting of $C_{p,u}^{N}$ values was only a method proposed for determining β, however, it is unclear if these values actually have a physical meaning.

Determined earlier, the apparent activation energy for enthalpy relaxation was 757 kJ/mol for this unaged PC/ABS blend. Similar to Figure 4.7, the apparent activation energy could be determined from the slope of a log $|q_1|$ vs $1/T_f$ plot. The effect of different aging conditions on Δh^* was studied by determining the slopes plotted in Figure 4.23. The values of the slopes and corresponding activation energy, Δh^*, are summarized in Table 4.6.

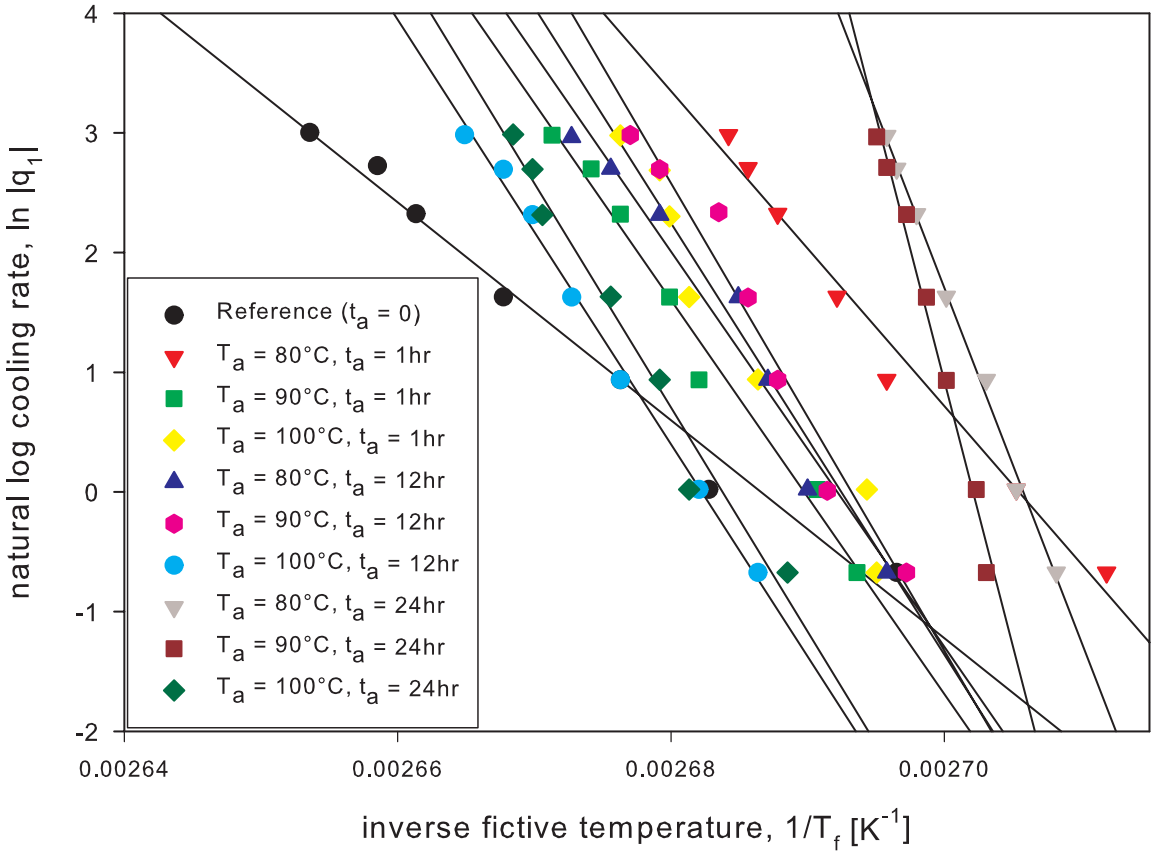

Figure 4.23: Dependence of fictive temperature on cooling rate for different aging conditions

Aging Temp., T_a	Aging Time, t_a					
	1 hr		12 hr		24 hr	
	kJ/mol	kK	kJ/mol	kK	kJ/mol	kK
80°C	1095	132	1373	165	2453	295
90°C	1368	165	1624	195	3674	442
100°C	1499	180	1475	177	1557	187

Table 4.6: Summary of activation energies (and Δh*/R) evaluated from slopes of Figure 4.23

When these values are plotted in Figure 4.24, the apparent activation energies for aging at T_a = 80 and 90°C indicate a dramatic increase in Δh^* with increased aging time, t_a , after 12 hours. This suggests that the blend remains poorly aged within this period at temperatures below $T_{g,ABS}$ but occur more rapidly as the temperature is increased. When aging at 100°C, it was not possible to progressively measure aging effects since relaxation occurred much too quickly. The apparent activation energies at 100°C remained at a constant level for the three aging times measured. What is surprising, however, is that Δh^* at 100°C is comparable to the poorly and intermediate aged states at about 1500 kJ/mol. The apparent inconsistent behaviour at 100°C suggests that the mechanisms during structural relaxations at sub-$T_{g,ABS}$ temperatures (Figure 4.4) would be very different from that at sub $T_{g,PC}$ temperatures in this blend. This supports the self-retarding theory during relaxation and could also be related to the unexpected behaviour exhibited in Figure 4.5 where the endothermic peak temperatures become concave-down.

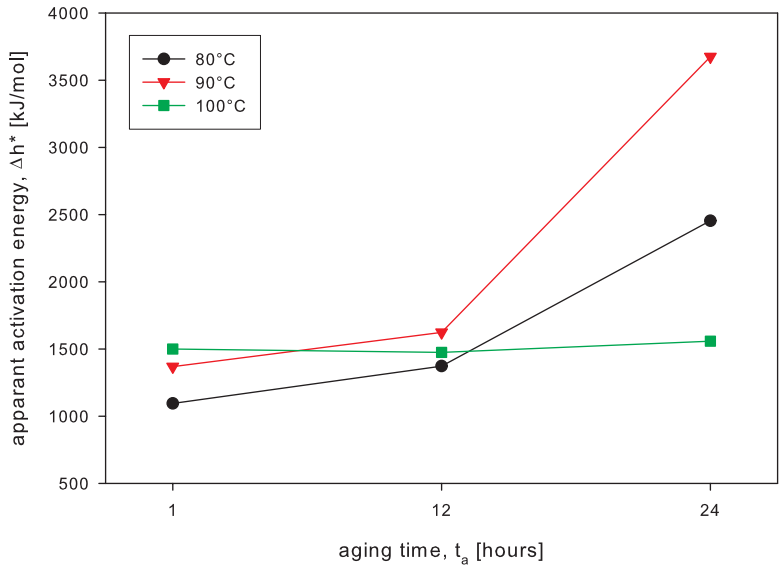

Figure 4.24: Interactions of aging temperature and time on apparent activation energy

From Table 4.6, three distinct activation energy regimes can be identified. First, a poorly aged state (80 – 90°C; 1 – 12 hrs) with relatively low activation energy. Secondly, an intermediate aged state (80 – 90°C; 24 hrs) with very high activation energy. Finally, a highly aged state (100°C; 1 – 24 hrs) with activation energy comparable to the poorly aged state.

The apparent anomalous behaviour at the aging temperature of 100°C, i.e. between the two component peaks, strongly suggests that aging studies for blends that exhibit two peaks should be

performed at a temperature below the first peak. It is evident that at 100°C, the ABS component has completely relaxed and any changes measured by DSC during aging are predominantly caused by relaxation in the PC component. Therefore, the optimal aging temperature lies between 80 and 90°C.

A normalized shift factor has been defined to determine the dependence of the peak endothermic temperature on enthalpy relaxation [Hutchinson and Ruddy 1988]. This factor, shown in equation (37), is used to obtain the non-linearity parameter, x.

$$\hat{s}(\bar{D}) = \Delta C_p \left(\frac{\partial T_p}{\partial \Delta H_a} \right)_{q_1, T_a, q_2} \qquad \textbf{(37)}$$

where ΔC_p is the difference between the heat capacity of the equilibrium liquid, C_{pl}, and equilibrium glass, C_{pg}, evaluated at the fictive temperature, T_f, which is an appropriate temperature describing the state of the material.

A *master shift* curve introduced for determining x is shown in Figure 4.25, where it can be determined rather precisely as described by Hutchinson and Ruddy (F(x) in figure is denoted as the shift factor).

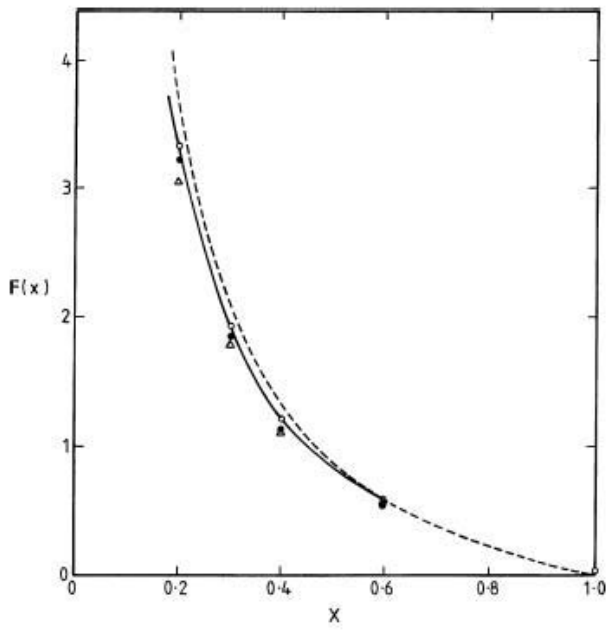

Figure 4.25: Master shift curve used for determining *x* [Hutchinson and Ruddy 1988]

From equation (37), it is necessary to determine the dependence of the peak endotherm temperature on enthalpy recovery. Such a relation is possible by determining a ratio of the slope for endothermic peak temperatures to the slope of enthalpy recovery, both as a function of aging time; (T_p vs log $|t_a|$) and ΔH_a vs log $|t_a|$ have both been previously determined in Figure 4.10 and Figure 4.11, respectively. As previously mentioned, $\left(\frac{\partial \Delta H_a}{\partial log|t_a|}\right)_{q_1,T_a,q_2}$ was determined to be 0.62 J/g per decade. However, the fact that there are two peak temperatures presents a complication in determining $\hat{s}\left(\bar{D}\right)$. It was possible to incorporate both relaxation peaks into an overall enthalpy relaxation for the blend, but the endothermic peak temperatures for each blend component cannot be combined.

With that said, the possibility of a shift factor for each individual component was investigated, although it would not be useful in characterizing the blend. In observing Figure 11, it is noticeable that the peak temperature for ABS remains constant, which leads to the shift factor associated with ABS to be approximately zero since $\left(\frac{\partial T_p}{\partial log|t_a|}\right)_{q_1,T_a,q_2} \approx 0$. In order to determine the shift factor associated with the PC component, a 2nd-order least squares curve-fit was necessary to be applied which was found to be

$$y = 1.27z^2 - 3.83z + 104.23 \quad \textbf{(38)}$$

where y represents the peak temperature, T_p, and z represents log $|t_a|$. The parameter required to determine the shift factor, $\left(\frac{\partial T_p}{\partial log|t_a|}\right)_{q_1,T_a,q_2} = 2.54z - 3.83$, implies that the shift factor is no longer a constant, but dependent on the aging time, t_a. Hence, without $\hat{s}\left(\bar{D}\right)$, it is not possible to determine either the TNM non-linearity parameter, x, or the non-exponentiality parameter, β.

Unlike analysis seen in PC alone [Hutchinson *et al.* 1999; Lee-Sullivan and Bettle 2005], it is not possible to read a value off the master curve as originally proposed by reference [Hutchinson and Ruddy 1988]. The inability to determine a shift factor for both components may only be related to this specific system of blend, and may not necessarily be the case for differing systems. In this case, it is clear that the two-peak behaviour complicates the analysis considerably.

4.5.2 Cowie-Ferguson Semi-Empirical Data Fit

Other than the phenomenological models described in section 1.3, a semi-empirical approach adopted by Cowie and Ferguson [1989; 1993] have been used to describe the physical aging process. According to Cowie and Ferguson, the enthalpy relaxed at any aging temperature and time can be expressed as:

$$\Delta H(T_a, t_a) = \Delta H_\infty(T_a)\,(1 - \Phi(t)) \qquad \textbf{(39)}$$

where $\Phi(t)$ is the KWW function in equation (9); $\Delta H_\infty(T_a)$ is the equilibrium excess enthalpy recovered after an infinite time. The experimental relaxation data obtained from the progressive physical aging study are shown in Figure 4.26 and have been fitted to the above expression using a curve-fitting routine with a least-squares minimization approach. This is therefore a 3-parameter curve-fitting routine. Ideally, sufficiently long aging times that show a plateau should be achieved, thus minimizing errors in the data fitting. However, it is evident in the figure that this condition has not been met. Moreover, a sufficiently long aging time to produce a point in the plateau region increases exponentially. The furthest experimental data point occurs at 42 days, but comparatively a point sufficiently further point in the plateau region would require upwards of 2 years. The resulting best fit parameters that produce the continuous curve shown are summarized in Table 4.7.

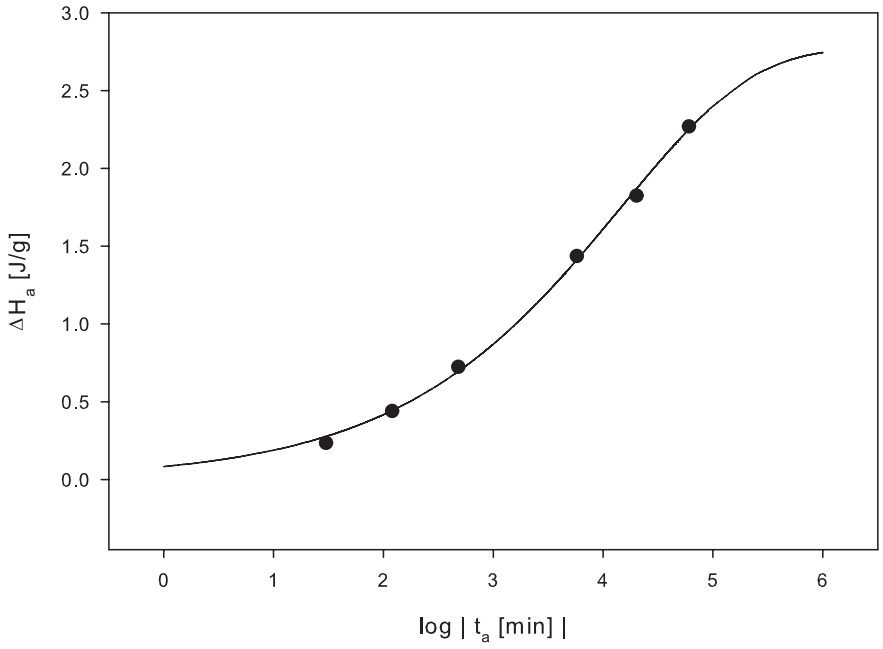

Figure 4.26: Enthalpy relaxation data (●) fit to Cowie-Ferguson expression (solid line)

β	Log (τ) [min]	ΔH_∞ [J/g]
0.37 ± 0.02	4.1 ± 0.2	2.75 ± 0.2

Table 4.7: Cowie-Ferguson parameters obtained from least-squares 3-parameter data fit

As described earlier, β is a measure of the breadth of this relaxation spectrum, but it can also be interpreted as a measure of co-operativity between the relaxation molecules. The greater the degree of co-operativity, the less time is required for relaxation. On the other hand, less co-operativity would require longer relaxation times and hence a broader spectrum. In comparison, β for a single polymer PC system was found to lie between $0.45 < \beta < 0.6$ [Hutchinson 1999; Lee-Sullivan and Bettle 2005]. While this suggests that there is a greater degree of co-operativity in the present PC/ABS blend than in PC alone, it also supports and confirms the intention that PC/ABS was to bring improved flow and processability characteristics over the PC component alone.

4.6 HYGROTHERMAL RESPONSE

4.6.1 Moisture Uptake Behaviour

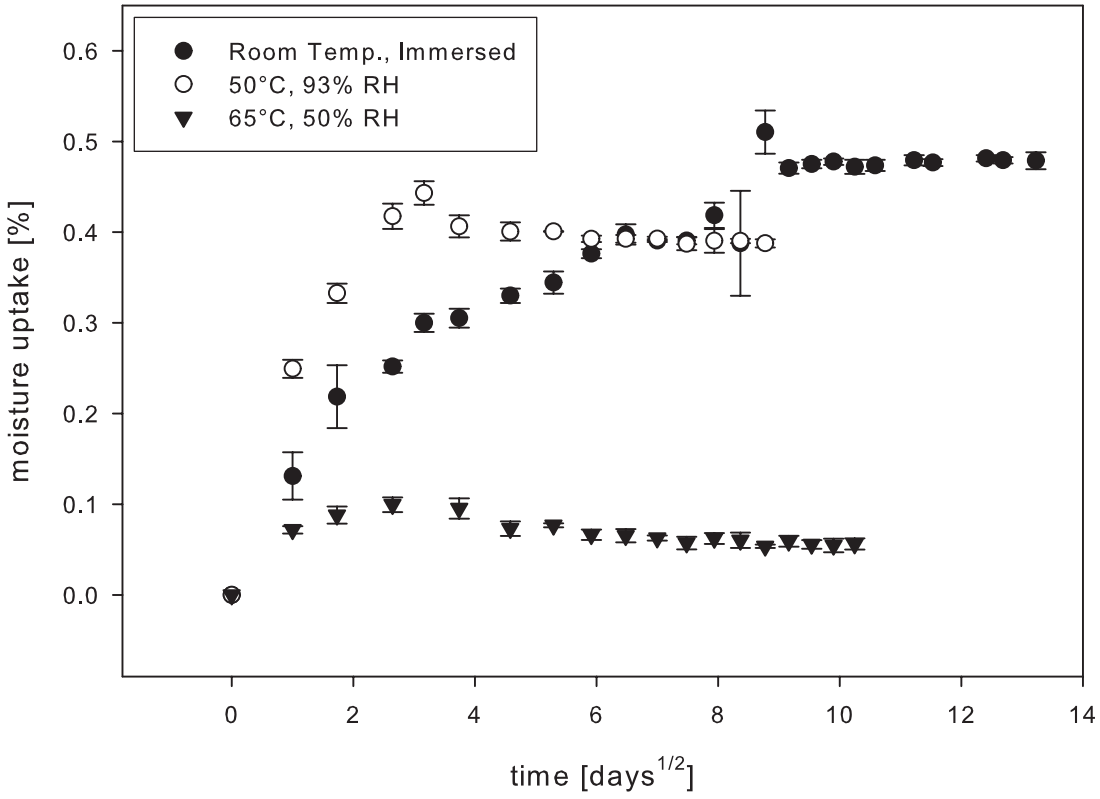

Figure 4.27: Moisture uptake behaviour of (●) fully immersed sample at room temperature (□) 50°C and 93% RH (▲) 65°C and 50% RH

The moisture uptake due to hygrothermal exposure is compared against the fully immersed sample at room temperature in Figure 4.27. The fully immersed moisture absorption samples (●) indicate that a steady equilibrium of moisture content is reached at approximately 0.5%. The moisture uptake quoted in the data sheet by the manufacturer of 0.11% after 24 hours appears to lend support to the accuracy of this study. Upon closer inspection, after the quick linear increase of the initial slope, there appears to be a small step before increasing again to the final equilibrium content of 0.5%. This resembles the anomalous two-stage diffusion behaviour as discussed by Cai and Weitsman [Cai and Weitsman 1994]. Formulations of the Fickian analytical solution according to equation (17) are fitted to the experimental data shown in Figure 4.28, providing an upper and lower bound. This illustrates more clearly the transition occurring from the lower concentration to the higher.

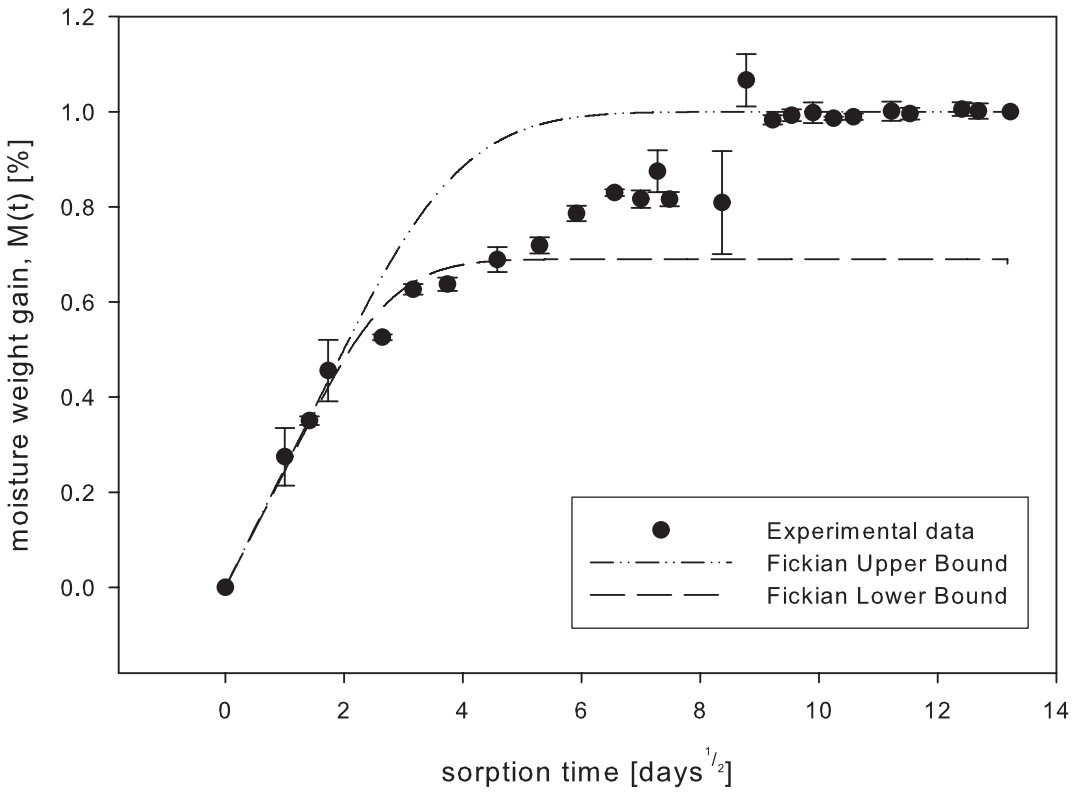

Figure 4.28: Overall moisture weight gain immersed at room temperature and Fickian bounds

The moisture uptake behaviour for hygrothermally conditioned at 50°C / 93% RH and at 65°C/50% RH as denoted by (○) and (▼), respectively, are also plotted in Figure 4.27. In contrast to the fully immersed sample, the moisture uptake is single-staged, with a slight overshoot before saturation. This is similar to the findings by Narkis *et al.* [1985] for glass-fibre reinforced PC which exhibits distinct differences in equilibrium liquid water sorption between 100°C and room temperature (0.6% and 0.3%, respectively). However, it was noted in that study that the anomalous (overshoot) behaviour was only observed for unfilled PC at 100°C before reaching saturation in 10 days.

In the present results, the overshoot is observed in both hygrothermal conditions although saturation did not occur as quickly. For 65°C/50% RH samples, saturation occurred closer to 35 days and the level was minimal at about 0.06%. In comparison, the equilibrating moisture content for the fully immersed sample was 0.5%. On the other hand, these results differed from the work by Thominette *et al.* [1996] on PC where an equilibrium moisture content of approximately 0.5% is reached, independent of the moisture absorption temperature.

By plotting the normalized overall weight gain in Figure 4.29 it can be seen that increasing the conditioning temperature, i.e. from room temperature to 50°C and then to 65°C, increases the rate of initial weight gain. As the diffusion coefficient for a system is proportional to the initial slope of the weight gain, the 65°C/50% RH sample has a greater diffusion coefficient than 50°C/93% RH sample. This was inspite of the relative humidity being doubled. However, the overall weight gain at saturation was very similar. These coefficients are determined according to equation (18) and tabulated in Table 4.8 along with the equilibrium moisture content and equilibrium time as discussed above.

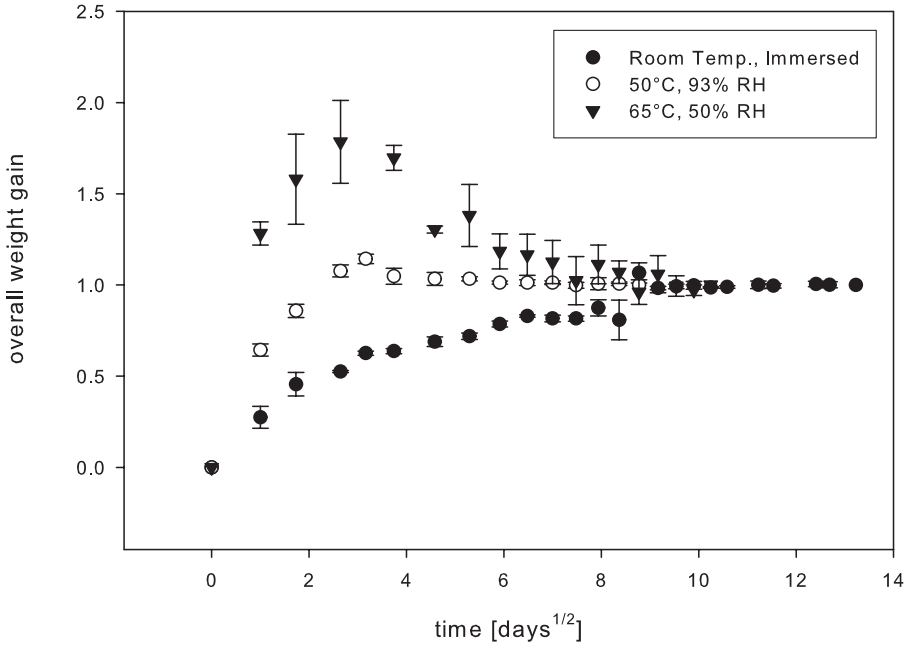

Figure 4.29: Overall weight gain of (●) fully immersed sample at room temperature (○) 50°C and 93% RH (▼) 65°C and 50% RH

Aging Temperature, T_a [°C]	Ambient Moisture Content	Diffusion Coefficient, D x 10^{-12} [m^2 s^{-1}]	Equilibrium Moisture, M_∞ [%]	Equilibrium Time, t_{eq} [days]
65	50% RH	22.67	0.06	~35
50	93% RH	5.67	0.4	~45
~23 (Room)	Immersed	1.15	0.5	~85

Table 4.8: Summary of moisture absorption behaviour with aging conditions

It can be seen from this study that the short-term (approximately first 30 days) moisture absorption behaviour is greatly dependent on the aging and moisture exposure. At the beginning of the exposure, the molecular structure of the samples contained excess free volume due to the cooling from above the glass transition temperature (after erasing the thermal history). With excess volume, water molecules are easily transported and fit into the polymer blend system. Therefore, the higher the moisture absorption temperature is, the greater the energy for the water molecules to diffuse into the polymer blend. This explains the overshoot at elevated temperatures. It should be noted, however, that even at the highest temperature with moisture content in this study (65°C), this temperature is still below the glass temperature of the component materials, hence does not cause rapid relaxation in the molecular structure. At room temperature, less thermal energy is available for the transport process, and therefore the slow approach to equilibrium.

However, it is seen in the long-term that aging is the ultimate driving force of this free volume study. After sufficient aging time, the free volume contraction during structural relaxation reaches a point where the diffusion mechanism can no longer transport anymore water molecules into the system. Moreover, in the case of the systems that overshoot, excessive moisture content has penetrated and eventually the contraction process *squeezes* out the excess moisture to attain equilibrium. If the opposite were true, in that moisture diffusion is the dominant process, it should be seen that any moisture absorbed would not be desorbed, as in the case of the overshooting behaviour. Although there was no desorption seen in the samples fully immersed at room temperature, by the time a significant amount of moisture could penetrate the polymer system, the free volume had already contracted due to aging to prevent much more moisture to diffuse through.

It can be seen in Figure 4.11 that the enthalpy relaxation behaviour has yet to show any signs of approaching equilibrium, where as the moisture uptake, which can be associated with the free volume, begins to approach equilibrium after 30 days. It is well known that enthalpy and volume are internal state properties measured during aging that provide similar but non-identical relaxing behaviour. In fact, it was noted by Kovacs [1958] and Petrie [1972] that the time required to reach equilibrium is considerably longer in enthalpy than in volume relaxation.

4.6.2 ATR-FTIR Measurements

Figure 4.30 through Figure 4.32 show the progressive changes in the FTIR spectra for the hygrothermally aged samples fully immersed at room temperature, 50°C and 93% RH, and 65°C and 50% RH, respectively.

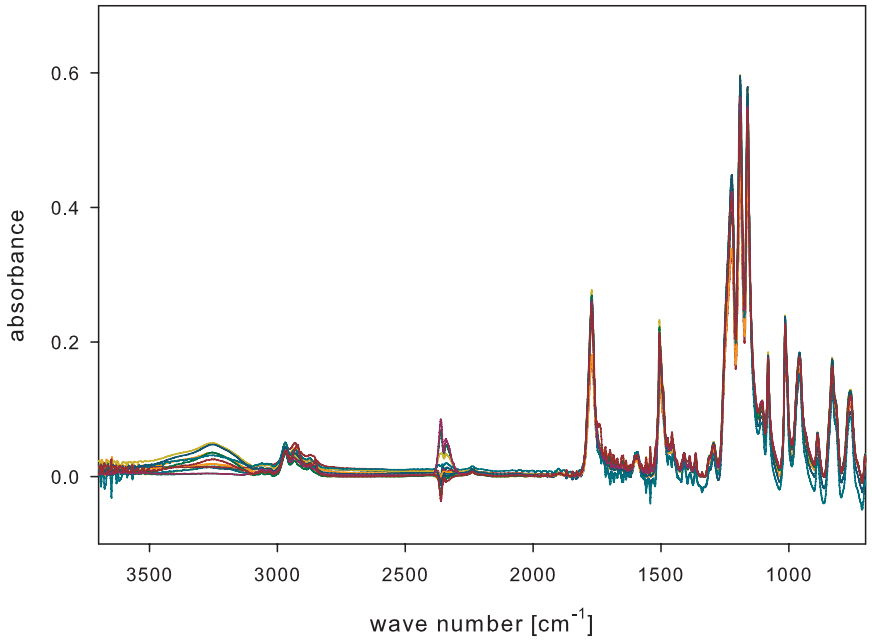

Figure 4.30: Progressive ATR-FTIR spectra of hygrothermally aged samples fully immersed at room temperature

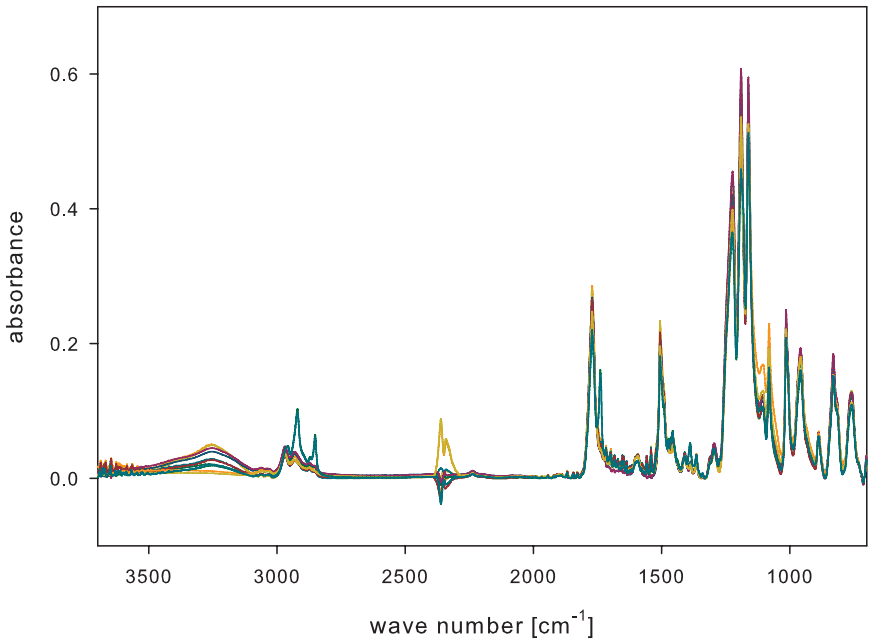

Figure 4.31: Progressive ATR-FTIR spectra of hygrothermally aged samples at 50°C and 93% RH

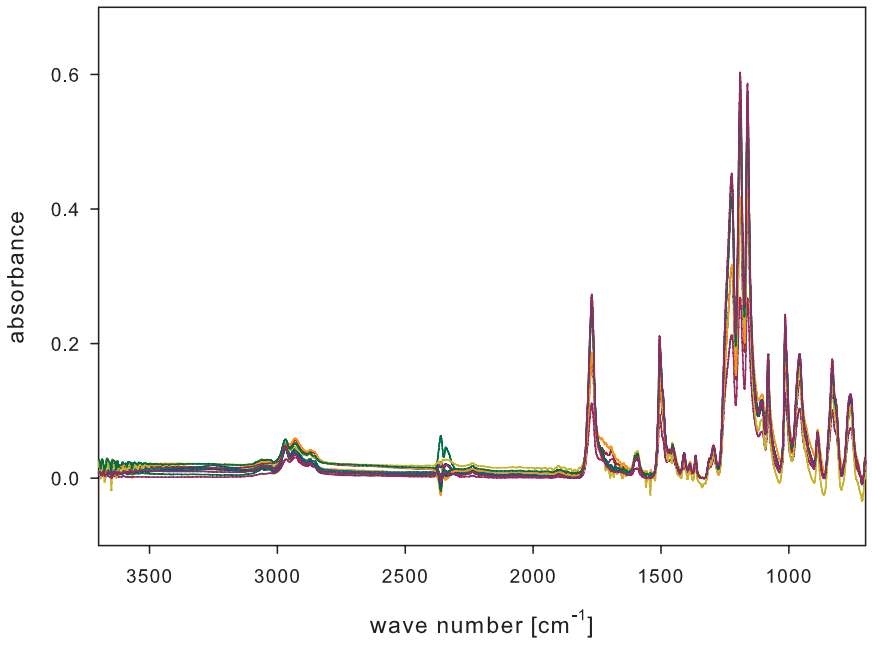

Figure 4.32: Progressive ATR-FTIR spectra of hygrothermally aged samples at 65°C and 50% RH

It is expected that the absorbance in the hydroxyl region (3000 – 3500 cm^{-1}) increases in intensity just as it did for physical aging at 80°C, which is seen to be the case in Figure 4.30 and Figure 4.31. Surprisingly however, hygrothermally aging at 65°C and 50% RH (Figure 4.32) does not produce similar results; the formation of hydroxyl groups for the duration of the study were not observed even though moisture is deliberately added to the study.

Upon closer inspection of the carbonyl region for the three hygrothermal conditions, no appreciable changes were found that indicated any changes occurred due to hygothermal conditioning. For example, the carbonyl region is shown in Figure 4.33 for the samples at 65°C and 50% RH.

Figure 4.34 illustrates the absorbance intensity values in the carbonyl region (normalized to the reference peak height) for the three hygrothermal conditions. Even though conditioning at 65°C well below $T_{g,PC}$ for physical aging or relaxation to occur, it is surprising that the addition of moisture does not affect the carbonyl bonds.

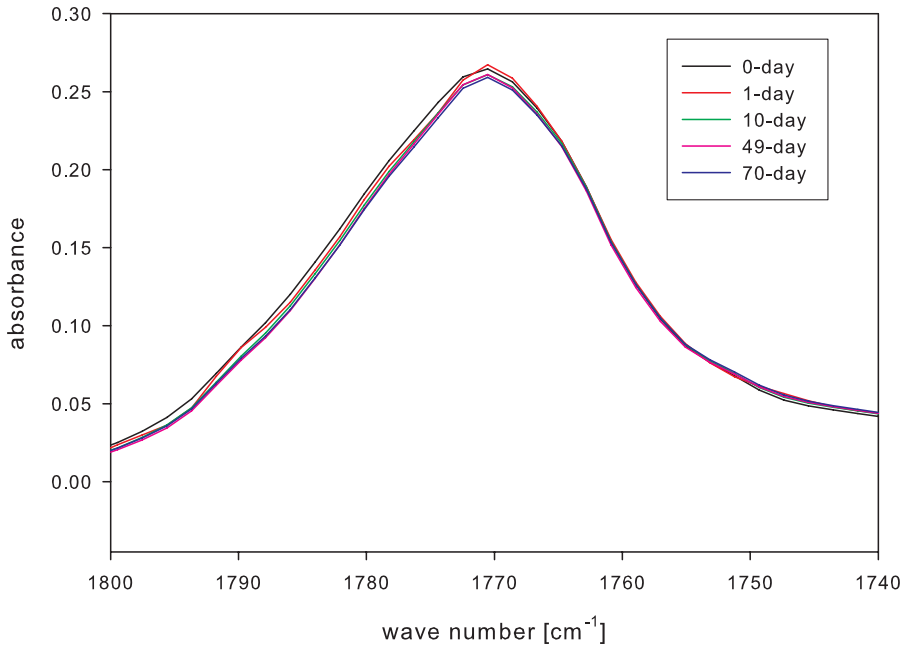

Figure 4.33: Absorbance of carbonyl region (1770 cm-1) at 65°C and 50% RH

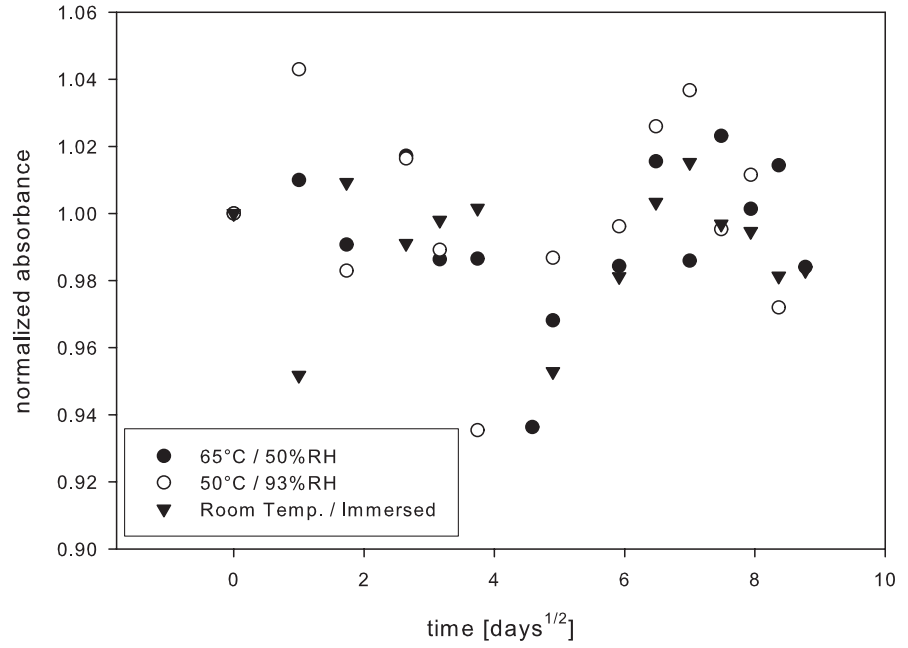

Figure 4.34: Normalized peak absorbance intensity of C=O aged at 65°C and 50% RH (●), 50°C and 93% RH (○) and fully immersed at room temperature (▼)

At 65°C, which is still within a reasonable temperature range of $T_{g,ABS}$ for relaxation in ABS to occur, Figure 4.35 shows a subtle decrease in the absorbance intensity in the butadiene region (▼). The normalized absorbances for the three hygrothermal conditions are illustrated in Figure

4.36. Although the data appears scattered and inconclusive of any other trends, it is noted that almost all of the data lie below unity, which indicates that the butadiene absorbance does tend to decrease during this hygrothermal study.

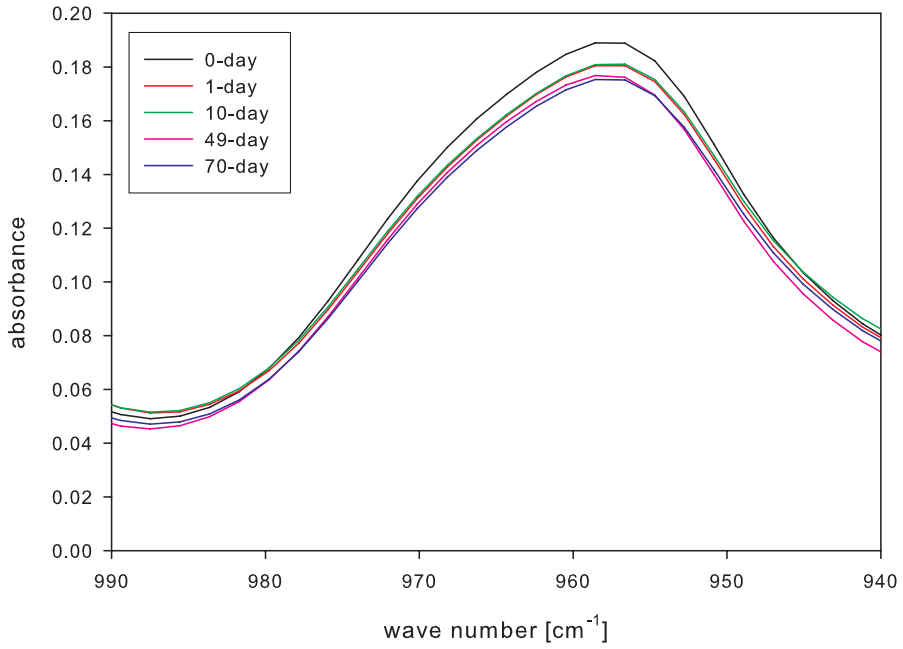

Figure 4.35: Absorbance of polybutadiene region (960 cm^{-1}) at 65°C and 50% RH

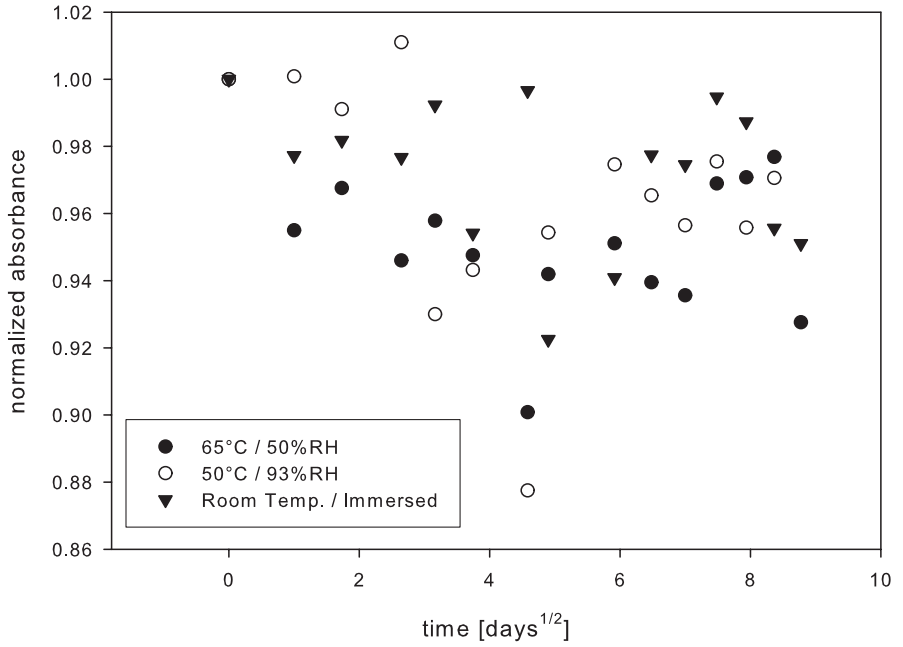

Figure 4.36: Normalized peak absorbance intensity of polybutadiene region aged at 65°C and 50% RH (●), 50°C and 93% RH (○) and immersed at room temperature (▼)

It may be tempting to associate the subtle decrease in the butadiene absorbance as a result of oxidation, as was seen in physical aging at 80°C, and further investigation is required to verify. It is as if these hygrothermal conditions pose a less severe environment for aging, not only because the temperature is lower as compared to the physical aging study at 80°C, but also due to lower presence of oxygen.

It can be reasoned that when fully immersed under water, the absence of oxygen prevents the oxidation process from occurring. At 50°C and 93% RH as well as 65°C and 50% RH where it is assumed that the presence of oxygen in the environment increases again with the decrease in moisture content, the oxidation process is more likely to happen. Moreover, the difference of aging in air and water (for polypropylene) has been studied in literature which has shown similar findings [Groff *et al.* 1996].

However, if there is little to no oxidation occurring, what is causing the hydroxyl (but not carbonyl) region to increase in absorbance? Although further investigation is necessary, it is plausible that hydrogen bonding has occurred, which has been shown in other studies [Zhang et al. 2002; Malek and Chong 2000] to cause absorbance increases within the same region.

The FTIR spectra shown in Figure 4.37 illustrates the final state of the 3 hygrothermal conditions in comparison to the unaged state. As previously mentioned, the presence of hydroxyl groups was not observed in the 65°C and 50% RH condition. However, it appears that the hydroxyl groups (between 3000–3500 cm^{-1}) in the other two hygrothermal conditions reach the same point of saturation. If the mechanism is indeed hydrogen bonding, then the formation of hydrogen bonds is independent of moisture concentration in the environment.

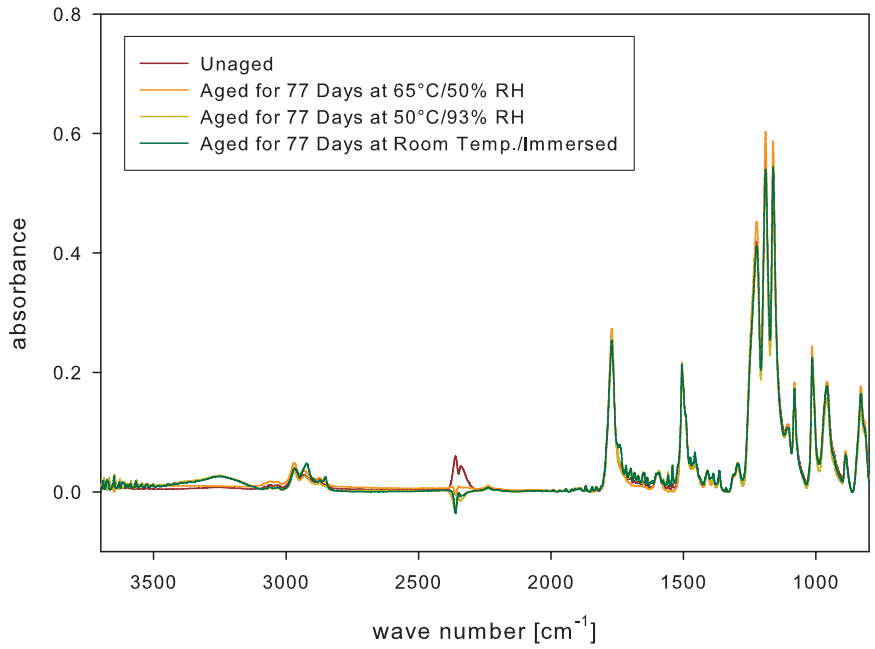

Figure 4.37: ATR-FTIR spectra of 3 hygrothermal conditions at end of aging study

Once again, it can be seen in the spectra shown in Figure 4.30 through Figure 4.32 that the characteristic C≡N absorption band for the acrylonitrile component occurring near 2250 cm^{-1} is almost undetectable.

Chapter 5 CONCLUSIONS AND RECOMMENDATIONS

5.1 CONCLUSIONS

The goal of this work was to characterize molecular processes associated with physical aging and hygrothermal moisture absorption in a polycarbonate/acrylonitrile-butadiene-styrene (PC/ABS) blend. Based on three different sets of experimental studies using Differential Scanning Calorimetry (DSC) and Fourier Transform Infrared Spectroscopy (FTIR), the following conclusions can be made:

(i) Using DSC analysis, it can be concluded that the apparent activation energy for enthalpy relaxation for the unaged material is 757 kJ/mol. This value which falls between the activation energies for PC and ABS does not follow a simple rule-of-mixtures. When PC/ABS is aged at 80 and 90°C, there are signs of self-retardation behaviour during relaxation but this phenomenon is absent when aging at 100°C. This suggests that the practical aging temperature range for studying physical aging for this blend is between 80 to 90°C.

(ii) A subsequent progressive aging study conducted at 80°C concluded that enthalpy relaxation occurred at a rate of 0.62 J/g per decade of aging time. This is very similar to reported values for polycarbonate. The enthalpy relaxation process has yet to reach equilibrium for the 42-day study. However, T_g of the ABS component was found to be insensitive to aging time. The T_g of the PC component decreased (shifted towards that of ABS) suggesting that the miscibility of the two components improved with aging time.

Enthalpic relaxation can be expected to continue at 80^{o}C even after 42 days of thermal aging. However, the molecular processes associated with the enthalpic relaxation are not linked with conformational rearrangements. FTIR aging data for nearly 80 days showed no sign of transformation from high energy, *trans-cis*, conformation to low energy, *trans-trans*, conformation, which was reported for polycarbonate alone.

However, FTIR studies revealed that butadiene group was oxidized, forming hydroxyl and carbonyl groups after approximately 10 days of aging and appear to stabilize after 25 days of aging. Carbonyl groups continue to form after 25 days of aging, which is tied to the aging of the PC component.

(iii) An attempt to curve fit the relaxation data using a phenomenological indicates that multiple endothermic peaks cause complications in applying the well-known Tool-Narayanaswamy-Moynihan model. A semi-empirical model proposed by Cowie and Ferguson was applied instead to fit the experimental data which provided a reasonable estimate of the relaxation behaviour. Aging at 80°C or the period investigated did not reach equilibrium and it is expected that aging times of upwards of 2 years will be necessary to minimize the errors associated with the data fitting to provide a better fit of the model.

In addition, an alternative analytical method was proposed to evaluate the differences in relaxation mechanisms as the aging temperature changes from $T_{g,ABS}$ to sub-$T_{g,PC}$. Using the concept of an apparent activation energy, it was found that enthalpy relaxation increased with aging time, except for samples aged at 100°C, suggesting that mechanisms during structural relaxation at sub-$T_{g,ABS}$ are very different from that at sub-$T_{g,PC}$ temperatures.

(iv) Hygrothermal studies were conducted to understand the combined effects of moisture absorption and thermal aging. It can be concluded that moisture uptake in the presence of heat in PC/ABS follows diffusion theory where the equilibrium moisture content is dependent and proportional to the surrounding environment's moisture content. Different hygrothermal conditions results in different moisture absorption curves, e.g. two-stage as opposed to overshooting. The effect of temperature is perhaps most prominent in the initial moisture absorption rate. The absorption rate, as characterized by the coefficient of diffusion, is strongly dependent on the environmental condition.

It is intuitive that volumetric contraction during thermal aging and free volume expansion due to moisture swelling are competing mechanisms in the present hygrothermal studies. However, our work indicates that the volumetric relaxation mechanism appears to eventually overcome the swelling of moisture diffusion. Regardless of the conditioning environment, saturation occurs at approximately 36 days. Hygrothermal aging in fact prevents the oxidation from occurring due to the absence of oxygen as demonstrated in the results of PC/ABS fully immersed in water. There is some but not conclusive evidence that hydrogen bonds are formed during hygrothermal aging and that the amount of hydrogen bonds formed saturates over time.

5.2 RECOMMENDATIONS

To further this study, the following recommendations to future work can be made:

(i) progressive physical aging studies at different temperatures, and adapt the enthalpy relaxation data to the semi-empirical model for comparisons of parameters, β and τ

(ii) volumetric relaxation study by TMA for comparison of fictive relaxation rate

(iii) hygrothermal conditions with the same temperature as those currently studied with different relative humidity, or the same relative humidity at other (higher) temperatures

REFERENCES

1. Alfrey T, Gurnee EF and Lloyd WG. *Journal of Polymer Science – Polymer Symposia Part C*, 12: 249–261, 1966.
2. Alpert NL, Keiser WE and Szymanski HA. "Theory and Practice of Infrared Spectroscopy", Plenum Press, New York, 1970.
3. (ASTM) American Society for Testing and Materials, D570 Standard Test Method for Water Absorption of Plastics, 1998.
4. (ASTM) American Society for Testing and Materials, E967 Temperature Calibration of Differential Scanning Calorimeters and Differential Thermal Analyzers, 1983.
5. (ASTM) American Society for Testing and Materials, E968 Heat Flow Calibration of Differential Scanning Calorimeters, 1983.
6. (ASTM) American Society for Testing and Materials, E1269 Standard Test Method for Determining Specific Heat Capacity by Differential Scanning Calorimetry, 2001.
7. (ASTM) American Society for Testing and Materials, E1356 Standard Test Method for Assignment of the Glass Transition Temperatures by Differential Scanning Calorimetry, 2003.
8. (ASTM) American Society for Testing and Materials, E1545 Standard Test Method for Assignment of the Glass Transition Temperature by Thermomechanical Analysis, 2000.
9. Avramov I. *Journal of Mining and Metallurgy*, 36B(1): 11–28, 2000.
10. Balart R, Lopez J, Garcia D and Salvador MD. *European Polymer Journal*, 41: 2150–2160, 2005.
11. Bauwens-Crowet C and Bauwens JC. *Polymer*, 27(5): 709–713, 1986.
12. Biddle MB and Christy MR. *Appliance Manufacturer*, 5: 57, 1992.
13. Cai LW and Weitsman Y. *Journal of Composite Materials*, 28(2): 130–154, 1994.
14. Callister WD. "Materials science and engineering – an introduction", John Wiley & Sons Inc., Toronto, Canada, 1997.
15. Cheng TW, Keskkula H and Paul DR. *Journal of Applied Polymer Science*, 45: 531–551, 1992.
16. Choquette SJ, Travis JC, Zhu CJ and Duewer DL. "Handbook of Vibrational Spectroscopy: Wave Number Standards for Near-Infrared Spectroscopy", John Wiley & Sons Ltd, Chichester, 2002.

17. Cohen MH and Turnbull D. *Journal of Chemical Physics*, 31: 1164–1169, 1959.
18. Coleman PB. "Practical Sampling Techniques for Infrared Analysis", CRC Press, Boca Raton, 1993.
19. Cowie JMG and Ferguson R. *Macromolecules* 22(5): 2307–2312, 1989.
20. Cowie JMG and Ferguson R. *Macromolecules* 22(5): 2312–2317, 1989.
21. Cowie JMG and Ferguson R. *Polymer* 34(10): 2135–2141, 1993.
22. Crank JS and Park GS. "Diffusion in Polymers", Academic Press, Oxford, 1975.
23. Doolittle AK. *Journal of Applied Physics*, 22(9): 1471–1475, 1951.
24. Dykeman D and Lee-Sullivan P. *Polymer Engineering and Science*, 43(2): 383–397, 2003.
25. Eguiazabal JI and Nazabal J. *Journal of Polymer Engineering and Science*, 30: 527, 1990.
26. Ferrillo RG (Cytec Industries) and Achorn PJ. *Journal of Applied Polymer Science*, 64(1): 191–195, 1997.
27. Fick A. *Ann. Der. Phys.*, 94: 59–86, 1855.
28. Fulcher GS. *Journal of the American Ceramic Society*, 8(6): 339, 1925.
29. Garton A. "Infrared Spectroscopy of Polymer Blends, Composites and surfaces", Sellier Druck GmbH, Freising, Germany, 1992.
30. Groff I, Franzese R, Landro LD, Pagano MR and Genoni M. *Polymer Testing* 15: 347–361, 1996.
31. Guest MJ and Van Daele R. *Journal of Applied Polymer Science*, 55: 1417–1429, 1995.
32. Gugumus F. *Polymer Degradation and Stability*, 62(8): 235–243, 1998.
33. Hadac J, Slobodian P and Saha P. *Journal of Thermal Analysis and Calorimetry*, 80, 181–185, 2005.
34. Heymans N. *Polymer*, 38(14), 3435–3440, 1997.
35. Heymans N and Van Rossum S. *Journal of Materials Science*, 37: 4273–4277, 2002.
36. Ho CH and Vu-Khanh T. *Theoretical and Applied Fracture Mechanics*, 41, 103–114, 2004.
37. Hodge IM. *Macromolecules*, 20(11): 2897–2908, 1987.
38. Hodge IM. *Journal of Non-Crystalline Solids*, 169: 211–266, 1994.
39. Hodge IM. *Journal of Research of the National Institute of Standards and Technology*, 102(2): 195–205, 1997.
40. Hutchinson JM. *Progress in Polymer Science*, 20(4): 703–760, 1995.
41. Hutchinson JM and Kumar P. *Thermochimica Acta*, 391: 197–217, 2002.

42. Hutchinson JM and Ruddy M. *Journal of Polymer Science: Part B: Polymer Physics*, 26(11): 2341–2366, 1988.
43. Hutchinson JM, Smith S, Horne B and Gourlay GM. *Macromolecules*, 32: 5046–5061, 1999.
44. Hutchinson JM, Tong AB and Jiang Z. *Thermochimica Acta*, 335: 27–42, 1999.
45. Keitz JD, Barlow JW and Paul DR. *Journal of Applied Polymer Science*, 29(10): 3131–3145, 1984.
46. Kovacs AJ. *Journal of Polymer Science*, 30 : 131–147, 1958.
47. Kovacs AJ. *Fortschritte der Hochpolymeren – Forschung*, 3: 394, 1963.
48. Kovacs AJ, Aklonis JJ, Hutchinson JM and Ramos AR. *Journal of Polymer Science, Polymer Physics Edition*, 17(7): 1097–1162, 1979.
49. Kuczynski J, Snyder RW and Padolak PP. *Polymer Degradation and Stability*, 43(2): 285–291, 1994.
50. Lee S and Knaebel KS. *Journal of Applied Polymer Science*, 64(3): 455–476, 1997.
51. Lee-Sullivan P and Bettle M. *Journal of Thermal Analysis and Calorimetry*, 81(1): 169–177, 2005.
52. Li XG and Huang MR. *Polymer International*, 48: 387–391, 1999.
53. Li C, Zhang Y and Zhang Y. *Journal of Applied Polymer Science*, 89: 589–595, 2003.
54. Liu LB, Yee AF and Gidley DW. *Journal of Polymer Science: Part B: Polymer Physics*, 30, 221–230, 1992.
55. Lodge TP, Wood ER and Halley JC. *Journal of Polymer Science: Part B: Physics*, 44: 756–763, 2006.
56. Lu J, Wong Y and Shen D. *Polymer Journal*, 32(7): 610–615, 2000.
57. Malek J. *Thermochimica Acta*, 313(2): 181–190, 1998.
58. Malek J. *Macromolecules*, 31(23): 8312–8322, 1998.
59. Malek J and Montserrat S. *Thermochimica Acta*, 313(2): 191–200, 1998.
60. Malek J and Mitsuhashi T. *Journal of Thermal Analysis and Calorimetry*, 57(3): 707–716, 1999.
61. Malek J and Shanelova J. *Journal of Thermal Analysis and Calorimetry*, 60(3): 975–988, 2000.
62. Malek MA and Chong CS. *Vibrational Spectroscopy*, 24: 181–184, 2000.

63. Más J, Vidaurre A, Meseguer JM, Romero F, Monleon Pradas M, Gomez Ribelles JL, Maspoch MLL, Santana OO, Pages P and Perez-Folch J. *Journal of Applied Polymer Science*, 83: 1507–1516, 2002.
64. *MatWeb – Online Material Data Sheet*: Acrylonitrile Butadiene Styrene (ABS), Molded, URL: http://www.matweb.com/search/SpecificMaterial.asp?bassnum=O1100, Date Accessed: Sept. 2005.
65. *MatWeb – Online Material Data Sheet*: Polycarbonate (PC), Molded, URL: http://www.matweb.com/search/SpecificMaterial.asp?bassnum=O3100, Date Accessed: Sept. 2005.
66. McCrum N, Wiliams G and Read B. "Anelastic and Dielectric Effects in Polymeric Solids", Dover, New York, 1967.
67. McKenna GB and Simon SL. The glass transition: Its measurement and underlying physics. In S. Z. D. Cheng, editor, Handbook of Thermal Analysis and Calorimetry. Vol. 3: Applications to Polymers and Plastics, Chapter 2, pages 49–109. Elsevier, Amsterdam, 2002.
68. Menard KP. "Dynamic Mechanical Analysis A Practical Introduction", CRC Press LLC, Florida, pp. 4, 6, 18, 92, 1999.
69. Montgomery DC. Design and Analysis of Experiments. John Wiley & Sons, Inc., Fifth edition, 2001.
70. Motyakin MV and Schlick S. *Polymer Degradation and Stability*, 76: 25–36, 2002.
71. Moynihan CT, Easteal AJ, Wilder J and Tucker J. *Journal of Physical Chemistry*, 78: 2673–2677, 1974.
72. Moynihan CT, Easteal AJ and DeBolt MA. *Journal of the American Ceramic Society*, 59(1-2): 12–16, 1976.
73. Moynihan CT, Macedo PB, Gupta PK, Monrose CJ, DeBolt MA, Dill JF, Dom BE, Drake PW, Easteal AJ, Elerman PB, Moeller RP, Sasabe H and Wilder JA. *Ann. N. Y. Acad. Sci.*, 279: 15, 1976.
74. Moynihan CT, Lee SK, Tatsumisago M, and Minami T. *Thermochimica Acta*, 280-281: 153–162, 1996.
75. Narkis M, Chaouat-Sibony S, Nicolais L, Apicella A, and Bell JP. *Polymer Communications*, 26(11): 339–342, 1985.

76. Nigam I, Nigam D and Mathur GN. *Polymer-Plastics Technology and Engineering*, 44(5): 815–832, 2005.
77. Ning YC. "Structural Identification of Organic Compounds with Spectroscopic Techniques", Wiley-VCH Verlag GmbH & Co. KGaA, Weinheim, 2002.
78. NUANCE (Northwestern University, Atomic and Nanoscale Characterization Experimental Center), Evanston, IL 60208-3108, 2006 – Retrieved May, 2006: http://www.nuance.northwestern.edu/KeckII/ftir2.asp.
79. Patty, BS. *Annual Technical Conference - ANTEC, Conference Proceedings: Special Areas*, 3: 4054–4061, 2004.
80. Petrie SEB. *Journal of Polymer Science, Macromolecular Reviews*, 10(7), 1255–1272, 1972.
81. Plazek DJ and Bero CA. *Journal of Physics: Condensed Matte*r, 15: S789–S802, 2003.
82. Qayyum MM and White JR. *Journal of Applied Polymer Science*, 43: 129–144, 1991.
83. Ram A, Zibler O and Kenig S. *Polymer Engineering and Science*, 25(9): 535–540, 1985.
84. Richardson MJ and Savill NG. *Polymer*, 16: 753–757, 1975.
85. Rjeb A, Tajounte L, Chafik El Idrissi M, Letarte S, Adnot A, Roy D, Claire Y, Périchaud A and Kaloustian J, *Journal of Applied Polymer Science*, 77(2): 1742–1748, 2000.
86. Roy S. "Hygrothermal Modeling of Polymers and Polymer Matrix Composites", Time Dependent and Nonlinear Effects in Polymers and Composites, ASTM STP 1357, Schapery, R. A. and Sun, C. T., Eds., American Society for Testing and Materials, West Conshohocken, PA, pp. 338–352, 2000.
87. Rusch KC. *Journal of Macromolecules Science, Physics B2(3),* 421–447, 1968.
88. Santana OO, Maspoch MLL and Martinez AB. *Polymer Bulletin*, 41: 721–728, 1998.
89. Sato M, Koshino T, Kajitani Y, Inamu I and Kubo Y. *Journal of Applied Polymer Science*, 93: 1616–1622, 2004.
90. Schultheisz CR and McKenna GB. *Polymeric Materials Science and Engineering*, Proceedings of the ACS Division of PMSE, 76, 221–222, 1997.
91. Seyler RJ. *STP 1249: Assignment of the Glass Transition*. American Society for Testing and Materials (ASTM), Philadelphia, 1994.
92. Silverstein RM, Bassler GC, and Morill TC, "Spectrometric Identification of Organic Compounds", 5th Ed., John Wiley & Sons, Inc., USA, 1991.

93. Simon SL and McKenna GB. *Thermochimica Acta*, 348: 77–89, 2000.
94. Simon SL. *Thermochimica Acta*, 374(1): 55–71, 2001.
95. Slobodian P, Lengalova A, and Saha P. *Journal of Thermal Analysis and Calorimetry*, 71: 387–393, 2003.
96. Struik LCE. "Physical aging in amorphous polymers and other materials", Elsevier, New York, 1978.
97. Stuart BH. "Infrared Spectroscopy: Fundamentals and Applications", John Wiley & Sons, Ltd., 2004.
98. Su CC and Shih CK. *Journal of Applied Polymer Science*, 100: 3840–3849, 2006.
99. Tammann G and Hesse W. *Journal of Inorganic and General Chemistry*, 156(4): 245–257, 1926.
100. Thomas LC. TP 006 — Modulated DSC Paper 1: Why Modulated DSC? An Overview and Summary of Advantages and Disadvantages Relative to Traditional DSC. Technical report, TA Instruments, 2005.
101. Thomas LC. TP 008 — Modulated DSC Paper 3: Modulated DSC Basics; Optimization of MDSC Experimental Conditions. Technical report, TA Instruments, 2005.
102. Thomas LC. TP 010 — Modulated DSC Paper 5: Measurement of Glass Transitions and Enthalpic Recovery. Technical report, TA Instruments, 2005.
103. Thominette NAF, Paris D, Pays MF, and Verdu J. *Journal of Materials Science Letters*, 15: 1001–1002, 1996.
104. Tool AQ. *United States Bureau of Standards - Journal of Research*, 34(2): 199–211, 1945.
105. Tool AQ. *United States Bureau of Standards – Journal of Research*, 37(2): 73–90, 1946.
106. Tool AQ. *American Ceramic Society - Journal*, 29(9): 240–253, 1946.
107. Turnbull D and Cohen MH. *Journal of Chemical Physics*, 34: 120–125, 1961.
108. Vogel H. *Physik Zeitschrift*, 22: 645–646, 1921.
109. Vrentas JD, Duda JL and Huang JW. *Macromolecules*, 19(6): 1718–1724, 1986.
110. Wang CH. *Annual Technical Conference - ANTEC, Conference Proceedings*, Vol. 2, 1946–1948, 1995.
111. Zhang Z, Mo Z, Zhang H, Zhang Y, Na T, An Y, Wang X and Zhao X. *Journal of Polymer Science: Part B: Polymer Physics*, 40: 1957–1964, 2002.

APPENDIX A

CYCOLOY C6600 DATA SHEET

GE Plastics

Cycoloy* Resin C6600

Americas: COMMERCIAL

Nonbrominated, nonchlorinated FR PC+ABS with balanced flow, impact and hydrolytic stability for a wide variety of applications including business equipmer nonitors, enclosures, among others.

TYPICAL PROPERTIES [1]	TYPICAL VALUE	UNIT	STANDARD
MECHANICAL			
Tensile Stress, yld, Type I, 50 mm/min	63	MPa	ASTM D 638
Tensile Stress, brk, Type I, 50 mm/min	49	MPa	ASTM D 638
Tensile Strain, yld, Type I, 50 mm/min	4	%	ASTM D 638
Tensile Strain, brk, Type I, 50 mm/min	80	%	ASTM D 638
Tensile Modulus, 50 mm/min	3000	MPa	ASTM D 638
Flexural Stress, yld, 1.3 mm/min, 50 mm span	94	MPa	ASTM D 790
Flexural Modulus, 1.3 mm/min, 50 mm span	2620	MPa	ASTM D 790
IMPACT			
Izod Impact, notched, 23°C	550	J/m	ASTM D 256
Instrumented Impact Total Energy, 23°C	51	J	ASTM D 3763
Instrumented Impact Total Energy, -30°C	51	J	ASTM D 3763
THERMAL			
Vicat Softening Temp, Rate B/50	99	°C	ASTM D 1525
HDT, 1.82 MPa, 3.2mm, unannealed	83	°C	ASTM D 648
HDT, 0.45 MPa, 6.4 mm, unannealed	98	°C	ASTM D 648
HDT, 1.82 MPa, 6.4 mm, unannealed	90	°C	ASTM D 648
Relative Temp Index, Elec	80	°C	UL 746B
Relative Temp Index, Mech w/impact	70	°C	UL 746B
Relative Temp Index, Mech w/o impact	80	°C	UL 746B
PHYSICAL			
Specific Gravity	1.19	-	ASTM D 792
Water Absorption, 24 hours	0.11	%	ASTM D 570
Mold Shrinkage, flow, 3.2 mm	0.4 - 0.6	%	GE Method
Melt Flow Rate, 260°C/2.16 kgf	21.5	g/10 min	ASTM D 1238
ELECTRICAL			
Volume Resistivity	>1.E+15	Ohm-cm	IEC 60093
Surface Resistivity, ROA	>1.E+15	Ohm	IEC 60093
Dielectric Strength, in oil, 3.2 mm	17	kV/mm	IEC 60243-1
Relative Permittivity, 50/60 Hz	2.7	-	IEC 60250

1) Typical values only. Variations within normal tolerances are possible for variose colours.All values are measured at least after 48 hours storage at 230C/50% relative humidity.
All properties, expect the melt volume rate are measured on injection moulded samples.
All samples are prepared according to ISO 294.

2) Only typical data for material selection purpose.Not to be used for part or tool design.
3) This rating is not intended to reflect hazards presented by this or any other material under actual fire conditions.
4) Own measurement according to UL.

Source, GMD, Last Update:07/25/2005

GE Plastics

Cycoloy* Resin C6600

Americas: COMMERCIAL

TYPICAL PROPERTIES [1]	TYPICAL VALUE	UNIT	STANDARD
ELECTRICAL			
Relative Permittivity, 50/60 Hz	2.7	-	IEC 60250
Relative Permittivity, 1 MHz	2.7	-	IEC 60250
Dissipation Factor, 50/60 Hz	0.004	-	IEC 60250
Dissipation Factor, 1 MHz	0.006	-	IEC 60250
FLAME CHARACTERISTICS			
UL Recognized, 94V-2 Flame Class Rating (3)	0.76	mm	UL 94
UL Recognized, 94V-0 Flame Class Rating (3)	1.49	mm	UL 94
UL Recognized, 94-5VB Rating (3)	2	mm	UL 94

1) Typical values only. Variations within normal tolerances are possible for variose colours.All values are measured at least after 48 hours storage at 230C/50% relative humidity.
All properties, expect the melt volume rate are measured on injection moulded samples.
All samples are prepared according to ISO 294.

2) Only typical data for material selection purpose.Not to be used for part or tool design.
3) This rating is not intended to reflect hazards presented by this or any other material under actual fire conditions.
4) Own measurement according to UL.

Source, GMD, Last Update:07/25/2005

GE Plastics

Cycoloy* Resin C6600
Americas: COMMERCIAL

PROCESSING PARAMETERS	TYPICAL VALUE	UNIT
Injection Molding		
Drying Temperature	80 - 90	°C
Drying Time	3 - 4	hrs
Drying Time (Cumulative)	8	hrs
Maximum Moisture Content	0.04	%
Melt Temperature	245 - 275	°C
Nozzle Temperature	245 - 275	°C
Front - Zone 3 Temperature	245 - 275	°C
Middle - Zone 2 Temperature	220 - 275	°C
Rear - Zone 1 Temperature	220 - 255	°C
Mold Temperature	60 - 80	°C
Back Pressure	0.3 - 0.7	MPa
Screw Speed	40 - 70	rpm
Shot to Cylinder Size	30 - 80	%
Vent Depth	0.038 - 0.076	mm

• NOTE: Back Pressure, Screw Speed, Shot to Cylinder Size and Vent Depth are only mentioned as general guidelines. These may not apply or need adjustment in specific situations such as low shot sizes, thin wall molding and gas-assist molding.

1) Typical values only. Variations within normal tolerances are possible for variose colours.All values are measured at least after 48 hours storage at 230C/50% relative humidity.
All properties, expect the melt volume rate are measured on injection moulded samples.
All samples are prepared according to ISO 294.

2) Only typical data for material selection purpose.Not to be used for part or tool design.
3) This rating is not intended to reflect hazards presented by this or any other material under actual fire conditions.
4) Own measurement according to UL.

Source, GMD, Last Update:07/25/2005

APPENDIX B

STATISTICAL ANALYSIS (ANOVA)

General Linear Model

Between-Subjects Factors

		N
AgingTime	.50	4
	2.00	4
	8.00	4
	96.00	4
	336.00	4
	1008.00	4

Multivariate Tests(c)

Effect		Value	F	Hypothesis df	Error df	Sig.
Intercept	Pillai's Trace	1.000	33173.658	6.000	13.000	.000
	Wilks' Lambda	.000	33173.658	6.000	13.000	.000
	Hotelling's Trace	15310.919	33173.658	6.000	13.000	.000
	Roy's Largest Root	15310.919	33173.658	6.000	13.000	.000
AgingTime	Pillai's Trace	2.851	3.758	30.000	85.000	.000
	Wilks' Lambda	.000	13.009	30.000	54.000	.000
	Hotelling's Trace	159.657	60.670	30.000	57.000	.000
	Roy's Largest Root	151.331	428.771	6.000	17.000	.000

Tests of Between-Subjects Effects

Source	Dependent Variable	Type III Sum of Squares	df	Mean Square	F	Sig.
Corrected Model	TpABS	7.611	5	1.522	1.419	.265
	TpPC	36.220	5	7.244	6.755	.001
	TgABS	14.191	5	2.838	2.260	.092
	TgPC	18.306	5	3.661	3.373	.025
	logEnthalpy	2.951	5	.590	385.826	.000
	Tf	96.737	5	19.347	11.335	.000
Intercept	TpABS	184940.171	1	184940.171	172435.038	.000
	TpPC	252896.752	1	252896.752	235809.718	.000
	TgABS	184673.407	1	184673.407	147062.727	.000
	TgPC	259143.227	1	259143.227	238744.5	.000
	logEnthalpy	.085	1	.085	55.789	.000
	Tf	197780.570	1	197780.570	115877.623	.000
AgingTime	TpABS	7.611	5	1.522	1.419	.265
	TpPC	36.220	5	7.244	6.755	.001
	TgABS	14.191	5	2.838	2.260	.092
	TgPC	18.306	5	3.661	3.373	.025
	logEnthalpy	2.951	5	.590	385.826	.000
	Tf	96.737	5	19.347	11.335	.000
Error	TpABS	19.305	18	1.073		
	TpPC	19.304	18	1.072		
	TgABS	22.603	18	1.256		
	TgPC	19.538	18	1.085		
	logEnthalpy	.028	18	.002		
	Tf	30.723	18	1.707		
Total	TpABS	184967.088	24			
	TpPC	252952.276	24			
	TgABS	184710.202	24			
	TgPC	259181.071	24			
	logEnthalpy	3.063	24			
	Tf	197908.030	24			
Corrected Total	TpABS	26.917	23			
	TpPC	55.524	23			
	TgABS	36.794	23			
	TgPC	37.844	23			
	logEnthalpy	2.978	23			
	Tf	127.460	23			

Custom Hypothesis Tests

Contrast Results (K Matrix)

AgingTime Polynomial Contrast			Dependent Variable					
			TpABS	TpPC	TgABS	TgPC	logEnthalpy	Tf
Linear	Contrast Estimate		.631	-.325	.312	-1.114	.843	-4.844
	Hypothesized Value		0	0	0	0	0	0
	Difference (Estimate - Hypothesized)		.631	-.325	.312	-1.114	.843	-4.844
	Std. Error		.518	.518	.560	.609	.020	.653
	Sig.		.239	.539	.584	.084	.000	.000
	95% Confidence Interval for Difference	Lower Bound	-.457	-1.412	-.865	-2.394	.802	-6.216
		Upper Bound	1.719	.763	1.489	.166	.884	-3.471
Quadratic	Contrast Estimate		-.683	2.856	.089	1.564	-.146	.153
	Hypothesized Value		0	0	0	0	0	0
	Difference (Estimate - Hypothesized)		-.683	2.856	.089	1.564	-.146	.153
	Std. Error		.518	.518	.560	.609	.020	.653
	Sig.		.204	.000	.876	.019	.000	.818
	95% Confidence Interval for Difference	Lower Bound	-1.771	1.768	-1.088	.284	-.187	-1.220
		Upper Bound	.405	3.944	1.266	2.844	-.105	1.525
Cubic	Contrast Estimate		-.950	-.779	-1.644	.067	-.045	-.496
	Hypothesized Value		0	0	0	0	0	0
	Difference (Estimate - Hypothesized)		-.950	-.779	-1.644	.067	-.045	-.496
	Std. Error		.518	.518	.560	.609	.020	.653
	Sig.		.083	.150	.009	.914	.032	.458
	95% Confidence Interval for Difference	Lower Bound	-2.038	-1.867	-2.822	-1.214	-.086	-1.868
		Upper Bound	.138	.309	-.467	1.347	-.004	.877

Order 4	Contrast Estimate		.236	-.408	.831	.552	.008	.661
	Hypothesized Value		0	0	0	0	0	0
	Difference (Estimate - Hypothesized)		.236	-.408	.831	.552	.008	.661
	Std. Error		.518	.518	.560	.609	.020	.653
	Sig.		.654	.441	.155	.377	.672	.325
	95% Confidence Interval for Difference	Lower Bound	-.852	-1.496	-.346	-.728	-.033	-.711
		Upper Bound	1.324	.680	2.008	1.832	.050	2.034
Order 5	Contrast Estimate		-.284	.147	.218	.451	.056	-.129
	Hypothesized Value		0	0	0	0	0	0
	Difference (Estimate - Hypothesized)		-.284	.147	.218	.451	.056	-.129
	Std. Error		.518	.518	.560	.609	.020	.653
	Sig.		.591	.779	.702	.469	.011	.846
	95% Confidence Interval for Difference	Lower Bound	-1.372	-.941	-.959	-.829	.014	-1.502
		Upper Bound	.804	1.235	1.395	1.731	.097	1.243

Univariate Test Results

Source	Dependent Variable	Sum of Squares	df	Mean Square	F	Sig.
Contrast	TpABS	7.611	5	1.522	1.419	.265
	TpPC	36.220	5	7.244	6.755	.001
	TgABS	14.191	5	2.838	2.260	.092
	TgPC	18.306	5	3.661	3.373	.025
	logEnthalpy	2.951	5	.590	385.826	.000
	Tf	96.737	5	19.347	11.335	.000
Error	TpABS	19.305	18	1.073		
	TpPC	19.304	18	1.072		
	TgABS	22.603	18	1.256		
	TgPC	19.538	18	1.085		
	logEnthalpy	.028	18	.002		
	Tf	30.723	18	1.707		

Post Hoc Tests
AgingTime

Multiple Comparisons

Tukey HSD

Dependent Variable	AgingTime (I)	AgingTime (J)	Mean Difference (I-J)	Std. Error	Sig.	95% Confidence Interval	
						Lower Bound	Upper Bound
TpABS	.50	2.00	.5375	.73230	.975	-1.7898	2.8648
		8.00	-.5400	.73230	.974	-2.8673	1.7873
		96.00	-.9000	.73230	.817	-3.2273	1.4273
		336.00	-1.0850	.73230	.679	-3.4123	1.2423
		1008.00	-.0100	.73230	1.000	-2.3373	2.3173
	2.00	.50	-.5375	.73230	.975	-2.8648	1.7898
		8.00	-1.0775	.73230	.685	-3.4048	1.2498
		96.00	-1.4375	.73230	.399	-3.7648	.8898
		336.00	-1.6225	.73230	.278	-3.9498	.7048
		1008.00	-.5475	.73230	.973	-2.8748	1.7798
	8.00	.50	.5400	.73230	.974	-1.7873	2.8673
		2.00	1.0775	.73230	.685	-1.2498	3.4048
		96.00	-.3600	.73230	.996	-2.6873	1.9673
		336.00	-.5450	.73230	.973	-2.8723	1.7823
		1008.00	.5300	.73230	.976	-1.7973	2.8573
	96.00	.50	.9000	.73230	.817	-1.4273	3.2273
		2.00	1.4375	.73230	.399	-.8898	3.7648
		8.00	.3600	.73230	.996	-1.9673	2.6873
		336.00	-.1850	.73230	1.000	-2.5123	2.1423
		1008.00	.8900	.73230	.824	-1.4373	3.2173
	336.00	.50	1.0850	.73230	.679	-1.2423	3.4123
		2.00	1.6225	.73230	.278	-.7048	3.9498
		8.00	.5450	.73230	.973	-1.7823	2.8723

		96.00	.1850	.73230	1.000	-2.1423	2.5123
		1008.00	1.0750	.73230	.687	-1.2523	3.4023
	1008.00	.50	.0100	.73230	1.000	-2.3173	2.3373
		2.00	.5475	.73230	.973	-1.7798	2.8748
		8.00	-.5300	.73230	.976	-2.8573	1.7973
		96.00	-.8900	.73230	.824	-3.2173	1.4373
		336.00	-1.0750	.73230	.687	-3.4023	1.2523
TpPC	.50	2.00	2.2800	.73228	.057	-.0472	4.6072
		8.00	3.6425(*)	.73228	.001	1.3153	5.9697
		96.00	3.0700(*)	.73228	.006	.7428	5.3972
		336.00	1.7925	.73228	.192	-.5347	4.1197
		1008.00	.9500	.73228	.783	-1.3772	3.2772
	2.00	.50	-2.2800	.73228	.057	-4.6072	.0472
		8.00	1.3625	.73228	.455	-.9647	3.6897
		96.00	.7900	.73228	.883	-1.5372	3.1172
		336.00	-.4875	.73228	.984	-2.8147	1.8397
		1008.00	-1.3300	.73228	.480	-3.6572	.9972
	8.00	.50	-3.6425(*)	.73228	.001	-5.9697	-1.3153
		2.00	-1.3625	.73228	.455	-3.6897	.9647
		96.00	-.5725	.73228	.967	-2.8997	1.7547
		336.00	-1.8500	.73228	.168	-4.1772	.4772
		1008.00	-2.6925(*)	.73228	.018	-5.0197	-.3653
	96.00	.50	-3.0700(*)	.73228	.006	-5.3972	-.7428
		2.00	-.7900	.73228	.883	-3.1172	1.5372
		8.00	.5725	.73228	.967	-1.7547	2.8997
		336.00	-1.2775	.73228	.522	-3.6047	1.0497
		1008.00	-2.1200	.73228	.086	-4.4472	.2072
	336.00	.50	-1.7925	.73228	.192	-4.1197	.5347
		2.00	.4875	.73228	.984	-1.8397	2.8147
		8.00	1.8500	.73228	.168	-.4772	4.1772
		96.00	1.2775	.73228	.522	-1.0497	3.6047
		1008.00	-.8425	.73228	.854	-3.1697	1.4847
	1008.00	.50	-.9500	.73228	.783	-3.2772	1.3772
		2.00	1.3300	.73228	.480	-.9972	3.6572
		8.00	2.6925(*)	.73228	.018	.3653	5.0197
		96.00	2.1200	.73228	.086	-.2072	4.4472
		336.00	.8425	.73228	.854	-1.4847	3.1697
TgABS	.50	2.00	2.0000	.79238	.169	-.5182	4.5182
		8.00	1.0075	.79238	.796	-1.5107	3.5257
		96.00	-.3225	.79238	.998	-2.8407	2.1957
		336.00	.1975	.79238	1.000	-2.3207	2.7157
		1008.00	.8250	.79238	.898	-1.6932	3.3432
	2.00	.50	-2.0000	.79238	.169	-4.5182	.5182
		8.00	-.9925	.79238	.806	-3.5107	1.5257
		96.00	-2.3225	.79238	.081	-4.8407	.1957
		336.00	-1.8025	.79238	.254	-4.3207	.7157
		1008.00	-1.1750	.79238	.679	-3.6932	1.3432
	8.00	.50	-1.0075	.79238	.796	-3.5257	1.5107
		2.00	.9925	.79238	.806	-1.5257	3.5107

		96.00	-1.3300	.79238	.562	-3.8482	1.1882
		336.00	-.8100	.79238	.904	-3.3282	1.7082
		1008.00	-.1825	.79238	1.000	-2.7007	2.3357
	96.00	.50	.3225	.79238	.998	-2.1957	2.8407
		2.00	2.3225	.79238	.081	-.1957	4.8407
		8.00	1.3300	.79238	.562	-1.1882	3.8482
		336.00	.5200	.79238	.985	-1.9982	3.0382
		1008.00	1.1475	.79238	.699	-1.3707	3.6657
	336.00	.50	-.1975	.79238	1.000	-2.7157	2.3207
		2.00	1.8025	.79238	.254	-.7157	4.3207
		8.00	.8100	.79238	.904	-1.7082	3.3282
		96.00	-.5200	.79238	.985	-3.0382	1.9982
		1008.00	.6275	.79238	.965	-1.8907	3.1457
	1008.00	.50	-.8250	.79238	.898	-3.3432	1.6932
		2.00	1.1750	.79238	.679	-1.3432	3.6932
		8.00	.1825	.79238	1.000	-2.3357	2.7007
		96.00	-1.1475	.79238	.699	-3.6657	1.3707
		336.00	-.6275	.79238	.965	-3.1457	1.8907
TgPC	.50	2.00	1.4775	.86165	.540	-1.2609	4.2159
		8.00	2.1750	.86165	.169	-.5634	4.9134
		96.00	1.9125	.86165	.277	-.8259	4.6509
		336.00	2.6300	.86165	.064	-.1084	5.3684
		1008.00	1.2250	.86165	.714	-1.5134	3.9634
	2.00	.50	-1.4775	.86165	.540	-4.2159	1.2609
		8.00	.6975	.86165	.962	-2.0409	3.4359
		96.00	.4350	.86165	.995	-2.3034	3.1734
		336.00	1.1525	.86165	.761	-1.5859	3.8909
		1008.00	-.2525	.86165	1.000	-2.9909	2.4859
	8.00	.50	-2.1750	.86165	.169	-4.9134	.5634
		2.00	-.6975	.86165	.962	-3.4359	2.0409
		96.00	-.2625	.86165	1.000	-3.0009	2.4759
		336.00	.4550	.86165	.994	-2.2834	3.1934
		1008.00	-.9500	.86165	.874	-3.6884	1.7884
	96.00	.50	-1.9125	.86165	.277	-4.6509	.8259
		2.00	-.4350	.86165	.995	-3.1734	2.3034
		8.00	.2625	.86165	1.000	-2.4759	3.0009
		336.00	.7175	.86165	.957	-2.0209	3.4559
		1008.00	-.6875	.86165	.964	-3.4259	2.0509
	336.00	.50	-2.6300	.86165	.064	-5.3684	.1084
		2.00	-1.1525	.86165	.761	-3.8909	1.5859
		8.00	-.4550	.86165	.994	-3.1934	2.2834
		96.00	-.7175	.86165	.957	-3.4559	2.0209
		1008.00	-1.4050	.86165	.590	-4.1434	1.3334
	1008.00	.50	-1.2250	.86165	.714	-3.9634	1.5134
		2.00	.2525	.86165	1.000	-2.4859	2.9909
		8.00	.9500	.86165	.874	-1.7884	3.6884
		96.00	.6875	.86165	.964	-2.0509	3.4259
		336.00	1.4050	.86165	.590	-1.3334	4.1434
logEnthalpy	.50	2.00	-.2715(*)	.02765	.000	-.3594	-.1836

		8.00	-.4866(*)	.02765	.000	-.5745	-.3987
		96.00	-.7851(*)	.02765	.000	-.8730	-.6973
		336.00	-.8885(*)	.02765	.000	-.9764	-.8006
		1008.00	-.9811(*)	.02765	.000	-1.0690	-.8932
	2.00	.50	.2715(*)	.02765	.000	.1836	.3594
		8.00	-.2151(*)	.02765	.000	-.3030	-.1272
		96.00	-.5136(*)	.02765	.000	-.6015	-.4258
		336.00	-.6170(*)	.02765	.000	-.7049	-.5291
		1008.00	-.7096(*)	.02765	.000	-.7975	-.6217
	8.00	.50	.4866(*)	.02765	.000	.3987	.5745
		2.00	.2151(*)	.02765	.000	.1272	.3030
		96.00	-.2985(*)	.02765	.000	-.3864	-.2107
		336.00	-.4019(*)	.02765	.000	-.4898	-.3140
		1008.00	-.4945(*)	.02765	.000	-.5824	-.4066
	96.00	.50	.7851(*)	.02765	.000	.6973	.8730
		2.00	.5136(*)	.02765	.000	.4258	.6015
		8.00	.2985(*)	.02765	.000	.2107	.3864
		336.00	-.1034(*)	.02765	.016	-.1912	-.0155
		1008.00	-.1959(*)	.02765	.000	-.2838	-.1080
	336.00	.50	.8885(*)	.02765	.000	.8006	.9764
		2.00	.6170(*)	.02765	.000	.5291	.7049
		8.00	.4019(*)	.02765	.000	.3140	.4898
		96.00	.1034(*)	.02765	.016	.0155	.1912
		1008.00	-.0926(*)	.02765	.036	-.1805	-.0047
	1008.00	.50	.9811(*)	.02765	.000	.8932	1.0690
		2.00	.7096(*)	.02765	.000	.6217	.7975
		8.00	.4945(*)	.02765	.000	.4066	.5824
		96.00	.1959(*)	.02765	.000	.1080	.2838
		336.00	.0926(*)	.02765	.036	.0047	.1805
Tf	.50	2.00	2.2500	.92380	.196	-.6859	5.1859
		8.00	2.6000	.92380	.100	-.3359	5.5359
		96.00	3.6250(*)	.92380	.011	.6891	6.5609
		336.00	5.1250(*)	.92380	.000	2.1891	8.0609
		1008.00	6.1750(*)	.92380	.000	3.2391	9.1109
	2.00	.50	-2.2500	.92380	.196	-5.1859	.6859
		8.00	.3500	.92380	.999	-2.5859	3.2859
		96.00	1.3750	.92380	.675	-1.5609	4.3109
		336.00	2.8750	.92380	.057	-.0609	5.8109
		1008.00	3.9250(*)	.92380	.005	.9891	6.8609
	8.00	.50	-2.6000	.92380	.100	-5.5359	.3359
		2.00	-.3500	.92380	.999	-3.2859	2.5859
		96.00	1.0250	.92380	.871	-1.9109	3.9609
		336.00	2.5250	.92380	.117	-.4109	5.4609
		1008.00	3.5750(*)	.92380	.012	.6391	6.5109
	96.00	.50	-3.6250(*)	.92380	.011	-6.5609	-.6891
		2.00	-1.3750	.92380	.675	-4.3109	1.5609
		8.00	-1.0250	.92380	.871	-3.9609	1.9109
		336.00	1.5000	.92380	.595	-1.4359	4.4359
		1008.00	2.5500	.92380	.111	-.3859	5.4859

	336.00	.50	-5.1250(*)	.92380	.000	-8.0609	-2.1891
		2.00	-2.8750	.92380	.057	-5.8109	.0609
		8.00	-2.5250	.92380	.117	-5.4609	.4109
		96.00	-1.5000	.92380	.595	-4.4359	1.4359
		1008.00	1.0500	.92380	.860	-1.8859	3.9859
	1008.00	.50	-6.1750(*)	.92380	.000	-9.1109	-3.2391
		2.00	-3.9250(*)	.92380	.005	-6.8609	-.9891
		8.00	-3.5750(*)	.92380	.012	-6.5109	-.6391
		96.00	-2.5500	.92380	.111	-5.4859	.3859
		336.00	-1.0500	.92380	.860	-3.9859	1.8859

Based on observed means.
* The mean difference is significant at the .05 level.

Homogeneous Subsets

TpABS

Tukey HSD

	N	Subset
AgingTime	1	1
2.00	4	86.9125
.50	4	87.4500
1008.00	4	87.4600
8.00	4	87.9900
96.00	4	88.3500
336.00	4	88.5350
Sig.		.278

Means for groups in homogeneous subsets are displayed.
Based on Type III Sum of Squares, the error term is Mean Square(Error) = 1.073.
a Uses Harmonic Mean Sample Size = 4.000.
b Group sizes are unequal, harmonic mean of the group sizes is used. Type I error levels not guaranteed.
c Alpha = .05.

TpPC

Tukey HSD

	N	Subset		
AgingTime	1	2	3	1
8.00	4	100.9650		
96.00	4	101.5375	101.5375	
2.00	4	102.3275	102.3275	102.3275
336.00	4	102.8150	102.8150	102.8150
1008.00	4		103.6575	103.6575
.50	4			104.6075
Sig.		.168	.086	.057

Means for groups in homogeneous subsets are displayed.
Based on Type III Sum of Squares, the error term is Mean Square(Error) = 1.072.
a Uses Harmonic Mean Sample Size = 4.000.
b Group sizes are unequal, harmonic mean of the group sizes is used. Type I error levels not guaranteed.
c Alpha = .05.

TgABS

Tukey HSD

AgingTime	N	Subset

	1	1
2.00	4	86.3375
8.00	4	87.3300
1008.00	4	87.5125
336.00	4	88.1400
.50	4	88.3375
96.00	4	88.6600
Sig.		.081

Means for groups in homogeneous subsets are displayed.
Based on Type III Sum of Squares, the error term is Mean Square(Error) = 1.256.
a Uses Harmonic Mean Sample Size = 4.000.
b Group sizes are unequal, harmonic mean of the group sizes is used. Type I error levels not guaranteed.
c Alpha = .05.

TgPC
Tukey HSD

	N	Subset
AgingTime	1	1
336.00	4	103.0600
8.00	4	103.5150
96.00	4	103.7775
2.00	4	104.2125
1008.00	4	104.4650
.50	4	105.6900
Sig.		.064

Means for groups in homogeneous subsets are displayed.
Based on Type III Sum of Squares, the error term is Mean Square(Error) = 1.485.
a Uses Harmonic Mean Sample Size = 4.000.
b Group sizes are unequal, harmonic mean of the group sizes is used. Type I error levels not guaranteed.
c Alpha = .05.

logEnthalpy

Tukey HSD

AgingTime	N	Subset					
	1	2	3	4	5	6	1
.50	4	-.6284					
2.00	4		-.3569				
8.00	4			-.1418			
96.00	4				.1567		
336.00	4					.2601	
1008.00	4						.3526
Sig.		1.000	1.000	1.000	1.000	1.000	1.000

Means for groups in homogeneous subsets are displayed.

Based on Type III Sum of Squares, the error term is Mean Square(Error) = .002.

a Uses Harmonic Mean Sample Size = 4.000.

b Group sizes are unequal, harmonic mean of the group sizes is used. Type I error levels not guaranteed.

c Alpha = .05.

Tf

Tukey HSD

AgingTime	N	Subset		
	1	2	3	1
1008.00	4	87.9000		
336.00	4	88.9500	88.9500	
96.00	4	90.4500	90.4500	
8.00	4		91.4750	91.4750
2.00	4		91.8250	91.8250
.50	4			94.0750
Sig.		.111	.057	.100

Means for groups in homogeneous subsets are displayed.

Based on Type III Sum of Squares, the error term is Mean Square(Error) = 1.707.

a Uses Harmonic Mean Sample Size = 4.000.

b Group sizes are unequal, harmonic mean of the group sizes is used. Type I error levels not guaranteed.

c Alpha = .05.

ANOVA Assumptions Verification

Interactive Graph

Notes

Output Created		14-FEB-2007 11:15:05
Comments		
Input	Data	C:\Documents and Settings\j3tang\My Documents\My Work\Research (Part 2)\Peak Shift\PeakShift Data Analysis.sav
	Active Dataset	DataSet1
	Filter	<none>
	Weight	<none>
	Split File	<none>
Syntax		IGRAPH /VIEWNAME='Scatterplot' /X1 = VAR(PRE_5) TYPE = CATEGORICAL /Y = VAR (SRE_5) TYPE = SCALE /COORDINATE = VERTICAL /X1LENGTH=3.0 /YLENGTH=3.0 /X2LENGTH=3.0 /CHARTLOOK='NONE' /CATORDER VAR(PRE_5) (ASCENDING VALUES OMITEMPTY) /SCATTER COINCIDENT = NONE.
Resources	Elapsed Time	0:00:00.19
	Processor Time	0:00:00.13

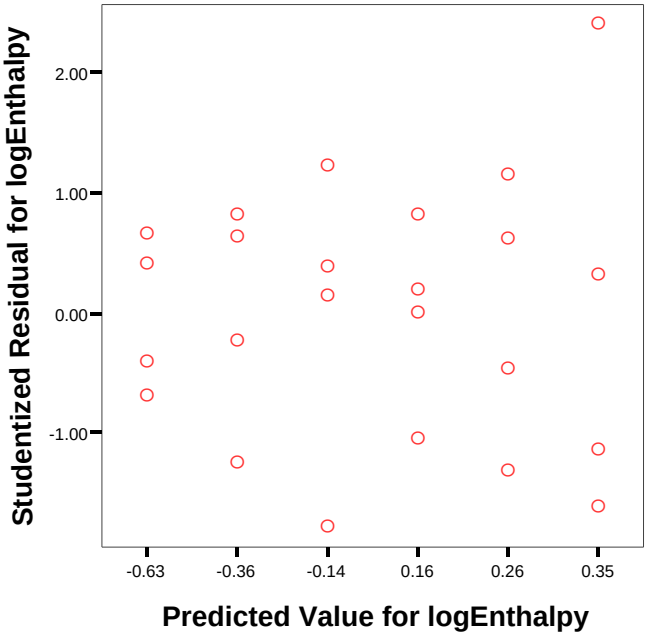

Interactive Graph

Notes

Output Created	14-FEB-2007 11:21:40
Comments	

Input	Data	C:\Documents and Settings\j3tang\My Documents\My Work\Research (Part 2)\Peak Shift\PeakShift Data Analysis.sav
	Active Dataset	DataSet1
	Filter	<none>
	Weight	<none>
	Split File	<none>
Syntax		IGRAPH /VIEWNAME='Scatterplot' /X1 = VAR(PRE_2) TYPE = CATEGORICAL /Y = VAR (SRE_2) TYPE = SCALE /COORDINATE = VERTICAL /X1LENGTH=3.0 /YLENGTH=3.0 /X2LENGTH=3.0 /CHARTLOOK='NONE' /CATORDER VAR(PRE_2) (ASCENDING VALUES OMITEMPTY) /SCATTER COINCIDENT = NONE.
Resources	Elapsed Time	0:00:00.02
	Processor Time	0:00:00.02

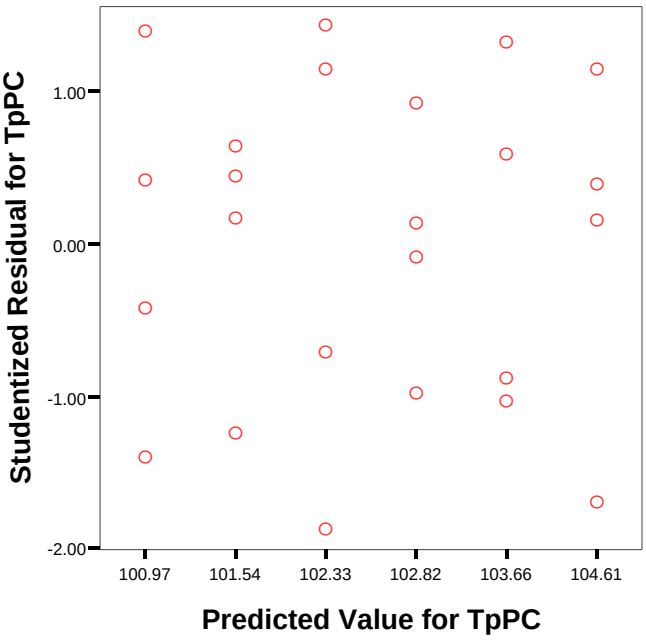

Interactive Graph

Notes

Output Created		14-FEB-2007 11:23:04
Comments		
Input	Data	C:\Documents and Settings\j3tang\My Documents\My Work\Research (Part 2)\Peak Shift\PeakShift Data Analysis.sav
	Active Dataset	DataSet1
	Filter	<none>
	Weight	<none>
	Split File	<none>
Syntax		IGRAPH /VIEWNAME='Scatterplot' /X1 = VAR(PRE_1) TYPE = CATEGORICAL /Y = VAR (SRE_1) TYPE = SCALE /COORDINATE = VERTICAL /X1LENGTH=3.0 /YLENGTH=3.0 /X2LENGTH=3.0 /CHARTLOOK='NONE' /CATORDER VAR(PRE_1) (ASCENDING VALUES OMITEMPTY) /SCATTER COINCIDENT = NONE.
Resources	Elapsed Time	0:00:00.00
	Processor Time	0:00:00.00

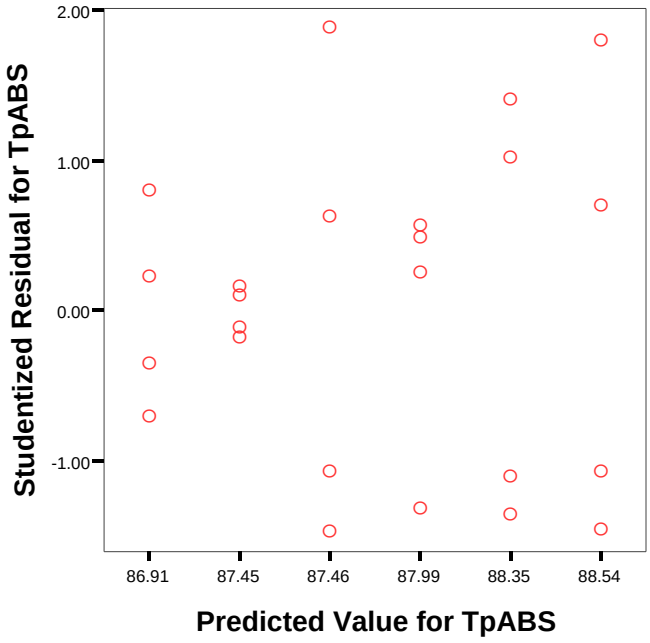

Interactive Graph

Notes

Output Created		14-FEB-2007 11:24:14
Comments		
Input	Data	C:\Documents and Settings\j3tang\My Documents\My Work\Research (Part 2)\Peak Shift\PeakShift Data Analysis.sav
	Active Dataset	DataSet1
	Filter	<none>
	Weight	<none>
	Split File	<none>
Syntax		IGRAPH /VIEWNAME='Scatterplot' /X1 = VAR(PRE_4) TYPE = CATEGORICAL /Y = VAR (SRE_4) TYPE = SCALE /COORDINATE = VERTICAL /X1LENGTH=3.0 /YLENGTH=3.0 /X2LENGTH=3.0 /CHARTLOOK='NONE' /CATORDER VAR(PRE_4) (ASCENDING VALUES OMITEMPTY) /SCATTER COINCIDENT = NONE.
Resources	Elapsed Time	0:00:00.03
	Processor Time	0:00:00.03

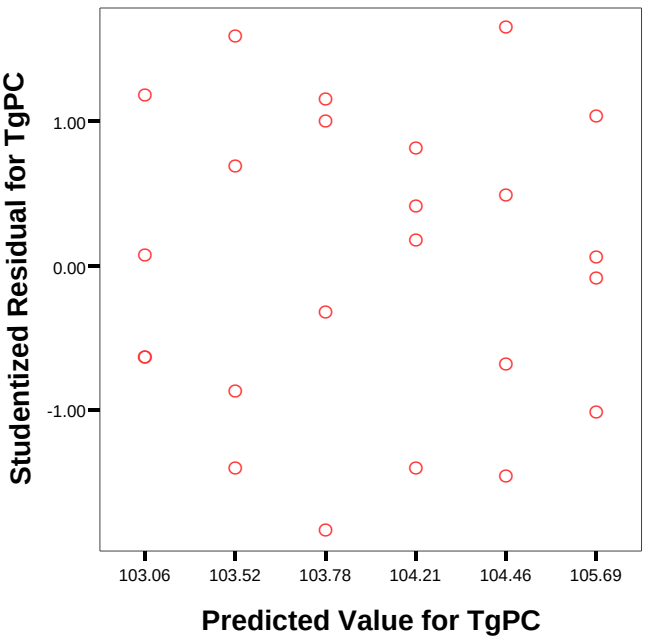

Interactive Graph

Notes

Output Created		14-FEB-2007 11:25:05
Comments		
Input	Data	C:\Documents and Settings\j3tang\My Documents\My Work\Research (Part 2)\Peak Shift\PeakShift Data Analysis.sav
	Active Dataset	DataSet1
	Filter	<none>
	Weight	<none>
	Split File	<none>
Syntax		IGRAPH /VIEWNAME='Scatterplot' /X1 = VAR(PRE_3) TYPE = CATEGORICAL /Y = VAR (SRE_3) TYPE = SCALE /COORDINATE = VERTICAL /X1LENGTH=3.0 /YLENGTH=3.0 /X2LENGTH=3.0 /CHARTLOOK='NONE' /CATORDER VAR(PRE_3) (ASCENDING VALUES OMITEMPTY) /SCATTER COINCIDENT = NONE.
Resources	Elapsed Time	0:00:00.01
	Processor Time	0:00:00.02

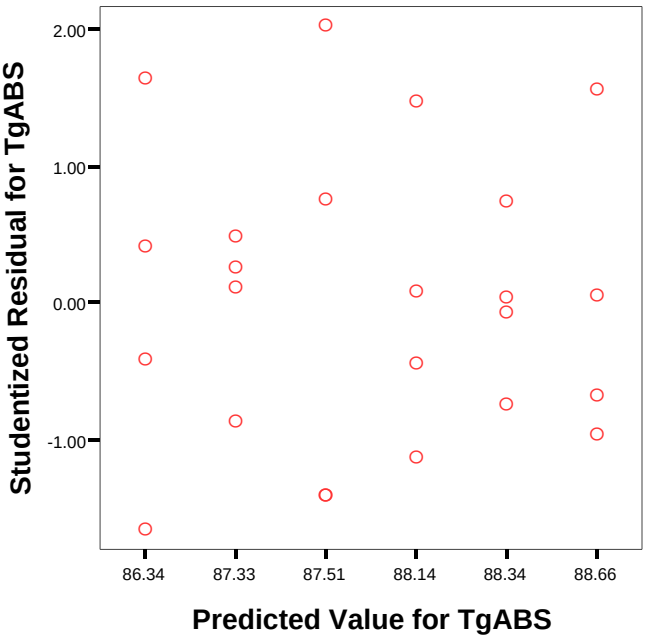

Interactive Graph

Notes

Output Created	14-FEB-2007 11:26:03
Comments	

Input	Data	C:\Documents and Settings\j3tang\My Documents\My Work\Research (Part 2)\Peak Shift\PeakShift Data Analysis.sav
	Active Dataset	DataSet1
	Filter	<none>
	Weight	<none>
	Split File	<none>
Syntax		IGRAPH /VIEWNAME='Scatterplot' /X1 = VAR(PRE_6) TYPE = CATEGORICAL /Y = VAR (SRE_6) TYPE = CATEGORICAL /COORDINATE = VERTICAL /X1LENGTH=3.0 /YLENGTH=3.0 /X2LENGTH=3.0 /CHARTLOOK='NONE' /CATORDER VAR(PRE_6) (ASCENDING VALUES OMITEMPTY) /CATORDER VAR(SRE_6) (ASCENDING VALUES OMITEMPTY) /SCATTER COINCIDENT = NONE.
Resources	Elapsed Time	0:00:00.02
	Processor Time	0:00:00.03

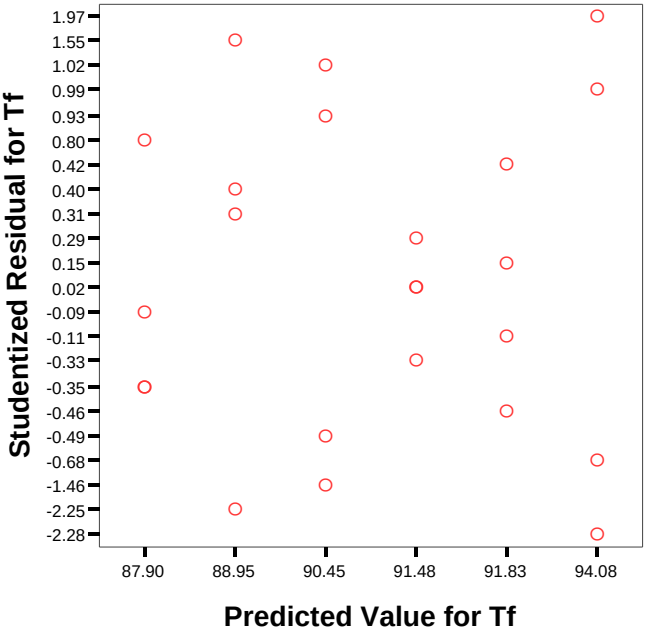

PPlot

Notes

Output Created		14-FEB-2007 11:31:46
Comments		
Input	Data	C:\Documents and Settings\j3tang\My Documents\My Work\Research (Part 2)\Peak Shift\PeakShift Data Analysis.sav
	Active Dataset	DataSet1
	Filter	<none>
	Weight	<none>
	Split File	<none>
	N of Rows in Working Data File	24
	Date	<none>
Missing Value Handling	Definition of Missing	User-defined missing values are treated as missing.
	Cases Used	For a given sequence or time series variable, cases with missing values are not used in the analysis. Cases with negative or zero values are also not used, if the log transform is requested.
Syntax		PPLOT /VARIABLES=SRE_5 /NOLOG /NOSTANDARDIZE /TYPE=Q-Q /FRACTION=BLOM /TIES=MEAN /DIST=NORMAL.
Resources	Elapsed Time	0:00:01.01
	Processor Time	0:00:00.72
Use	From	First observation
	To	Last observation
Time Series Settings (TSET)	Amount of Output	PRINT = DEFAULT
	Saving New Variables	NEWVAR = CURRENT
	Maximum Number of Lags in Autocorrelation or Partial Autocorrelation Plots	MXAUTO = 16
	Maximum Number of Lags Per Cross-Correlation Plots	MXCROSS = 7

Maximum Number of New Variables Generated Per Procedure	MXNEWVAR = 60
Maximum Number of New Cases Per Procedure	MXPREDICT = 1000
Treatment of User-Missing Values	MISSING = EXCLUDE
Confidence Interval Percentage Value	CIN = 95
Tolerance for Entering Variables in Regression Equations	TOLER = .0001
Maximum Iterative Parameter Change	CNVERGE = .001
Method of Calculating Std. Errors for Autocorrelations	ACFSE = IND
Length of Seasonal Period	Unspecified
Variable Whose Values Label Observations in Plots	Unspecified
Equations Include	CONSTANT

Model Description

Model Name		MOD_1
Series or Sequence	1	Studentized Residual for logEnthalpy
Transformation		None
Non-Seasonal Differencing		0
Seasonal Differencing		0
Length of Seasonal Period		No periodicity
Standardization		Not applied
Distribution	Type	Normal
	Location	estimated
	Scale	estimated
Fractional Rank Estimation Method		Blom's
Rank Assigned to Ties		Mean rank of tied values

Applying the model specifications from MOD_1

Case Processing Summary

	Studentized Residual for logEnthalpy

Series or Sequence Length		24
Number of Missing Values in the Plot	User-Missing	0
	System-Missing	0

The cases are unweighted.

Estimated Distribution Parameters

		Studentized Residual for logEnthalpy
Normal Distribution	Location	.0000
	Scale	1.02151

The cases are unweighted.

Studentized Residual for logEnthalpy

Normal Q-Q Plot of Studentized Residual for logEnthalpy

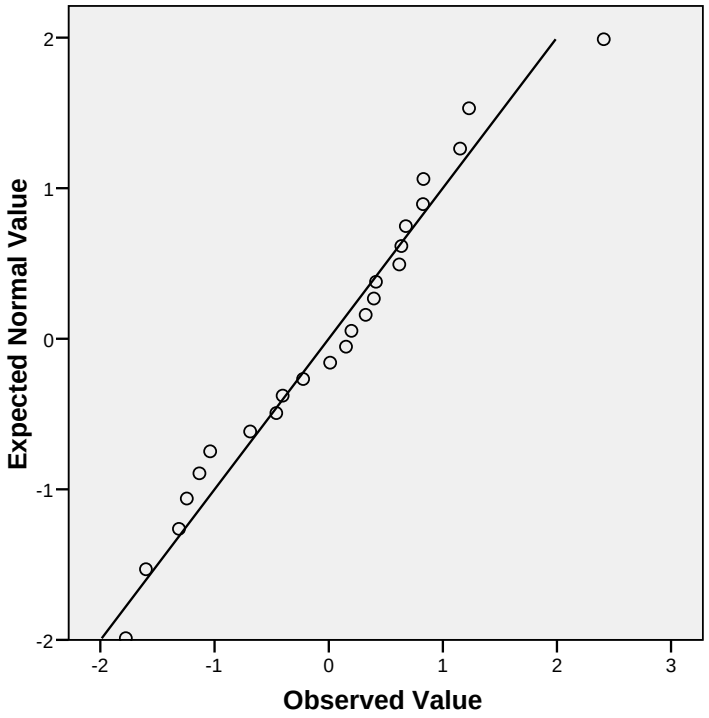

Detrended Normal Q-Q Plot of Studentized Residual for logEnthalpy

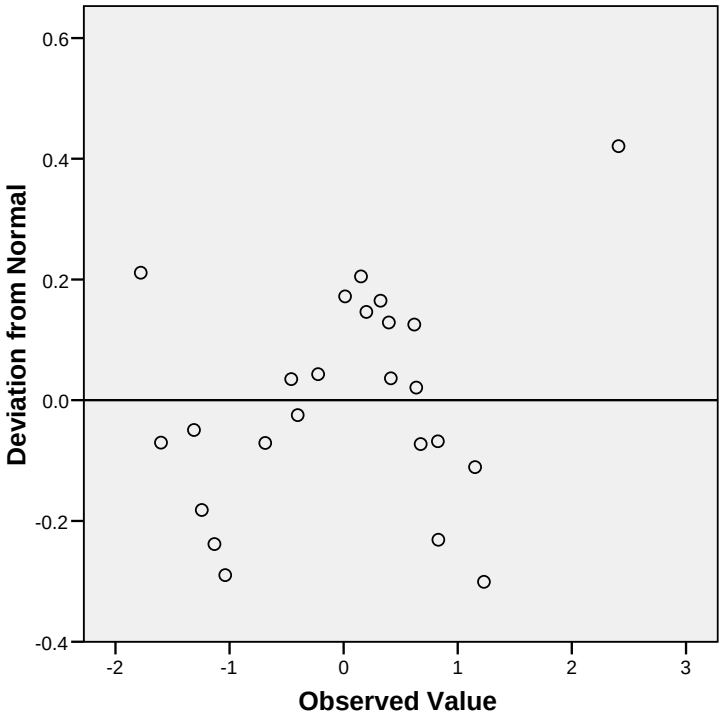

PPlot

Notes

Output Created		14-FEB-2007 11:32:59
Comments		
Input	Data	C:\Documents and Settings\j3tang\My Documents\My Work\Research (Part 2)\Peak Shift\PeakShift Data Analysis.sav
	Active Dataset	DataSet1
	Filter	<none>
	Weight	<none>
	Split File	<none>
	N of Rows in Working Data File	24
	Date	<none>
Missing Value Handling	Definition of Missing	User-defined missing values are treated as missing.
	Cases Used	For a given sequence or time series variable, cases with missing values are not used in the analysis. Cases with negative or zero values are also not used, if the log transform is requested.
Syntax		PPLOT /VARIABLES=SRE_2 /NOLOG /NOSTANDARDIZE /TYPE=Q-Q /FRACTION=BLOM /TIES=MEAN /DIST=NORMAL.
Resources	Elapsed Time	0:00:00.64
	Processor Time	0:00:00.77
Use	From	First observation
	To	Last observation
Time Series Settings (TSET)	Amount of Output	PRINT = DEFAULT
	Saving New Variables	NEWVAR = CURRENT
	Maximum Number of Lags in Autocorrelation or Partial Autocorrelation Plots	MXAUTO = 16

Maximum Number of Lags Per Cross-Correlation Plots	MXCROSS = 7
Maximum Number of New Variables Generated Per Procedure	MXNEWVAR = 60
Maximum Number of New Cases Per Procedure	MXPREDICT = 1000
Treatment of User-Missing Values	MISSING = EXCLUDE
Confidence Interval Percentage Value	CIN = 95
Tolerance for Entering Variables in Regression Equations	TOLER = .0001
Maximum Iterative Parameter Change	CNVERGE = .001
Method of Calculating Std. Errors for Autocorrelations	ACFSE = IND
Length of Seasonal Period	Unspecified
Variable Whose Values Label Observations in Plots	Unspecified
Equations Include	CONSTANT

Model Description

Model Name		MOD_2
Series or Sequence	1	Studentized Residual for TpPC
Transformation		None
Non-Seasonal Differencing		0
Seasonal Differencing		0
Length of Seasonal Period		No periodicity
Standardization		Not applied
Distribution	Type	Normal
	Location	estimated
	Scale	estimated
Fractional Rank Estimation Method		Blom's
Rank Assigned to Ties		Mean rank of tied values

Applying the model specifications from MOD_2

Case Processing Summary

		Studentized Residual for TpPC
Series or Sequence Length		24
Number of Missing Values in the Plot	User-Missing	0
	System-Missing	0

The cases are unweighted.

Estimated Distribution Parameters

		Studentized Residual for TpPC
Normal Distribution	Location	.0000
	Scale	1.02151

The cases are unweighted.

Studentized Residual for TpPC

Normal Q-Q Plot of Studentized Residual for TpPC

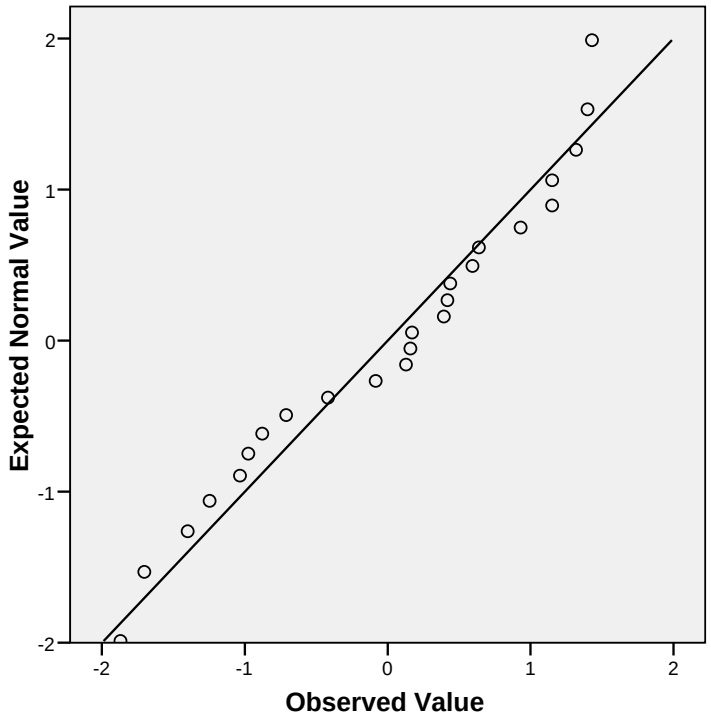

Detrended Normal Q-Q Plot of Studentized Residual for TpPC

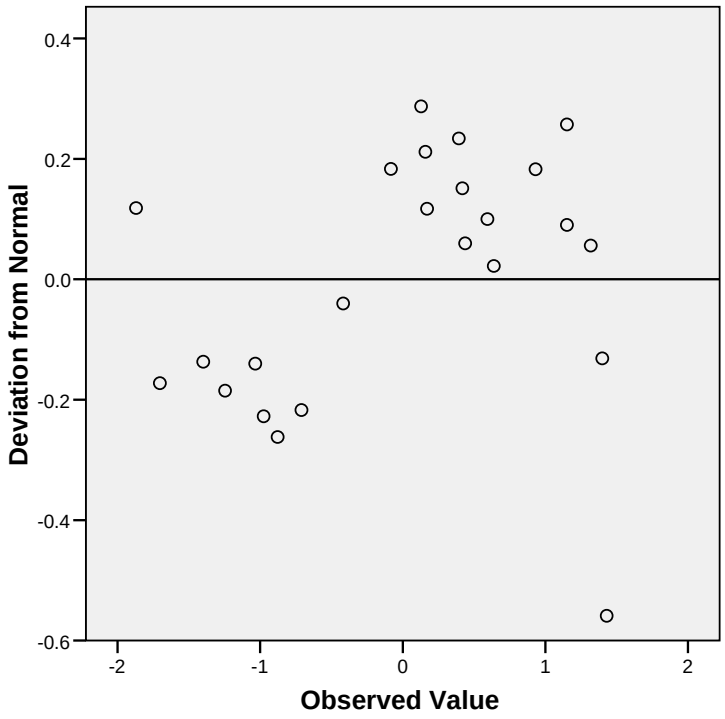

PPlot

Notes

Output Created		14-FEB-2007 11:33:37
Comments		
Input	Data	C:\Documents and Settings\j3tang\My Documents\My Work\Research (Part 2)\Peak Shift\PeakShift Data Analysis.sav
	Active Dataset	DataSet1
	Filter	<none>
	Weight	<none>
	Split File	<none>
	N of Rows in Working Data File	24
	Date	<none>
Missing Value Handling	Definition of Missing	User-defined missing values are treated as missing.
	Cases Used	For a given sequence or time series variable, cases with missing values are not used in the analysis. Cases with negative or zero values are also not used, if the log transform is requested.
Syntax		PPLOT /VARIABLES=SRE_1 /NOLOG /NOSTANDARDIZE /TYPE=Q-Q /FRACTION=BLOM /TIES=MEAN /DIST=NORMAL.
Resources	Elapsed Time	0:00:00.64
	Processor Time	0:00:00.75
Use	From	First observation
	To	Last observation
Time Series Settings (TSET)	Amount of Output	PRINT = DEFAULT
	Saving New Variables	NEWVAR = CURRENT
	Maximum Number of Lags in Autocorrelation or Partial Autocorrelation Plots	MXAUTO = 16

Maximum Number of Lags Per Cross-Correlation Plots	MXCROSS = 7
Maximum Number of New Variables Generated Per Procedure	MXNEWVAR = 60
Maximum Number of New Cases Per Procedure	MXPREDICT = 1000
Treatment of User-Missing Values	MISSING = EXCLUDE
Confidence Interval Percentage Value	CIN = 95
Tolerance for Entering Variables in Regression Equations	TOLER = .0001
Maximum Iterative Parameter Change	CNVERGE = .001
Method of Calculating Std. Errors for Autocorrelations	ACFSE = IND
Length of Seasonal Period	Unspecified
Variable Whose Values Label Observations in Plots	Unspecified
Equations Include	CONSTANT

Model Description

Model Name		MOD_3
Series or Sequence	1	Studentized Residual for TpABS
Transformation		None
Non-Seasonal Differencing		0
Seasonal Differencing		0
Length of Seasonal Period		No periodicity
Standardization		Not applied
Distribution	Type	Normal
	Location	estimated
	Scale	estimated
Fractional Rank Estimation Method		Blom's
Rank Assigned to Ties		Mean rank of tied values

Applying the model specifications from MOD_3

Case Processing Summary

		Studentized Residual for TpABS
Series or Sequence Length		24
Number of Missing Values in the Plot	User-Missing	0
	System-Missing	0

The cases are unweighted.

Estimated Distribution Parameters

		Studentized Residual for TpABS
Normal Distribution	Location	.0000
	Scale	1.02151

The cases are unweighted.

Studentized Residual for TpABS

Normal Q-Q Plot of Studentized Residual for TpABS

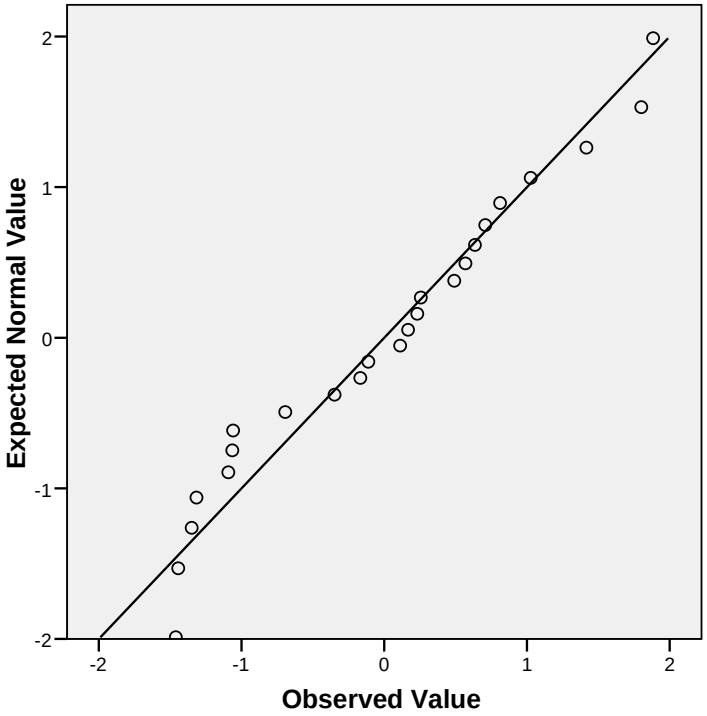

Detrended Normal Q-Q Plot of Studentized Residual for TpABS

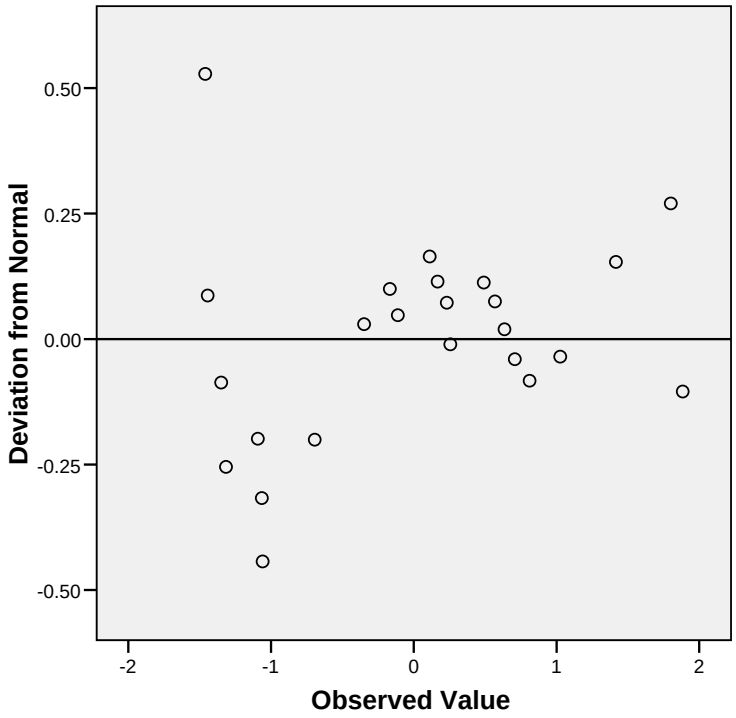

PPlot

Notes

Output Created		14-FEB-2007 11:34:19
Comments		
Input	Data	C:\Documents and Settings\j3tang\My Documents\My Work\Research (Part 2)\Peak Shift\PeakShift Data Analysis.sav
	Active Dataset	DataSet1
	Filter	<none>
	Weight	<none>
	Split File	<none>
	N of Rows in Working Data File	24
	Date	<none>
Missing Value Handling	Definition of Missing	User-defined missing values are treated as missing.
	Cases Used	For a given sequence or time series variable, cases with missing values are not used in the analysis. Cases with negative or zero values are also not used, if the log transform is requested.
Syntax		PPLOT /VARIABLES=SRE_4 /NOLOG /NOSTANDARDIZE /TYPE=Q-Q /FRACTION=BLOM /TIES=MEAN /DIST=NORMAL.
Resources	Elapsed Time	0:00:00.61
	Processor Time	0:00:00.66
Use	From	First observation
	To	Last observation
Time Series Settings (TSET)	Amount of Output	PRINT = DEFAULT
	Saving New Variables	NEWVAR = CURRENT
	Maximum Number of Lags in Autocorrelation or Partial Autocorrelation Plots	MXAUTO = 16
	Maximum Number of Lags Per Cross-Correlation Plots	MXCROSS = 7

Maximum Number of New Variables Generated Per Procedure	MXNEWVAR = 60
Maximum Number of New Cases Per Procedure	MXPREDICT = 1000
Treatment of User-Missing Values	MISSING = EXCLUDE
Confidence Interval Percentage Value	CIN = 95
Tolerance for Entering Variables in Regression Equations	TOLER = .0001
Maximum Iterative Parameter Change	CNVERGE = .001
Method of Calculating Std. Errors for Autocorrelations	ACFSE = IND
Length of Seasonal Period	Unspecified
Variable Whose Values Label Observations in Plots	Unspecified
Equations Include	CONSTANT

Model Description

Model Name		MOD_4
Series or Sequence	1	Studentized Residual for TgPC
Transformation		None
Non-Seasonal Differencing		0
Seasonal Differencing		0
Length of Seasonal Period		No periodicity
Standardization		Not applied
Distribution	Type	Normal
	Location	estimated
	Scale	estimated
Fractional Rank Estimation Method		Blom's
Rank Assigned to Ties		Mean rank of tied values

Applying the model specifications from MOD_4

Case Processing Summary

		Studentized Residual for TgPC
Series or Sequence Length		24
Number of Missing Values in the Plot	User-Missing	0
	System-Missing	0

The cases are unweighted.

Estimated Distribution Parameters

		Studentized Residual for TgPC
Normal Distribution	Location	.0000
	Scale	1.02151

The cases are unweighted.

Studentized Residual for TgPC

Normal Q-Q Plot of Studentized Residual for TgPC

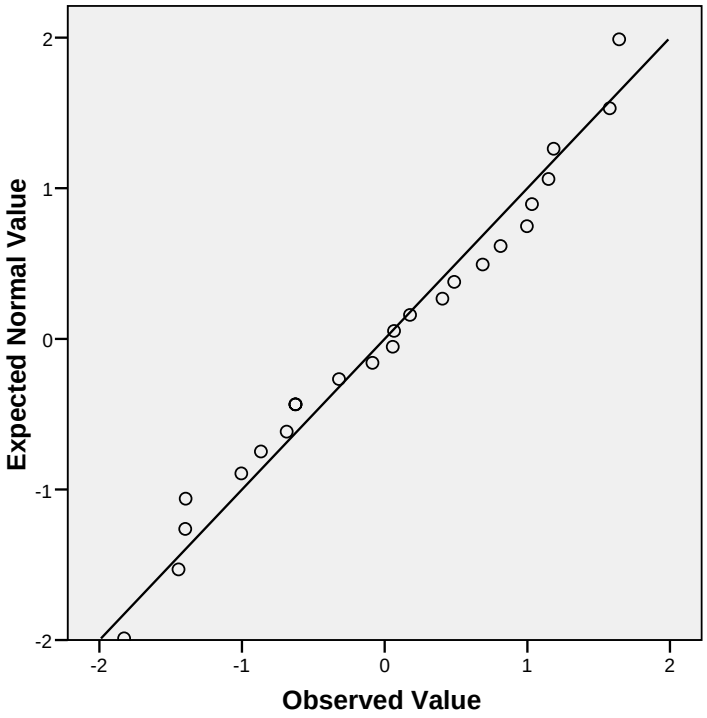

Detrended Normal Q-Q Plot of Studentized Residual for TgPC

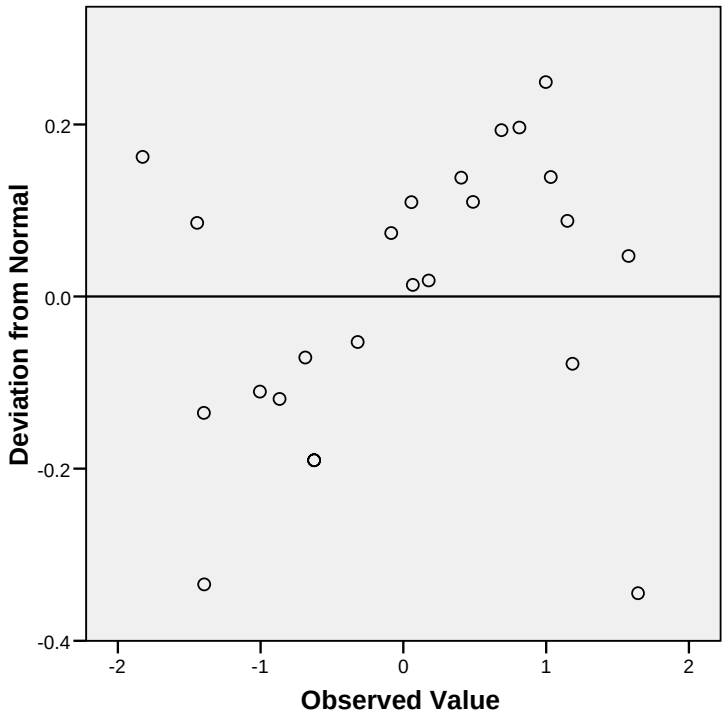

PPlot

Notes

Output Created		14-FEB-2007 11:34:53
Comments		
Input	Data	C:\Documents and Settings\j3tang\My Documents\My Work\Research (Part 2)\Peak Shift\PeakShift Data Analysis.sav
	Active Dataset	DataSet1
	Filter	<none>
	Weight	<none>
	Split File	<none>
	N of Rows in Working Data File	24
	Date	<none>
Missing Value Handling	Definition of Missing	User-defined missing values are treated as missing.
	Cases Used	For a given sequence or time series variable, cases with missing values are not used in the analysis. Cases with negative or zero values are also not used, if the log transform is requested.
Syntax		PPLOT /VARIABLES=SRE_3 /NOLOG /NOSTANDARDIZE /TYPE=Q-Q /FRACTION=BLOM /TIES=MEAN /DIST=NORMAL.
Resources	Elapsed Time	0:00:00.62
	Processor Time	0:00:00.72
Use	From	First observation
	To	Last observation
Time Series Settings (TSET)	Amount of Output	PRINT = DEFAULT
	Saving New Variables	NEWVAR = CURRENT
	Maximum Number of Lags in Autocorrelation or Partial Autocorrelation Plots	MXAUTO = 16
	Maximum Number of Lags Per Cross-Correlation Plots	MXCROSS = 7

Maximum Number of New Variables Generated Per Procedure	MXNEWVAR = 60
Maximum Number of New Cases Per Procedure	MXPREDICT = 1000
Treatment of User-Missing Values	MISSING = EXCLUDE
Confidence Interval Percentage Value	CIN = 95
Tolerance for Entering Variables in Regression Equations	TOLER = .0001
Maximum Iterative Parameter Change	CNVERGE = .001
Method of Calculating Std. Errors for Autocorrelations	ACFSE = IND
Length of Seasonal Period	Unspecified
Variable Whose Values Label Observations in Plots	Unspecified
Equations Include	CONSTANT

Model Description

Model Name		MOD_5
Series or Sequence	1	Studentized Residual for TgABS
Transformation		None
Non-Seasonal Differencing		0
Seasonal Differencing		0
Length of Seasonal Period		No periodicity
Standardization		Not applied
Distribution	Type	Normal
	Location	estimated
	Scale	estimated
Fractional Rank Estimation Method		Blom's
Rank Assigned to Ties		Mean rank of tied values

Applying the model specifications from MOD_5

Case Processing Summary

		Studentized Residual for TgABS
Series or Sequence Length		24
Number of Missing Values in the Plot	User-Missing	0
	System-Missing	0

The cases are unweighted.

Estimated Distribution Parameters

		Studentized Residual for TgABS
Normal Distribution	Location	.0000
	Scale	1.02151

The cases are unweighted.

Studentized Residual for TgABS

Normal Q-Q Plot of Studentized Residual for TgABS

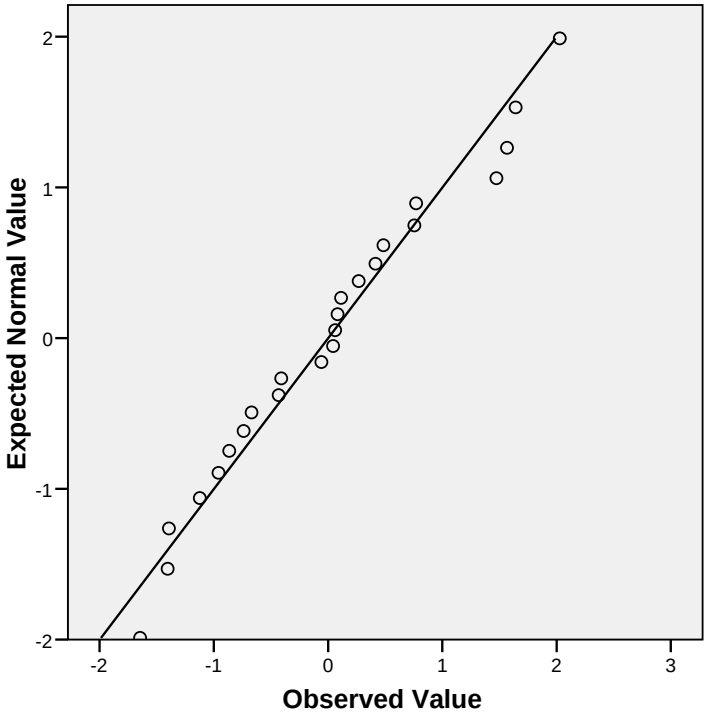

Detrended Normal Q-Q Plot of Studentized Residual for TgABS

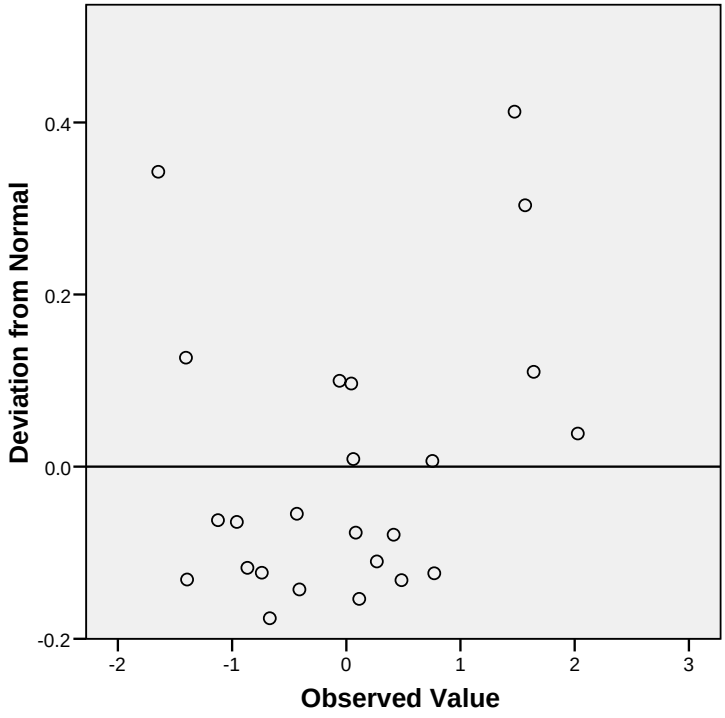

PPlot

Notes

Output Created		14-FEB-2007 11:35:52
Comments		
Input	Data	C:\Documents and Settings\j3tang\My Documents\My Work\Research (Part 2)\Peak Shift\PeakShift Data Analysis.sav
	Active Dataset	DataSet1
	Filter	<none>
	Weight	<none>
	Split File	<none>
	N of Rows in Working Data File	24
	Date	<none>
Missing Value Handling	Definition of Missing	User-defined missing values are treated as missing.
	Cases Used	For a given sequence or time series variable, cases with missing values are not used in the analysis. Cases with negative or zero values are also not used, if the log transform is requested.
Syntax		PPLOT /VARIABLES=SRE_6 /NOLOG /NOSTANDARDIZE /TYPE=Q-Q /FRACTION=BLOM /TIES=MEAN /DIST=NORMAL.
Resources	Elapsed Time	0:00:00.62
	Processor Time	0:00:00.78
Use	From	First observation
	To	Last observation
Time Series Settings (TSET)	Amount of Output	PRINT = DEFAULT
	Saving New Variables	NEWVAR = CURRENT
	Maximum Number of Lags in Autocorrelation or Partial Autocorrelation Plots	MXAUTO = 16

Maximum Number of Lags Per Cross-Correlation Plots	MXCROSS = 7
Maximum Number of New Variables Generated Per Procedure	MXNEWVAR = 60
Maximum Number of New Cases Per Procedure	MXPREDICT = 1000
Treatment of User-Missing Values	MISSING = EXCLUDE
Confidence Interval Percentage Value	CIN = 95
Tolerance for Entering Variables in Regression Equations	TOLER = .0001
Maximum Iterative Parameter Change	CNVERGE = .001
Method of Calculating Std. Errors for Autocorrelations	ACFSE = IND
Length of Seasonal Period	Unspecified
Variable Whose Values Label Observations in Plots	Unspecified
Equations Include	CONSTANT

Model Description

Model Name		MOD_6
Series or Sequence	1	Studentized Residual for Tf
Transformation		None
Non-Seasonal Differencing		0
Seasonal Differencing		0
Length of Seasonal Period		No periodicity
Standardization		Not applied
Distribution	Type	Normal
	Location	estimated
	Scale	estimated
Fractional Rank Estimation Method		Blom's
Rank Assigned to Ties		Mean rank of tied values

Applying the model specifications from MOD_6

Case Processing Summary

		Studentized Residual for Tf
Series or Sequence Length		24
Number of Missing Values in the Plot	User-Missing	0
	System-Missing	0

The cases are unweighted.

Estimated Distribution Parameters

		Studentized Residual for Tf
Normal Distribution	Location	.0000
	Scale	1.02151

The cases are unweighted.

Studentized Residual for Tf

Normal Q-Q Plot of Studentized Residual for Tf

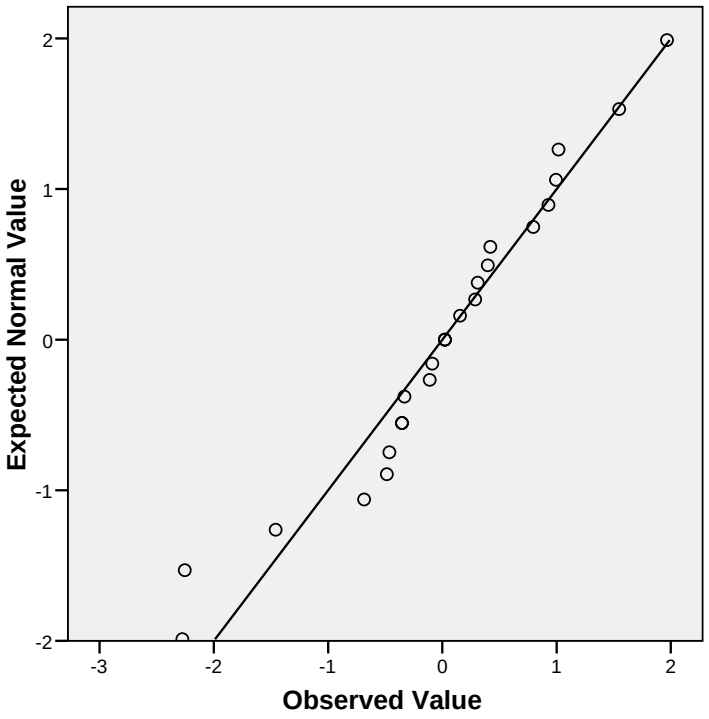

Detrended Normal Q-Q Plot of Studentized Residual for Tf

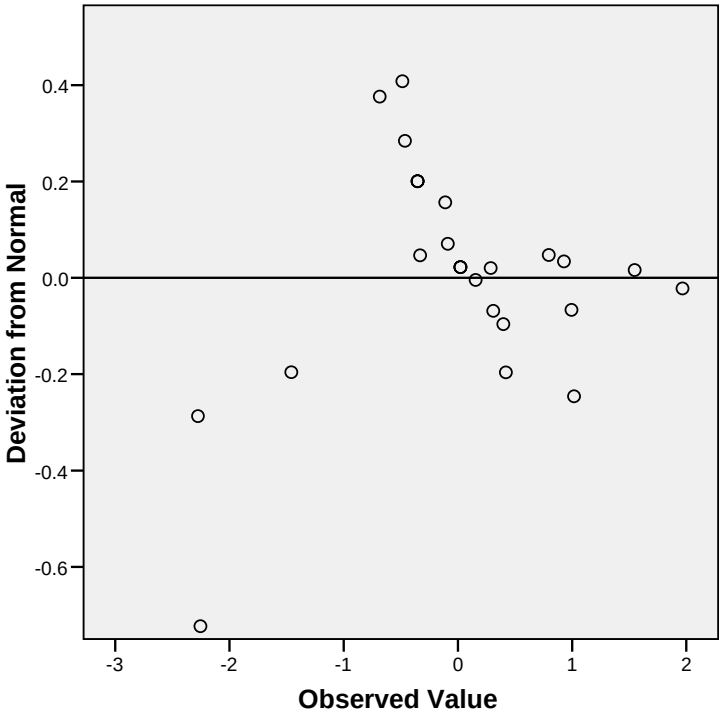

Interactive Graph

Notes

Output Created		14-FEB-2007 11:36:57
Comments		
Input	Data	C:\Documents and Settings\j3tang\My Documents\My Work\Research (Part 2)\Peak Shift\PeakShift Data Analysis.sav
	Active Dataset	DataSet1
	Filter	<none>
	Weight	<none>
	Split File	<none>
Syntax		IGRAPH /VIEWNAME='Scatterplot' /X1 = VAR(Case) TYPE = SCALE /Y = VAR(COO_5) TYPE = SCALE /COORDINATE = VERTICAL /X1LENGTH=3.0 /YLENGTH=3.0 /X2LENGTH=3.0 /CHARTLOOK='NONE' /SCATTER COINCIDENT = NONE.
Resources	Elapsed Time	0:00:00.01
	Processor Time	0:00:00.02

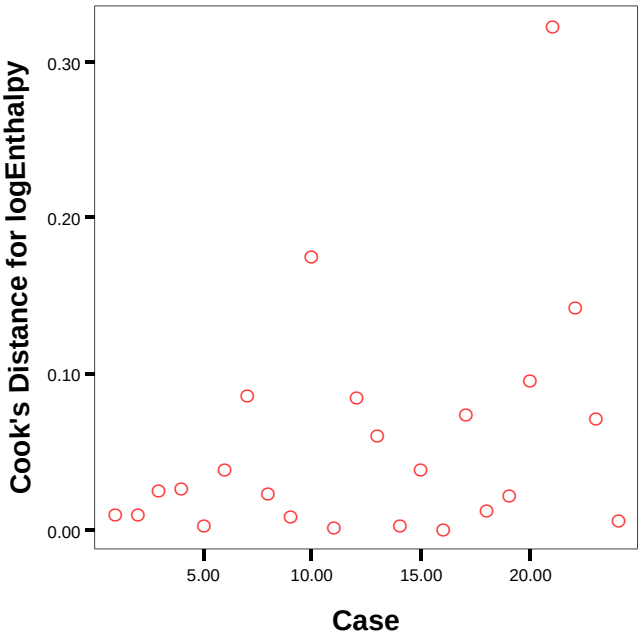

Interactive Graph

Notes

Output Created		14-FEB-2007 11:38:09
Comments		
Input	Data	C:\Documents and Settings\j3tang\My Documents\My Work\Research (Part 2)\Peak Shift\PeakShift Data Analysis.sav
	Active Dataset	DataSet1
	Filter	<none>
	Weight	<none>
	Split File	<none>
Syntax		IGRAPH /VIEWNAME='Scatterplot' /X1 = VAR(Case) TYPE = SCALE /Y = VAR(COO_2) TYPE = SCALE /COORDINATE = VERTICAL /X1LENGTH=3.0 /YLENGTH=3.0 /X2LENGTH=3.0 /CHARTLOOK='NONE' /SCATTER COINCIDENT = NONE.
Resources	Elapsed Time	0:00:00.02
	Processor Time	0:00:00.02

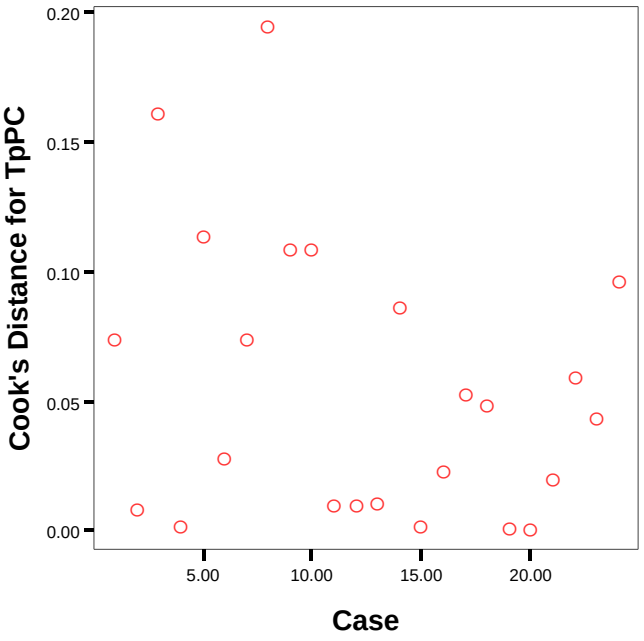

Interactive Graph

Notes

Output Created		14-FEB-2007 11:38:55
Comments		
Input	Data	C:\Documents and Settings\j3tang\My Documents\My Work\Research (Part 2)\Peak Shift\PeakShift Data Analysis.sav
	Active Dataset	DataSet1
	Filter	<none>
	Weight	<none>
	Split File	<none>
Syntax		IGRAPH /VIEWNAME='Scatterplot' /X1 = VAR(Case) TYPE = SCALE /Y = VAR(COO_1) TYPE = SCALE /COORDINATE = VERTICAL /X1LENGTH=3.0 /YLENGTH=3.0 /X2LENGTH=3.0 /CHARTLOOK='NONE' /SCATTER COINCIDENT = NONE.
Resources	Elapsed Time	0:00:00.02
	Processor Time	0:00:00.02

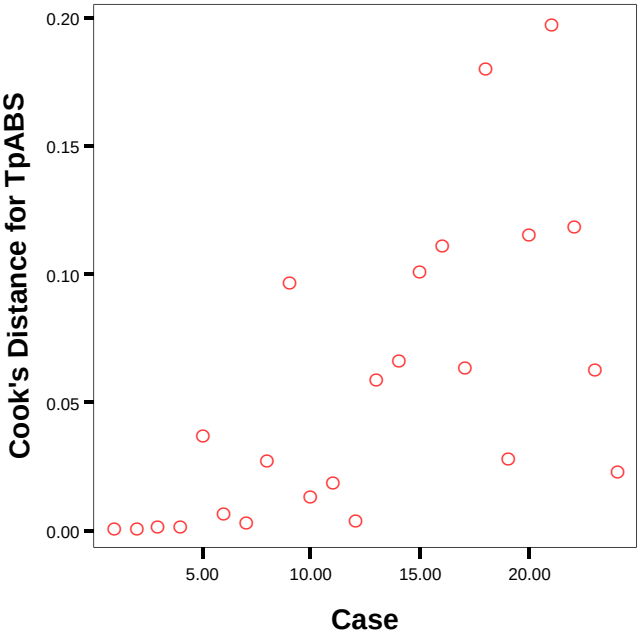

Interactive Graph

Notes

Output Created		14-FEB-2007 11:40:16
Comments		
Input	Data	C:\Documents and Settings\j3tang\My Documents\My Work\Research (Part 2)\Peak Shift\PeakShift Data Analysis.sav
	Active Dataset	DataSet1
	Filter	<none>
	Weight	<none>
	Split File	<none>
Syntax		IGRAPH /VIEWNAME='Scatterplot' /X1 = VAR(Case) TYPE = SCALE /Y = VAR(COO_4) TYPE = SCALE /COORDINATE = VERTICAL /X1LENGTH=3.0 /YLENGTH=3.0 /X2LENGTH=3.0 /CHARTLOOK='NONE' /SCATTER COINCIDENT = NONE.
Resources	Elapsed Time	0:00:00.00
	Processor Time	0:00:00.00

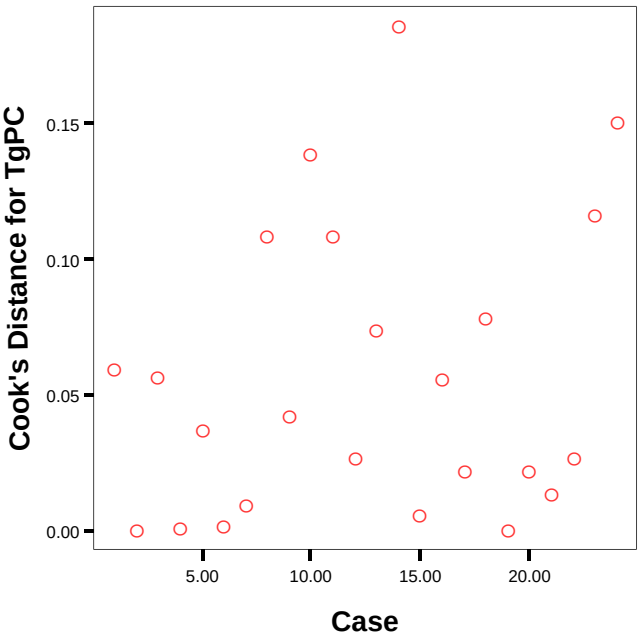

Interactive Graph

Notes

Output Created		14-FEB-2007 11:41:17
Comments		
Input	Data	C:\Documents and Settings\j3tang\My Documents\My Work\Research (Part 2)\Peak Shift\PeakShift Data Analysis.sav
	Active Dataset	DataSet1
	Filter	<none>
	Weight	<none>
	Split File	<none>
Syntax		IGRAPH /VIEWNAME='Scatterplot' /X1 = VAR(Case) TYPE = SCALE /Y = VAR(COO_3) TYPE = SCALE /COORDINATE = VERTICAL /X1LENGTH=3.0 /YLENGTH=3.0 /X2LENGTH=3.0 /CHARTLOOK='NONE' /SCATTER COINCIDENT = NONE.
Resources	Elapsed Time	0:00:00.02
	Processor Time	0:00:00.02

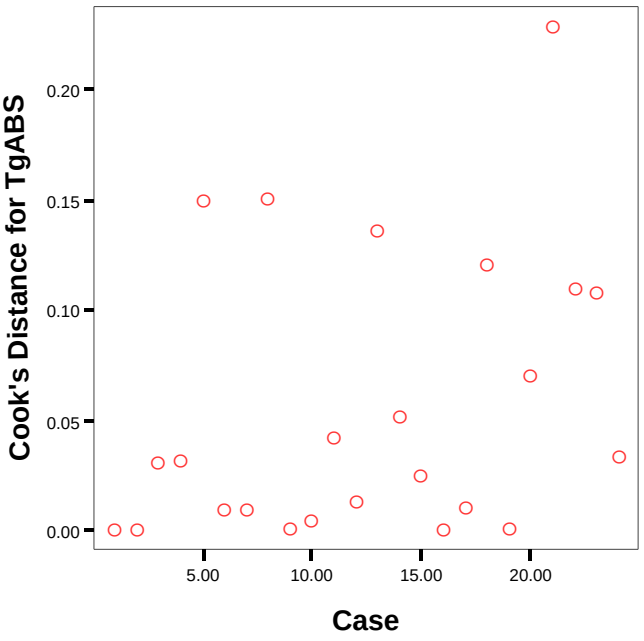

Interactive Graph

Notes

Output Created		14-FEB-2007 11:41:48
Comments		
Input	Data	C:\Documents and Settings\j3tang\My Documents\My Work\Research (Part 2)\Peak Shift\PeakShift Data Analysis.sav
	Active Dataset	DataSet1
	Filter	<none>
	Weight	<none>
	Split File	<none>
Syntax		IGRAPH /VIEWNAME='Scatterplot' /X1 = VAR(Case) TYPE = SCALE /Y = VAR(COO_6) TYPE = CATEGORICAL /COORDINATE = VERTICAL /X1LENGTH=3.0 /YLENGTH=3.0 /X2LENGTH=3.0 /CHARTLOOK='NONE' /CATORDER VAR(COO_6) (ASCENDING VALUES OMITEMPTY) /SCATTER COINCIDENT = NONE.
Resources	Elapsed Time	0:00:00.02
	Processor Time	0:00:00.02

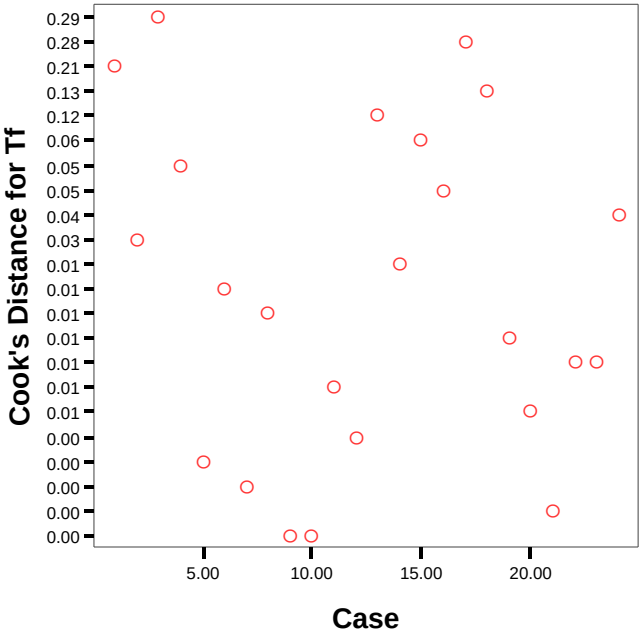

Univariate Analysis of Variance of Enthalpy Prior Transformation

Notes

Output Created		14-FEB-2007 12:04:54
Comments		
Input	Data	C:\Documents and Settings\j3tang\My Documents\My Work\Research (Part 2)\Peak Shift\PeakShift Data Analysis.sav
	Active Dataset	DataSet1
	Filter	<none>
	Weight	<none>
	Split File	<none>
	N of Rows in Working Data File	24
Missing Value Handling	Definition of Missing	User-defined missing values are treated as missing.
	Cases Used	Statistics are based on all cases with valid data for all variables in the model.
Syntax		UNIANOVA Enthalpy BY AgingTime /METHOD = SSTYPE(3) /INTERCEPT = INCLUDE /SAVE = PRED SRESID COOK /PRINT = DESCRIPTIVE /PLOT = RESIDUALS /CRITERIA = ALPHA(.05) /DESIGN = AgingTime .
Resources	Elapsed Time	0:00:00.41
	Processor Time	0:00:00.61
Variables Created or Modified	PRE_7	Predicted Value for Enthalpy
	SRE_7	Studentized Residual for Enthalpy
	COO_7	Cook's Distance for Enthalpy

Between-Subjects Factors

		N
AgingTime	.50	4
	2.00	4
	8.00	4
	96.00	4
	336.00	4
	1008.00	4

Descriptive Statistics

Dependent Variable: Enthalpy

AgingTime	Mean	Std. Deviation	N
.50	.2355	.01190	4
2.00	.4405	.03198	4
8.00	.7240	.06965	4
96.00	1.4365	.08572	4
336.00	1.8250	.15563	4
1008.00	2.2695	.32919	4
Total	1.1552	.77139	24

Tests of Between-Subjects Effects

Dependent Variable: Enthalpy

Source	Type III Sum of Squares	df	Mean Square	F	Sig.
Corrected Model	13.248(a)	5	2.650	108.926	.000
Intercept	32.026	1	32.026	1316.587	.000
AgingTime	13.248	5	2.650	108.926	.000
Error	.438	18	.024		
Total	45.712	24			
Corrected Total	13.686	23			

a R Squared = .968 (Adjusted R Squared = .959)

Dependent Variable: Enthalpy

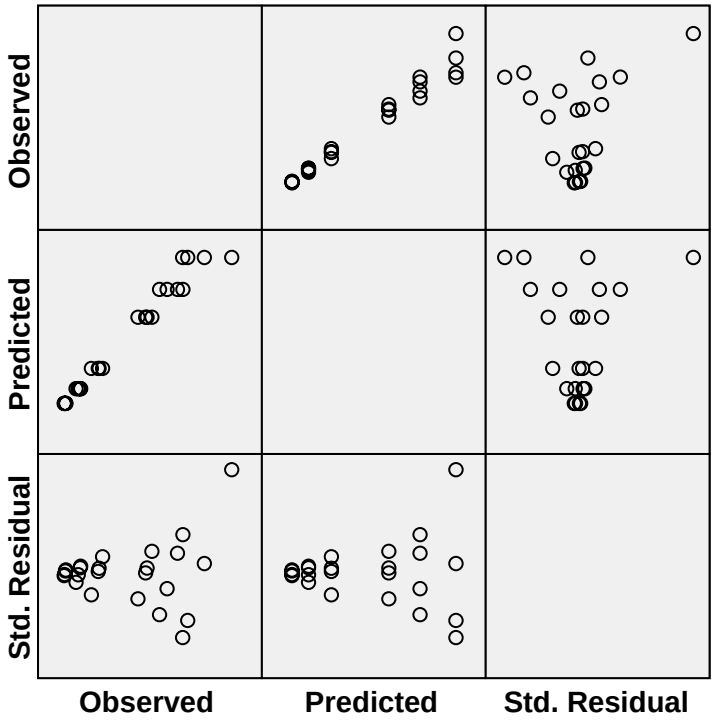

PPlot

Notes

Output Created		14-FEB-2007 12:05:56
Comments		
Input	Data	C:\Documents and Settings\j3tang\My Documents\My Work\Research (Part 2)\Peak Shift\PeakShift Data Analysis.sav
	Active Dataset	DataSet1
	Filter	<none>
	Weight	<none>
	Split File	<none>
	N of Rows in Working Data File	24
	Date	<none>
Missing Value Handling	Definition of Missing	User-defined missing values are treated as missing.
	Cases Used	For a given sequence or time series variable, cases with missing values are not used in the analysis. Cases with negative or zero values are also not used, if the log transform is requested.
Syntax		PPLOT

		/VARIABLES=SRE_7 /NOLOG /NOSTANDARDIZE /TYPE=Q-Q /FRACTION=BLOM /TIES=MEAN /DIST=NORMAL.	
Resources	Elapsed Time		0:00:00.64
	Processor Time		0:00:00.75
Use	From	First observation	
	To	Last observation	
Time Series Settings (TSET)	Amount of Output	PRINT = DEFAULT	
	Saving New Variables	NEWVAR = CURRENT	
	Maximum Number of Lags in Autocorrelation or Partial Autocorrelation Plots	MXAUTO = 16	
	Maximum Number of Lags Per Cross-Correlation Plots	MXCROSS = 7	
	Maximum Number of New Variables Generated Per Procedure	MXNEWVAR = 60	
	Maximum Number of New Cases Per Procedure	MXPREDICT = 1000	
	Treatment of User-Missing Values	MISSING = EXCLUDE	
	Confidence Interval Percentage Value	CIN = 95	
	Tolerance for Entering Variables in Regression Equations	TOLER = .0001	
	Maximum Iterative Parameter Change	CNVERGE = .001	
	Method of Calculating Std. Errors for Autocorrelations	ACFSE = IND	
	Length of Seasonal Period	Unspecified	
	Variable Whose Values Label Observations in Plots	Unspecified	
	Equations Include	CONSTANT	

Model Description

Model Name		MOD_7
Series or Sequence	1	Studentized Residual for Enthalpy
Transformation		None
Non-Seasonal Differencing		0
Seasonal Differencing		0
Length of Seasonal Period		No periodicity
Standardization		Not applied
Distribution	Type	Normal
	Location	estimated
	Scale	estimated
Fractional Rank Estimation Method		Blom's
Rank Assigned to Ties		Mean rank of tied values

Applying the model specifications from MOD_7

Case Processing Summary

		Studentized Residual for Enthalpy
Series or Sequence Length		24
Number of Missing Values in the Plot	User-Missing	0
	System-Missing	0

The cases are unweighted.

Estimated Distribution Parameters

		Studentized Residual for Enthalpy
Normal Distribution	Location	.0000
	Scale	1.02151

The cases are unweighted.

Studentized Residual for Enthalpy

Normal Q-Q Plot of Studentized Residual for Enthalpy

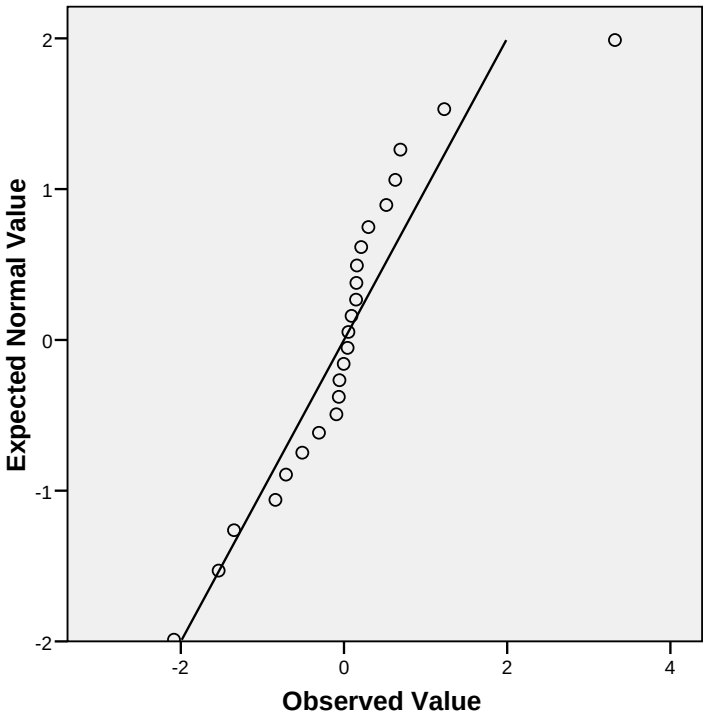

Detrended Normal Q-Q Plot of Studentized Residual for Enthalpy

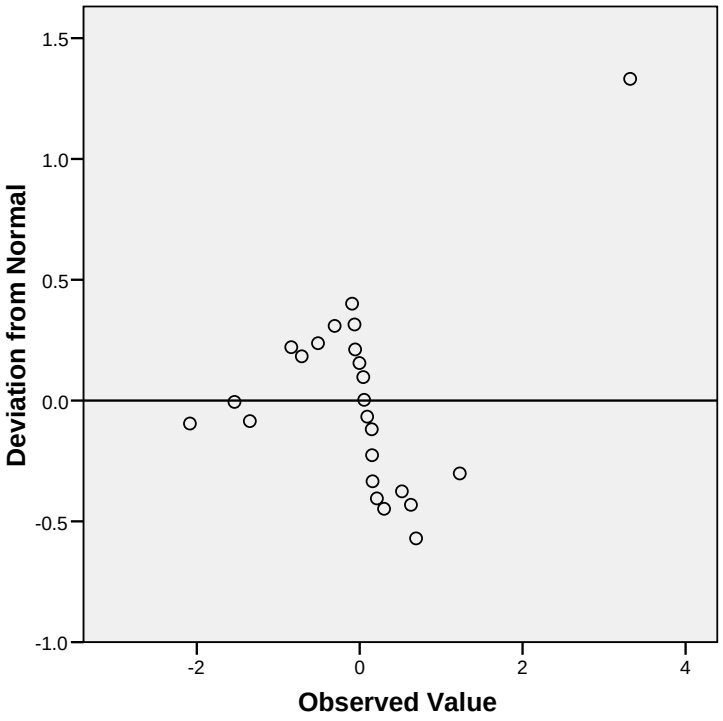

Interactive Graph

Notes

Output Created		14-FEB-2007 12:06:38
Comments		
Input	Data	C:\Documents and Settings\j3tang\My Documents\My Work\Research (Part 2)\Peak Shift\PeakShift Data Analysis.sav
	Active Dataset	DataSet1
	Filter	<none>
	Weight	<none>
	Split File	<none>
Syntax		IGRAPH /VIEWNAME='Scatterplot' /X1 = VAR(Case) TYPE = SCALE /Y = VAR(COO_7) TYPE = SCALE /COORDINATE = VERTICAL /X1LENGTH=3.0 /YLENGTH=3.0 /X2LENGTH=3.0 /CHARTLOOK='NONE' /SCATTER COINCIDENT = NONE.
Resources	Elapsed Time	0:00:00.02
	Processor Time	0:00:00.03

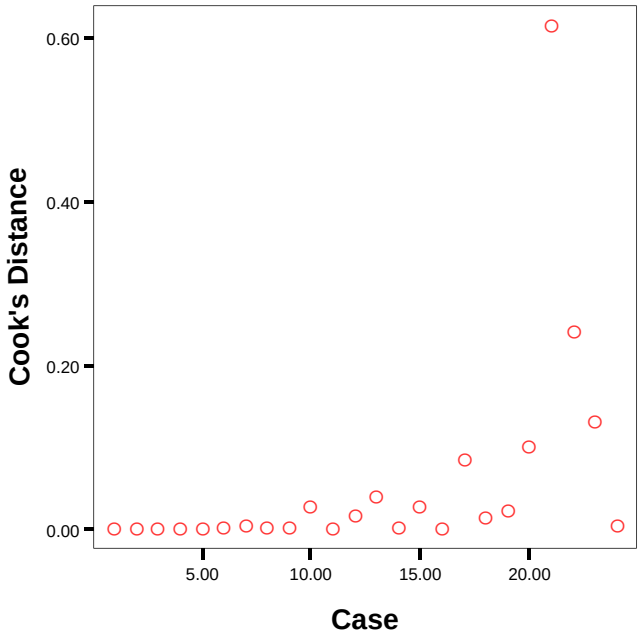

Interactive Graph

Notes

Output Created		14-FEB-2007 12:08:08
Comments		
Input	Data	C:\Documents and Settings\j3tang\My Documents\My Work\Research (Part 2)\Peak Shift\PeakShift Data Analysis.sav
	Active Dataset	DataSet1
	Filter	<none>
	Weight	<none>
	Split File	<none>
Syntax		IGRAPH /VIEWNAME='Scatterplot' /X1 = VAR(PRE_7) TYPE = CATEGORICAL /Y = VAR (SRE_7) TYPE = SCALE /COORDINATE = VERTICAL /X1LENGTH=3.0 /YLENGTH=3.0 /X2LENGTH=3.0 /CHARTLOOK='NONE' /CATORDER VAR(PRE_7) (ASCENDING VALUES OMITEMPTY) /SCATTER COINCIDENT = NONE.
Resources	Elapsed Time	0:00:00.03
	Processor Time	0:00:00.05